

ABSTRACT

Title of Document: LOSS OF CONTACT AND TIME DELAY
 DYNAMICS OF MILLING PROCESSES

Xinhua Long, Doctor of Philosophy, 2005

Directed By: Professor B. Balachandran
 Department of Mechanical Engineering

Considering the feed motion, the dynamics of constant spindle speed (CSS) milling processes is described by a set of delay differential equations with periodic coefficients and a variable time delay associated with each cutting tooth. This model, which has been developed for the first time as a part of this dissertation, is used to study the dynamics and stability of the system. The semi-discretization scheme, a numerical scheme with an analytical basis, is refined to examine the stability of periodic solutions of this system. This scheme can be used to predict not only the stability but also the chatter frequencies for a wide variety of milling operations ranging from full-immersion to partial-immersion operations. From the results obtained thus far, it can be stated that feed-rate effects can be neglected during full-immersion and high-immersion operations, where the influence of loss of contact nonlinearities is not pronounced. However, for low-immersion milling operations, where loss of contact effects have a strong influence on system stability behavior,

high feed-rate effects are pronounced and these effects can't be ignored. Along with investigations into the dynamics of CSS milling processes, in this dissertation, a better delay approximation has been used in the modeling of variable spindle speed (VSS) milling processes, and the benefits of VSS milling operations are discussed by comparing the stability charts of VSS milling operations with those obtained for CSS milling operations. The nonsmooth characteristics of milling processes are pointed out by presenting the simulated results for cutting forces. Work conducted with a nonsmooth mechanical system, a simplified system related to the milling process, is presented and the numerical results and experimental results obtained show evidence for grazing and other bifurcations in this nonsmooth system.

LOSS OF CONTACT AND TIME DELAY DYNAMICS OF MILLING PROCESSES

By

Xinhua Long

Dissertation submitted to the Faculty of the Graduate School of the
University of Maryland, College Park, in partial fulfillment
of the requirements for the degree of
Doctor of Philosophy
2006

Advisory Committee:

Professor B. Balachandran, Chair/Advisor

Associate Professor S.K. Gupta, Mechanical Engineering

Associate Professor B. Hunt, Mathematics and IPST

Assistant Professor M. Yu, Mechanical Engineering

Associate Professor G.M. Zhang, Mechanical Engineering

© Copyright by
Xinhua Long
2006

Dedication

To My Family

Acknowledgements

I wish to express my sincere and deep appreciation to Professor B. Balachandran for his encouragement, insightful guidance, all the patience, support, and enthusiasm. His guidance throughout this work has not only been of invaluable help to me during my Ph.D. study, but it will also guide me in my life beyond school.

I would like to thank Professors S. K. Gupta, B. Hunt, M., Yu, and G. M. Zhang for serving on my committee and for their time and efforts to help me in innumerable ways. I would also like to thank Professor B. Mann of the University of Missouri for providing experimental data and machining system parameters.

My thanks also go to Drs. Moustafa Al-Bassyiouni, He Li, Sergio Preidikman, Mr. Andrew James Dick, and Guojian Lin for their help and friendship during my doctoral study.

The financial support provided by the National Science Foundation (NSF grant DMI-0123708) is gratefully acknowledged.

Finally, I extend the warmest thanks and appreciation to my wife, Meixin, whose unwavering support made the completion of this dissertation possible.

Table of Contents

Dedication.....	ii
Acknowledgements.....	iii
Table of Contents.....	iv
List of Tables.....	vi
List of Figures.....	vii
Chapter 1.....	1
Introduction and Background.....	1
1.1. Introduction.....	1
1.2. Review of Research on Dynamics of Milling Processes.....	7
1.2.1. Cutting force model.....	7
1.2.2. Milling system models.....	7
1.2.3. Dynamics and stability issues.....	10
1.3. Nonsmooth Dynamics.....	14
1.4. Current Research.....	16
1.4.1. Research objectives.....	16
1.4.2. Organization of dissertation.....	18
Chapter 2.....	19
Model of Workpiece-Tool System.....	19
2.1. Feed Motion Effect on Time Delay.....	19
2.2. Feed Motion Effect on the Static Cutting Entry Angle and Exit Angle.....	24
2.3. Feed Motion Effect on the Static Uncut Chip Thickness.....	25
2.4. Feed Motion Effect on the Amplitude of Feed Mark Wave.....	28
2.5. Modeling of Milling Process System.....	30
2.6. Model with Two Time Delays.....	39
Chapter 3.....	44
Stability Analysis.....	44
3.1. Periodic Motions of Delay Differential System with Time-Periodic Coefficients.....	45
3.2. Semi-Discretization Method for System with Two Time Delays.....	47
3.3. Numerical Results for System with Two Time Delays.....	52
3.3.1. Single-degree-of-freedom system.....	52
3.3.2. Four-degree-of-freedom system.....	56
3.4. Semi-Discretization Method for System with Variable Time Delay.....	63
3.5. Results for Systems with Variable Time Delay.....	67
Chapter 4.....	80
Dynamics of Variable Spindle Speed (VSS) Milling Processes.....	80
4.1. Milling Model with Variable Spindle Speed.....	80
4.2. Numerical Results for VSS Milling Processes.....	84
Chapter 5.....	90
Nonsmooth Dynamics.....	90
5.1. Nonsmooth Characteristics of Milling Processes.....	90
5.2. Model of Impacted Beam.....	95

5.3. Experimental Arrangement.....	98
5.4. Results and Discussion	100
5.4.1. Results for hard impact.....	101
5.4.2. Grazing motions in systems with soft impacts	104
5.4.3. Bifurcation control.....	111
Chapter 6.....	113
Summary and Recommendation for Future Work.....	113
Appendix A.....	117
Coefficients in Impact Model	117
Appendix B.....	118
Matlab Program for Semi-Discretization Method for System with Two Time Delays	118
Appendix C.....	128
Matlab Program for Semi-Discretization Method for System with Variable Time Delay	128
Appendix D.....	137
Matlab Program for Semi-Discretization Method for Stability Analysis of VSS Milling Processes.....	137
Appendix E	146
FORTTRAN Program for Studying Impact System.....	146
Bibliography	153

List of Tables

3.1	Modal parameters of single-degree-of-freedom milling system (Mann et al. 2003)	53
3.2	Machining parameters of single-degree-of-freedom milling system (Mann et al. 2003)	53
3.3	Modal parameters of four-degree-of-freedom milling system.....	56
3.4	Machining parameters of four-degree-of-freedom milling system.....	56
3.5	Modal parameters of two-degree-of-freedom milling system.....	67
3.6	Machining parameters of two-degree-of-freedom milling system.....	67
4.1	Modal parameters of two-degree-of-freedom milling system.....	86
4.2	Machining parameters of two-degree-of-freedom milling system.....	87

List of Figures

1.1.	Different milling operations: (a) peripheral milling , (b) face milling, and (c) end milling.	2
1.2.	Milling operations with different feed directions: (a) up-milling operation and (b) down-milling operation.	3
1.3.	Stability chart of a milling process.....	5
1.4.	Illustration of loss of contact between tool and workpiece.....	11
2.1.	Tooth path of milling operation with two teeth: (a) system vibration dependent tooth path, (b) system vibration independent tooth path, and (c) quasi-static tooth path. The dashed and solid lines represent the paths of tooth 1 and tooth 2, respectively. O_1 is the position of tool center when the tooth 1 cuts the workpiece at point B and O_2 is the position of tool center when the tooth 2 cuts the workpiece at point A.	20
2.2.	Illustrations of geometric relationships for the three cases of Figure 2.1. θ' is the angular position of the first tooth, θ is the angular position of the second tooth, f is the feed speed, and τ is the time delay. The relationships are identical in cases (b) and (c).....	20
2.3.	Variable time delays for $\Omega=5000$ rpm, $R=9.53$ mm, and $N=2$	23
2.4.	Variable time delays for $\Omega=5000$ rpm, $f=0.5$ mm/tooth, and $N=2$	23
2.5.	Schematic diagram for cutting entry angle and exit angle.....	25
2.6.	Static uncut chip thickness for $R=9.53$ mm and $N=2$	26
2.7.	Normalized static uncut chip thickness for $R=9.53$ mm and $N=2$	26
2.8.	Schematic diagram for feed marks on the workpiece.	28
2.9.	Workpiece-Tool system model: (a) up-milling operation and (b) down-milling operation.....	31
2.10.	Cylindrical end mill with helical flutes and thin disk element.....	33
2.11.	Static deviation of entry or exit angle in cutting zone.	41
3.1.	Discretization scheme for two delays.	49
3.2.	Schematic diagram of experimental arrangement (Mann <i>et al.</i> , 2003).....	53
3.3.	Stability predictions for 25% immersion down-milling operations.....	54
3.4.	Stability predictions for 25% immersion up-milling operations.....	54
3.5.	Stability predictions for 25% immersion up-milling operations.....	58
3.6.	Stability predictions for 25% immersion down-milling operations.....	58
3.7.	Stability predictions for 10% immersion up-milling operations.....	59
3.8.	Stability predictions for 10% immersion down-milling operations.	59
3.9.	Poincaré section and trajectory.	60
3.10.	(a) Poincaré section of periodic orbit, (b) Poincaré section of period-two orbit, and (c) Poincaré section of quasi-periodic orbit.	62
3.11.	Bifurcation diagram for 10% immersion up-milling operation at spindle speed 14200 rpm.	62
3.12.	Discretization scheme for variable time delay.....	64
3.13.	Stability charts for 5% immersion down-milling operations.	69
3.14.	Normalized stability limit for 5% immersion down-milling operations.....	69

3.15.	Chatter frequencies for 5% immersion down-milling operations. The labels “PD” and “Hopf” are used to mark the period-doubling and Hopf bifurcation windows, respectively.	70
3.16.	Experimental results obtained for a 5% immersion down-milling case: (a) 1/rev sampled signals; (b) Poincaré sections; and (c) power spectra. The cases A, B, C, and D shown here correspond to cases A, B, C, and D of Figure 3.13. The symbols \circ , \square , Δ , and \bullet , are used to mark the Hopf chatter frequencies f_H , the period-doubling chatter frequencies f_{PD} , the tooth-passing frequencies f_{TP} , and the damped natural frequency, respectively.	71
3.17.	Stability charts for 5% immersion up-milling operations.	72
3.18.	Stability charts for 25% immersion: (a) down-milling operation and (b) up-milling operations	74
3.19.	Stability charts for 50% immersion: (a) down-milling operation and (b) up-milling operations	75
3.20.	Stability charts for 75% immersion: (a) down-milling operation and (b) up-milling operations.	76
3.21.	Stability charts for full-immersion milling operations.	77
3.22.	Chatter frequencies for full-immersion milling operations with $f=0.127$ mm/tooth.	77
3.23.	Stability predictions for 10% immersion down-milling operations.	78
3.24.	Stability predictions for 10% immersion up-milling operations.	79
4.1.	Exact and approximate delays for $\Omega_0 = 4000$ rpm: (a,b) $N=1, 2, RVA=0.1, RVF=0.1$, (c,d) $N=1, 2, RVA=0.2, RVF=0.2$, and (e,f) $N=1, 2, RVA=0.3, RVF=0.3$. (— Exact Delay; --- Approximated Delay (Current); Approximated Delay (Former)).	83
4.2.	Stability predictions for 25% immersion down-milling operations: (a) $RVA=0.1, RVF=0.1$, (b) $RVA=0.1, RVF=0.2$, (c) $RVA=0.2, RVF=0.1$, (d) $RVA=0.2, RVF=0.2$, (e) $RVA=0.2, RVF=0.3$, and (f) $RVA=0.3, RVF=0.3$	85
4.3.	Stability predictions for 5% immersion up-milling operations: (a) $RVA=0.05, RVF=0.05$, (b) $RVA=0.1, RVF=0.1$, (c) $RVA=0.1, RVF=0.2$, (d) $RVA=0.2, RVF=0.1$, (e) $RVA=0.2, RVF=0.2$, (f) $RVA=0.3, RVF=0.2$, (g) $RVA=0.2, RVF=0.3$, and (h) $RVA=0.3, RVF=0.3$	87
4.4.	Stability predictions for 5% immersion up-milling operations: (a) $RVA=0.05, RVF=0.05$, (b) $RVA=0.1, RVF=0.1$, (c) $RVA=0.1, RVF=0.2$, (d) $RVA=0.2, RVF=0.1$, (e) $RVA=0.2, RVF=0.2$, (f) $RVA=0.3, RVF=0.2$, (g) $RVA=0.2, RVF=0.3$, and (h) $RVA=0.3, RVF=0.3$	88
5.1.	Simulated cutting forces for four degree-of-freedom system during 10% immersion up-milling operations: (a) cutting during periodic motions when $ADOC=1.2$ mm and $\Omega=14200$ rpm, (b) cutting during period-doubled motions when $ADOC=2.4$ mm and $\Omega=14200$ rpm, (c) cutting during chaotic motions when $ADOC=4.8$ mm and $\Omega=14200$ rpm, and (d) cutting during period-doubled motions (including jump of workpiece cutting) when $ADOC=0.45$ mm at $\Omega=12330$ rpm.	92
5.2.	Experimental measurements of contact force in an impacted cantilever beam with a soft impact: (a) $\Omega/2\pi = 34.0$ Hz, periodic orbit, (b) $\Omega/2\pi = 33$ Hz, period-	

	doubled orbit, (c) $\Omega / 2\pi = 30.2$ Hz , period-doubled orbit, and (d) $\Omega / 2\pi = 30.0$ Hz , chaotic orbit.....	93
5.3.	Cutting force phase plots for the four cases shown in Figure 5.1.....	94
5.4.	Model of an elastic cantilever beam subjected to impacts.....	95
5.5.	Photograph of experimental set up for impact studies.....	99
5.6.	Schematic of experimental arrangement for impact studies.....	99
5.7.	Experimentally obtained bifurcation diagram on a Poincaré section for $D=0.074$ mm.....	102
5.8.	Numerically obtained bifurcation diagram on a Poincaré section for $D=0.074$ mm.....	103
5.9.	Phase plot for 40 Hz excitation frequency: (a) experimental result and (b) numerical result.....	103
5.10.	Phase plot for 112 Hz excitation frequency: (a) experimental result and (b) numerical result.....	104
5.11.	Possible grazing motions: (a) system with hard impact and (b) piecewise linear system.....	105
5.12.	Numerically obtained bifurcation diagram on a Poincaré section for $D=0.164$ mm, $k_c = 1.27 \times 10^5$ N/m, $c_c = 5.99$ N/(m/s), and $z_c = 0.1$ mm.....	106
5.13.	Numerical results obtained to illustrate a grazing bifurcation in a system with a soft impact: (a) $\Omega / 2\pi = 32.0$ Hz , periodic orbit prior to grazing, (b) $\Omega / 2\pi = 31.6$ Hz , periodic orbit grazing the hyper surface, and (c) $\Omega / 2\pi = 31.4$ Hz , chaotic orbit, immediately following the grazing impact. ...	107
5.14.	Experimental results obtained to illustrate a grazing bifurcation in a system with a soft impact: (a) $\Omega / 2\pi = 30.5$ Hz , periodic orbit prior to grazing, (b) $\Omega / 2\pi = 30.3$ Hz , periodic orbit grazing the hyper surface, and (c) $\Omega / 2\pi = 30.0$ Hz , chaotic orbit, immediately following the grazing impact. ...	108
5.15.	Experimental measurements of contact force in a system with a soft impact: (a) $\Omega / 2\pi = 30.5$ Hz , periodic orbit prior to grazing, (b) $\Omega / 2\pi = 30.3$ Hz , periodic orbit grazing the hyper surface, and (c) $\Omega / 2\pi = 30.0$ Hz , chaotic orbit, immediately following the grazing impact.....	109
5.16.	Numerical results used to illustrate a smooth bifurcation of a soft impact system: (a) $\Omega / 2\pi = 32.7$ Hz , periodic orbit and (b) $\Omega / 2\pi = 32.63$ Hz , period- doubled orbit.....	110
5.17.	Experimental results used to illustrate a smooth bifurcation of a soft impact system: (a) $\Omega / 2\pi = 34.0$ Hz , periodic orbit and (b) $\Omega / 2\pi = 33.0$ Hz , period- doubled orbit.....	110
5.18.	Experimental measurements of contact force in a system with a soft impact: (a) $\Omega / 2\pi = 34.0$ Hz , periodic orbit and (b) $\Omega / 2\pi = 33.0$ Hz , period-doubled orbit.	110
5.19.	Numerically obtained bifurcation diagrams for hard impact and feedback control: (a) $bu(q_1) = 0.2k_1 q_1(t) $ and (b) $bu(q_1) = -0.2k_1 q_1(t) $	112

Chapter 1

Introduction and Background

In this chapter, introductory and background information on prior research on milling processes and nonsmooth dynamics are presented. Along with a literature review on the different aspects of research on milling processes and nonsmooth dynamics, the shortcomings and limitations of previous efforts are examined and the issues to be addressed in the current efforts are also introduced.

1.1. Introduction

The milling process, a traditional operation of machining, is widely used in industry to manufacture mechanical components. In general, it is classified into peripheral milling, face milling, and end milling operations (Kalpakjian and Schmid, 2003). In peripheral milling, the milled surface is generated by teeth located on the periphery of the cutter body and the axis of cutter rotation is generally in a plane parallel to the workpiece surface being machined. In face milling, the milled surface results from the action of cutting edges located on the periphery and face of the cutter and the cutter is mounted on a spindle having an axis of rotation perpendicular to the workpiece surface. In end milling, the milling surface is generated by the teeth located on both the periphery and the tip of the cutter body and the cutter rotates on an axis perpendicular to the workpiece. End milling is the most versatile form of milling and it is used to machine die cavities, slots, contours, and profiles. Due to the interrupted

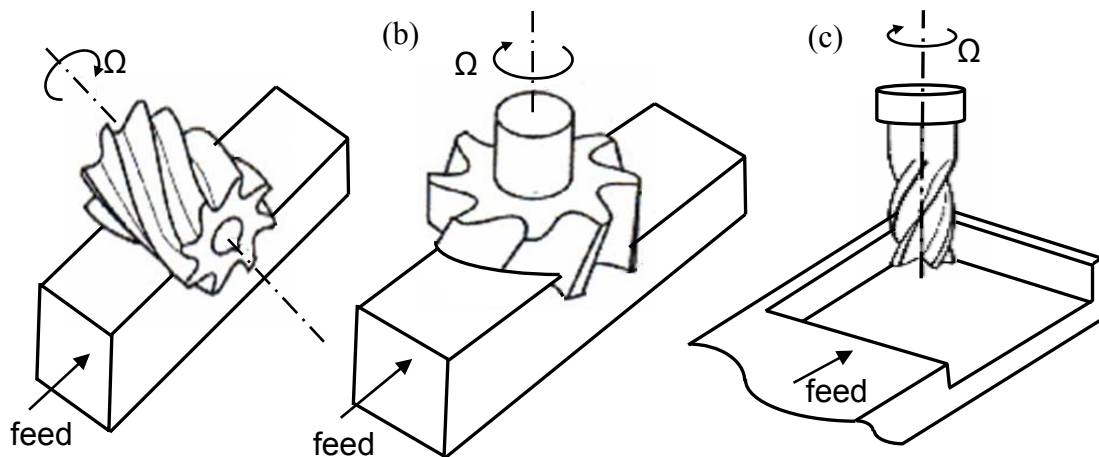


Figure 1.1: Different milling operations: (a) peripheral milling, (b) face milling, and (c) end milling.

nature of end milling, these teeth are usually made helical to reduce the impact that occurs when each tooth engages the workpiece. Depending on the nature of the feature to be machined, the axis of rotation of the end mill may be either perpendicular or parallel to the finished surface. The peripheral cutting edges generate a finished surface parallel to the axis of rotation, and the end cutting edges produce a finished surface perpendicular to the spindle. One also can say that an end milling operation is the combination of peripheral milling and face milling operations. Figure 1.1 is used to illustrate the peripheral milling, face milling, and end milling operations. Milling operations can also be classified into up-milling and down-milling according to the direction of the rotation with respect to the feed direction. As shown in Figure 1.2a, when the direction of the cutter rotation opposes the feed motion direction, the operation is referred to as up-milling. It is also called conventional milling. If the direction of cutter rotation is along the same direction as the feed motion direction, as shown in Figure 1.2b, the operation is referred to as down-milling operation. Down-milling is also called climb milling. The chip formation in down-

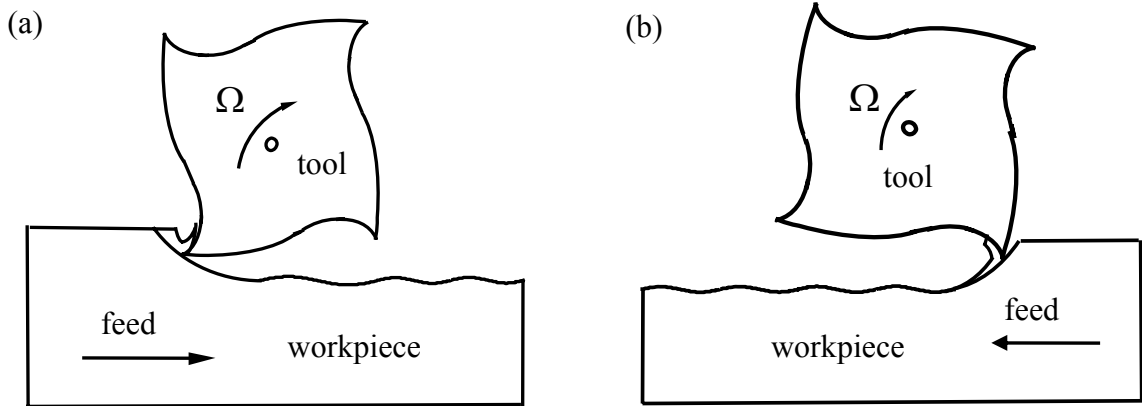


Figure 1.2: Milling operations with different feed directions: (a) up-milling operation and (b) down-milling operation.

milling is opposite to the chip formation in up-milling. As shown in Figure 1.2a, during up-milling, the cutter tooth begins to mill material with low chip thickness and the chip thickness increases gradually.

Although the investigations into the milling process have flourished in many areas of study during the past fifty years, research into the milling process is continually motivated by the ever increasing industrial demand for better performance.

Higher productivity and lower costs in material removal operations are always desirable in the manufacturing industry. Maintaining a good quality of the finished surface and a low tool wear are major challenges, when the material removal rate is increased. It is believed that the vibrations encountered during the milling process play a major role in determining the quality of the finished surface, the wear of tool, and the material removal rate. The cutting forces generated during a milling process induce dynamic deflections of the workpiece-tool system, which in turn modulate the cutting forces. In this self-excited system, when the energy input exceeds the energy

dissipated, the amplitude of vibration of the system will increase and result in an undesired relative vibration between the workpiece and the tool. This undesired relative vibration is one form of chatter vibrations. As discussed later in this dissertation, chatter vibrations can occur due to regenerative effects, loss of contact effects, and mode coupling effects. Chatter vibrations can result in a poor quality finished surface and high tool wear. Hence, these vibrations limit the material removal rate and result in a low productivity. As a result, avoiding and suppressing chatter vibrations is an important issue in the manufacturing industry.

Increasing workpiece-tool system damping is a direct and effective method to reduce the vibrations level and stabilize the milling process. However, there are several disadvantages; first, an existing system needs to undergo considerable modification to enhance the system damping. Second, there are limits to the level that the damping can be increased to. So, other approaches such as active methods need to be considered to suppress chatter vibrations. It is known that the level of vibration during a milling process is associated with the cutting force that is determined by the chip load; that is the volume of workpiece material that is removed during a given unit of time. Generally, reducing the chip load is one way to decrease the level of vibration of a system in certain milling operations. But a small chip load means a low material removal rate, a consequence of which is a lower production rate that is undesirable. The continuous variation of the cutting speed could help suppress chatter that develops during conventional, constant speed machining (Inamura and Sata, 1974). The improvement on the stability limit of cutting is dependent on the cutting speed, amplitude of speed variation, and frequency of speed variation. An alternate method

to avoid chatter vibration during a milling process is based on the stability chart (Figure 1.3), which is a graphical tool that was introduced by Tobias and Fishwick (1958a, b). This chart provides information about the onset of chatter vibrations in term of control parameters such as the axial depth of cut (ADOC) and the spindle speed. As shown in Figure 1.3, highly productive milling operations can be achieved by selecting appropriate spindle speeds that are associated with high process stability. To achieve this, a thorough understanding of the dynamics of the milling process is necessary to determine the stability, which depends on a number of different machining parameters. In addition, a good understanding of the dynamics of a milling process can be helpful for suppressing chatter efficiently by using system damping and active control techniques.

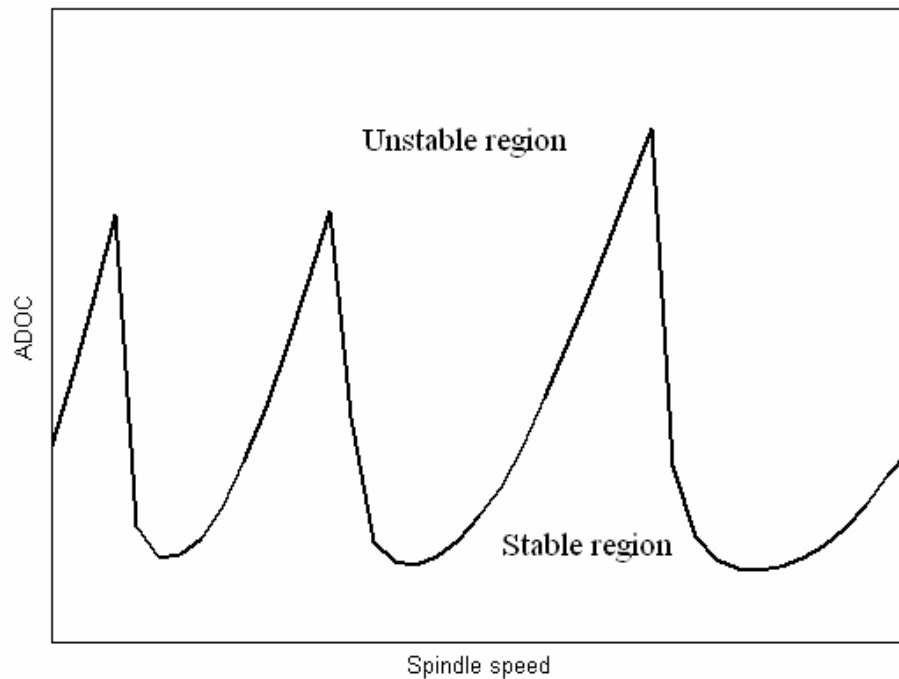


Figure 1.3: Stability chart of a milling process.

Since high speed milling can be beneficial to manufacturing industries through higher productivity, better finished surface, and longer tool life, it has received increased attention and it is becoming one of the most preferred and efficient cutting processes. There is no absolute criterion for using the qualifier “high speed” in milling, and it is a relative term based on the milling system, material properties of the workpiece, *etc.* Some sources relate the definition of high speed to system dynamics that depend on the natural frequency of the dominant mode of vibration (Smith and Tlusty, 1997), while others define it as any speed greater than 8,000 *rpm*. One of the features of high speed milling is low-immersion rate. During a low-immersion milling operation, there is loss of contact between the tool and the workpiece. At certain spindle speeds, one can achieve a substantial increase in stability limits (higher axial depths of cut in milling operations), which can be used to realize higher material removal rates by changing the feed direction. A good knowledge of milling dynamics is important and this knowledge can enable the selection of machining parameters such as spindle speed, axial depth of cut, and feed direction to achieve optimized operation planning.

Based on the above discussion, it can be discerned that studies on the dynamics of milling processes are very important for the modern manufacturing industry to improve quality and productivity. In the following section, a review of research on milling processes and related nonsmooth dynamics is presented and the current work is also outlined.

1.2. Review of Research on Dynamics of Milling Processes

1.2.1. Cutting force model

The cutting force is dependent on the following aspects: 1) cutter geometry, 2) workpiece geometry, 3) cutting conditions, 4) workpiece material properties, and 5) relative displacement between the workpiece and the tool.

In the literature, various models have been proposed to model the cutting forces as a function of the cutting parameters, such as the depth of cut and the dynamic uncut chip thickness [Taylor (1907), Kuster and Gygax (1990), and Endres, DeVor, and Kapoor (1995)]. Atlintas (2000) and Balachandran and Zhao (2000), used a linear cutting force model, where the cutting force is a linear function of the dynamic uncut chip thickness. It should be noted that Balachandran and Zhao (2000) considered loss of contact effects within their model. Stépán (1998, 2001) presented a nonlinear cutting force model, where the cutting force is a nonlinear function of the dynamic uncut chip thickness.

1.2.2. Milling system models

The milling process is a multi-point interrupted cutting process. The spindle speed and immersion rate determine the rate at which each cutting tooth enters and exits the workpiece. The whole cutting process can be regarded as a sequence of single point cutting operations with varying chip thickness values. This causes the coefficients in the system equations to be periodic in nature as opposed to the constant coefficients

present in the case of a turning process. In the early efforts to investigate milling processes, Martelotti (1941, 1945) pointed out that the true path of the cutter flute path is trochoidal. One can approximate this trochoidal path by a circular path when the feed rate is much smaller than the radius of the cutter tooth. In practical milling operations, this assumption is usually satisfied and this assumption simplifies the process analysis. Sridhar, Hohn, and Long (1968) developed a comprehensive milling simulation model for cutting operations with a straight tooth cutter. The chip thickness, in terms of the time delay effect, is time varying and it is determined by the displacements of the current state and the displacement of the state immediately preceding it. In this model, the loss of contact is ignored by assuming that each tooth is in contact with the workpiece over a constant time interval and that the workpiece is always engaged by the cutter. In addition, based on the above assumption, the feed-rate effects on the time delay are also ignored. This results in a constant time delay for constant spindle speed milling operations. Since the time delay plays a key role in regenerative chatter, it is necessary to investigate the feed-rate effects on the time delay. Considering the feed-rate effects on time delay and loss of contact effects, Balachandran (2001), Balachandran and Zhao (2000), Zhao and Balachandran (2001), and Balachandran and Gilsinn (2005) pointed out that the time delay along the X-direction is different from the time delay along the Y-direction, and they presented a nonlinear, non-homogeneous, and non-autonomous delay differential system with periodic coefficients and two time delays. Considering the effect of vibrations on the delay, Insperger and Stépán (2005) presented a model with a state dependent regenerative delay. As presented in Long and Balachandran (2004) and Long,

Balachandran, and Mann (2006), and also in the second chapter, the feed-rate effects on the time delay can lead to a state dependent delay. A new formulation is presented in these efforts and the second chapter of this dissertation.

The research efforts of Inamura and Sata (1974), Takemura, Hoshi, and Okushima (1974), and Sexton, Milne, and Stone (1977) showed that the continuous variation of the cutting speed could help suppress the chatter that normally develops during conventional, constant speed machining. Spindle speed variation is attracting increasing attention. Lin, DeVor, and Kapoor (1990) and Radulescu, Kapoor, and DeVor (1997a,b) pointed out that varying spindle speed machining can lead to a reduction in the amplitude of vibrations. They also showed that the stability of a workpiece-tool system was robust with respect to variations in the workpiece-tool system modal parameters by comparing the stability charts obtained for VSS machining with those obtained for CSS machining. Canniere, Brussel, and Bogaert (1981), Radulescu, Kapoor, and Devor (1997a, b), Insperger, Stépán, and Namachchivaya (2001), Sastry, Kapoor, and Devor (2002), and Namachchivaya and Beddini (2003) investigated sinusoidal spindle speed variation, a method to vary the spindle speed continuously around a nominal value, for suppressing chatter. Yilmaz, Al-Regib, and Ni (2002) presented random spindle speed variation for suppressing machine tool chatter during milling processes. Long and Balachandran (2005b) discussed the advantages of VSS machining by comparing the stability charts obtained for VSS milling processes with those of obtained for CSS milling processes. The dynamics of both sinusoidal spindle speed variation milling processes and random spindle speed variation milling processes are described by a set of delay

differential equations with time-periodic coefficients and a time varying delay. A time varying delay causes the stability analysis to be complicated. When the spindle speed is varied, the mechanism that causes the suppression of is not clear. At the same time, the time varying delay in a model of a VSS milling process can not be expressed as an explicit function of time. In general, an approximate solution for the delay is used. Efforts towards this end are presented later in this dissertation.

1.2.3. Dynamics and stability issues

As in self-excited systems (e.g., Nayfeh and Mook, 1979), there are regenerative effects in a milling process. This regenerative effect is in the form of a time-delay effect in the governing equations, and the physical basis for this effect is the cutting forces in the workpiece-tool system. In the context of milling processes, considerable research on chatter due to this time-delay effect has been carried out [Tlusty and Polacek (1963), Tobias (1965), Opitz, Dregger, and Roese (1966), Sridhar, Hohn, and Long (1968), Hanna and Tobias (1974), Minis and Yanushevsky (1993), Altintas and Budak (1995), Balachandran (2001), Faassen, van de Wouw, Oosterling and Nijmeijer, (2003)]. The mode coupling effect, which is present only in systems with multiple degrees of freedom, is due to the fact that the system mass vibrates simultaneously along different degrees of freedom with different amplitudes and different phases. This results in an elliptical motion of the tool. Some research on the effect of mode coupling has been carried out [Tlusty and Polacek (1963) and Gasparetto (2001)]. Aside from the regenerative effects and mode coupling effects, loss of contact is also a mechanism that leads to chatter [Davies and

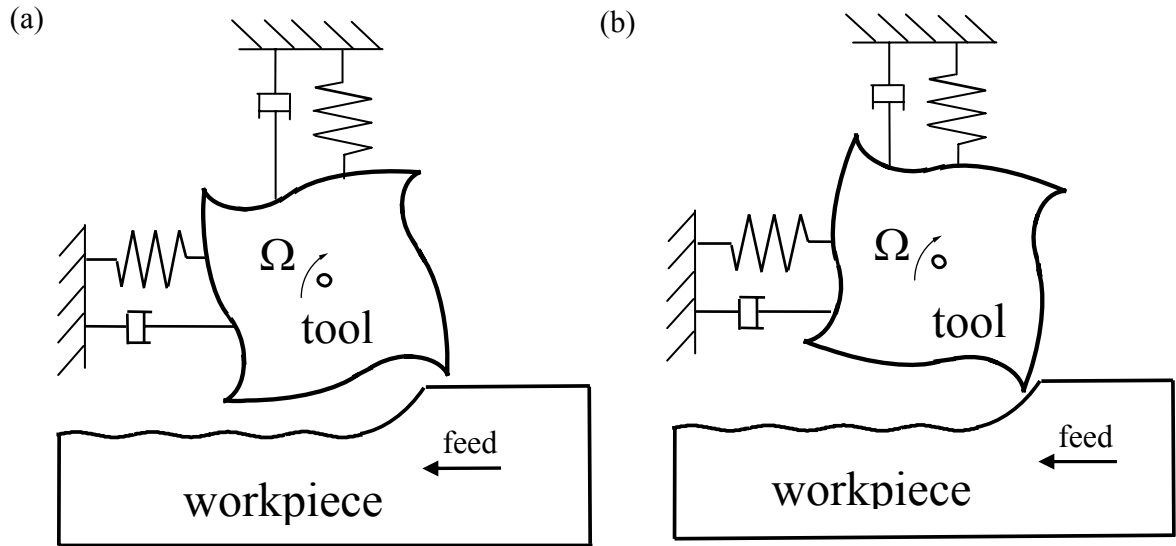


Figure 1.4: Illustration of loss of contact between tool and workpiece.

Balachandran (2000) and Balachandran (2001)]. During a milling operation, there are two types of loss of contact between the workpiece and tool. As shown in Figure 1.4a, one is due to all the teeth of the cutting tool not being in the cutting zone. Another one is due the relative vibrations between the workpiece and tool that results in the tool jump out of the workpiece (Figure 1.4b). As discussed in the studies of Balachandran (2001), Balachandran and Zhao (2000), and Zhao and Balachandran (2001), in general, the governing system of equations of a milling process is a nonlinear, non-homogeneous, delay-differential system with time-periodic coefficients. Over the years, this system of equations has been approximated on a physical basis as well as a mathematical basis to determine the stability of motions of the workpiece-tool system. These approximations are to do with consideration of nonlinearities, time-periodic nature of the cutting-force coefficients, and the feed terms. For example, if one does not consider multiple regenerative effects, loss of contact dynamics, friction, structural nonlinearities, and other sources of nonlinearities, then, the resulting system

of equations is linear [Tlusty and Polacek (1963), Opitz, Dregger, and Roesse (1966), Sridhar, Hohn, and Long (1968), Minis and Yanushevsky (1993), Altintas and Budak (1995)]. Tlusty and Polacek (1963) presented a frequency-domain approach based on transfer functions between the system displacements and cutting forces to determine the instability due to the regenerative effect. In milling processes, the orientations of the cutting forces and chip thickness are explicit periodic functions of time. If the cutting forces are averaged over the period of contact time of each cutter with the workpiece, then the resulting system of delay-differential equations no longer has time-periodic coefficients but rather constant coefficients. This type of averaging was carried out in the work of Opitz et al. (1966) who examined the stability of a face milling process and also in the work of Altintas and Budak (1995).

Prior to the stability analysis, Sridhar et al. (1968) dropped the feed terms from their model and then studied the stability of the zero solution of the resulting linear, homogeneous delay-differential system with periodic coefficients. Hahn (1961) presented an extension of Floquet's theorem for delay-differential equations with periodic coefficients. This provided a basis for the work of Sridhar et al. who numerically computed the fundamental matrix and the eigenvalues of this matrix. In the study of Minis and Yanushevsky (1993), as in previous studies [Sridhar et al. (1968) and Altintas and Budak (1995)], milling operations with straight fluted cutters are considered. They used Floquet theory to determine the stability of the zero solution of a linear, homogeneous delay-differential system. The periodic terms were expanded by using a Fourier expansion with the basic frequency defined by the spindle speed. The Hill's determinant (Nayfeh and Mook, 1979) was obtained and

zeroth-order and first-order truncations of the resulting characteristic equation were used to produce the stability charts in the space of spindle speed and depth of cut.

In the work of Hanna and Tobias (1974), face milling processes were considered and they were modeled with structural nonlinearities and cutting force nonlinearities. Quadratic and cubic nonlinearities were included in a delay-differential system with constant coefficients, and the stability of the zero solution of this system was studied. Unlike the model used by Hanna and Tobias (1965), the models used by Sridhar et al. (1968), Minis and Yanushevsky (1993), and Altintas and Budak (1995) are linear. While these linear models are useful for predicting the onset of chatter, they are not suited for understanding the nature of the instability as well as post instability motions. In the work of Balachandran and Zhao (2000) and Zhao and Balachandran (2001), loss of contact nonlinearities and feed-rate effects are considered. They pointed out that linear models can provide quite accurate stability predictions for high-immersion milling operations but inaccurate stability predictions for low-immersion operations. The stability of these operations represented in the space of spindle speed and depth of cut can be constructed through time-domain simulations of this nonlinear system. However, for determining the type of instability of the periodic motion of this nonlinear, non-homogeneous, non-autonomous, delay-differential system, numerical schemes with an analytical basis are required. In the present work, the semi-discretization method [Insperger and Stépán (2001, 2002)] has been improved to examine the stability of periodic solutions of systems with two time delays [Long and Balachandran (2006)] and systems with variable time delay [Long and Balachandran (2004) and Long Balachandran, and Mann (2006)].

As discussed in the previous section, the governing system of equations of a VSS milling process is a nonlinear, non-homogeneous, delay-differential system with time-periodic coefficients and a time varying delay. Lin *et al.* (1990), Altintas and Chan (1992), and Radulescu *et al.* (1997a,b) investigated the stability of VSS milling through time-domain simulations. These simulations are time consuming, and numerical schemes with an analytical basis can provide faster and more reliable stability prediction schemes. Tsao, McCarthy, and Kapoor (1993) used the angular position as an independent variable instead of time, and a full discretization scheme is used to analyze the stability of the resulting system. Sastry, Kapoor, DeVor, and Dullerud (2001) analyzed the stability of milling processes with sinusoidal spindle speed variation directly by using the full discretization scheme. Yilmaz, Al-Regib, and Ni (2001) also used the full discretization scheme to analyze the stability of a milling process with a random spindle speed variation. Sastry, Kapoor, and DeVor (2002) presented the Floquet theory based approach for stability analysis of a variable spindle speed face-milling process.

1.3. Nonsmooth Dynamics

Due to the loss of contact between the workpiece and tool, the cutting force shown in the right-hand side of governing equation of motion of milling processes are piecewise functions of time and uncut chip thickness, which are determined by the relative displacement of the current and previous state. A system with piecewise smooth right-hand side is an example of a nonsmooth system. In nonsmooth systems, there are many bifurcations that occur, which are different from the conventional bifurcations that occur in a smooth system. Following the work of Feigin (1970, 1974,

1995) on C-bifurcations in maps, many efforts have followed on bifurcations of solutions of nonsmooth maps [Lamba and Budd (1994), Nusse, Ott, and Yorke (1994), Banerjee and Grebogi (1999), Galvanetto (2001, 2004), Bernardo, Budd and Champneys (2001a,b), Zhusubaliyev and Mosekilde (2004)] and nonsmooth continuous-time systems [Leine (2000), Leine and van Campen (2002)]. Leine (2000) and Leine and van Campen (2002) have discussed some characteristics of discontinuous bifurcations by comparing them with the corresponding continuous bifurcations and they have examined bifurcations of periodic solutions in tri-linear spring systems and stick-slip systems.

As pointed out by Davis and Balachandran (2000), Balachandran (2001), and Stépán, Szalai, Mann, Bayly, Insperger, Gradišek, and Govekar (2005), milling processes with low-immersion operation can be investigated by using impact like models. The dynamics of mechanical systems with impacts has been extensively studied over the last several decades [Popp, Oestreich, and Hinrichs (1997), and Peterka, Kotera, and Čipera (2001)]. Pfeiffer and Glocker (1996) discussed the contact conditions and the use of Newton's impact law and Possion's impact law in detail. Following the work of Moon and Holmes (1979) with an elastic beam, Shaw (1985) and Fang and Wickert (1994) considered the dynamics of a vibro-impact cantilever beam modeled as a single-degree-of-freedom system. Wagg and Bishop (2002) discussed multiple mode effects in the impact dynamics of an elastic beam. Balachandran (2003) studied the dynamics of a system with cubic and loss of contact nonlinearities.

A special situation arises when an impact with a zero velocity occurs, namely, grazing impacts. Nordmark (1991) presented a discrete map to describe the dynamics of

grazing impacts. His results show that a special type of bifurcation occurs, when a stable periodic orbit undergoes a grazing impact as a scalar control parameter is varied. Stensson and Nordmark (1994) investigated the effects of low velocity impacts through experiments and numerical efforts. Although analytical and numerical results on grazing impacts and post-grazing phenomena have been extensively reported, experimental results have been less reported. The widespread presence of impact systems has motivated recent investigations into possible strategies for control of bifurcations and chaos in these systems. Casas and Grebogi (1997) used the OGY (Ott, Grebogi, and Yorke, 1990) method for controlling chaotic impacts. Control of grazing bifurcations in impacted elastic structural systems has not received much attention. As following with Long and Balachandran (2005a), experimental and numerical results are presented in this dissertation.

1.4. Current Research

1.4.1. Research objectives

The current investigation is motivated by an interest in improving the machining performance of milling processes. A fundamental understanding of the dynamics and stability of milling processes is sought and this understanding is to be used to optimize the control parameters and operations so that the productivity can be increased.

From the discussion of the previous sections, it is clear that the former models those were used to describe the dynamics of milling processes were simplified by ignoring the effects of feed motion on the time delay. The important, once of feed-rate effects

on the stability of milling processes has been less addressed. Linear regenerative theory can only be applied with reasonable accuracy to full-immersion CSS milling operations but not to partial-immersion CSS milling operations. It can not be applied to VSS milling operations either. Time-domain simulations can be used to study any milling operation. However, this approach is computationally expensive. A highly efficient method needs to be developed to examine the stability of wide range of milling processes. Loss of contact plays a key role in the low-immersion operation. This effects result in the system with a nonsmooth right-hand side. The characteristics of nonsmooth dynamics of a milling process has also received little attention.

To address these issues, the dissertation efforts have been carried out with the following specific objectives:

1. Develop a nonlinear, non-autonomous delay differential system model with time-periodic coefficients and a variable time delay for milling processes, where feed-rate effects can be important and validate this model by using experimental data and numerical results.
2. Extend the semi-discretization method for the stability analysis of periodic motions of nonlinear, non-autonomous delay differential system with time-periodic coefficients and either two discrete time delays or a time varying delay.
3. Investigate the stability and dynamics of the variable spindle speed milling process whose dynamics are described by a set of delay differential equations with time-periodic coefficients and a time varying delay.
4. Carry out experimental and numerical investigation with a nonsmooth mechanical

system and explore the bifurcations in this system.

1.4.2. Organization of dissertation

The rest of this work is organized as follows. In the next chapter, the development of system model is described and the model with two-time delays is revisited briefly. In Chapter 3, stability analyses of periodic solution are discussed and the semi-discretization method is presented. Numerical results obtained by using the semi-discretization for a system with two-time delays and a system with a variable time delay are presented. In the fourth chapter, investigations into the dynamics of variable spindle speed milling are carried out and the benefits of VSS milling are discussed. In the fifth chapter, the nonsmooth characteristics of a milling process are pointed out. The dynamics of an elastic beam subjected to repeat impact, which is similar to a simplified model of the milling process, is investigated by the means of experiments and simulations. In the last chapter, concluding remarks are presented and the contributions of this dissertation are highlighted along with an outline of the recommendations for future work. Appendices are also included to provide details of some coefficients that arise in the impact dynamics studies and the programs used in this dissertation. References are included at the end of the dissertation.

Chapter 2

Model of Workpiece-Tool System

Based on the assumption that the feed rate is much smaller than the radius of tool, in previous work, the governing equations of motion of constant spindle speed milling system with one constant time delay have been obtained [Minis and Yanushevsky (1993), Altintas and Budak (1995), Stépán et al. (2003), and Insperger et al. (2003a,b)]. Balachandran and Zhao (2000) and Zhao and Balachandran (2001) pointed out that the time delay along the X-direction is different from the delay along the Y-direction if the feed rate is considered.

Here, a new formulation for analyzing the dynamics and stability of end milling operations will be presented. In this formulation, consideration of the feed-rate effects leads to a non-autonomous delay-differential system with a variable time delay. The development of this formulation is described.

2.1. Feed Motion Effect on Time Delay

In Figure 2.1, the tooth paths of milling operation with two teeth are shown. Based on different assumptions on the motion of tool center such as the tool center is vibrating, feed motion without vibration, or quasi-static motion, three different tooth paths can be obtained as shown in Figures 2.1(a), 2.1(b), and 2.1(c). In Figure 2.1(a), the length \overline{AB} is the uncut chip thickness, and in Figures 2.1(b) and 2.1(c), this length is the static uncut chip thickness. The tool path shown in Figure 2.1(a) is dependent on the state variables used to describe the vibrations of the workpiece-tool system and the

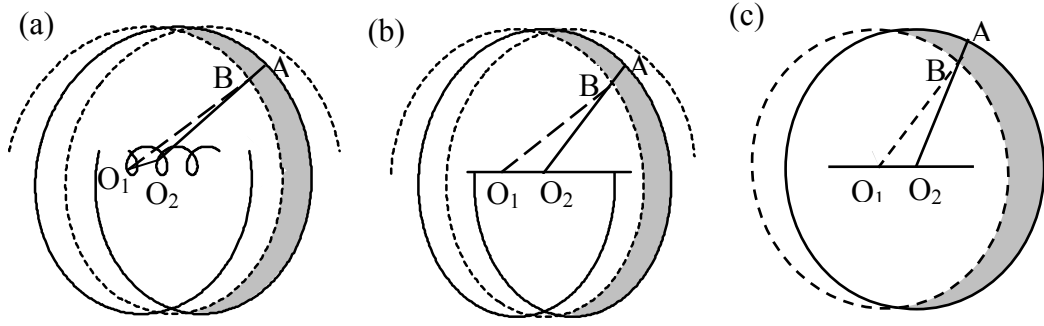


Figure 2.1: Tooth path of milling operation with two teeth: (a) system vibration dependent tooth path, (b) system vibration independent tooth path, and (c) quasi-static tooth path. The dashed and solid lines represent the paths of tooth 1 and tooth 2, respectively. O_1 is the position of tool center when the tooth 1 cuts the workpiece at point B and O_2 is the position of tool center when the tooth 2 cuts the workpiece at point A.

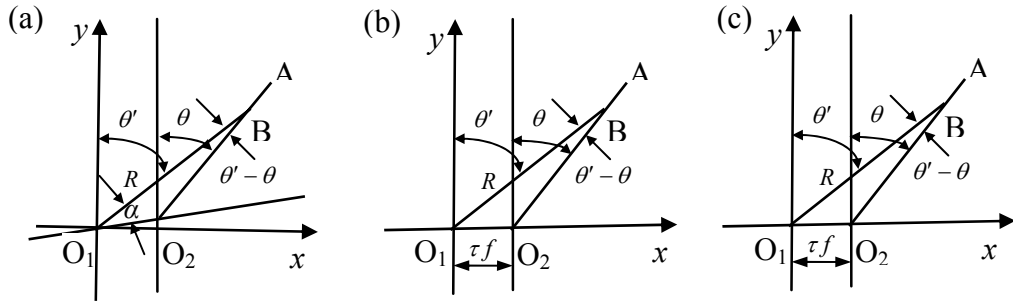


Figure 2.2: Illustrations of geometric relationships for the three cases of Figure 2.1. θ' is the angular position of the first tooth, θ is the angular position of the second tooth, f is the feed speed, and τ is the time delay. The relationships are identical in cases (b) and (c).

tooth paths shown in Figures 2.1(b) and 2.1(c) are independent of these vibratory states. In Figure 2.2, the geometric relationships among the rotation angle, time delay, feed distance and uncut chip thickness are illustrated for the three cases of Figure 2.1.

Considering the vibration of tool center, referring to Figure 2.2(a), one can obtain the

following relations:

$$\frac{\overline{o_1 o_2}}{\sin(\theta' - \theta)} = \frac{R}{\sin(\pi - \theta' + \theta - \alpha)} = \frac{R - \overline{AB}}{\sin \alpha} \quad (2.1)$$

$$\overline{o_1 o_2} = \sqrt{(x(t) - x(t - \tau) + f\tau)^2 + (y(t) - y(t - \tau))^2} \quad (2.2)$$

$$\alpha = \frac{\pi}{2} - \theta' - a \tan \left(\frac{y(t) - y(t - \tau)}{x(t) - x(t - \tau) + f\tau} \right) \quad (2.3)$$

From these three equations, one can discern that the time delay τ depends on the state variables $x(t)$, $y(t)$, $x(t - \tau)$, and $y(t - \tau)$ and that it is state dependent. In most of the previous research efforts, a circular tooth path is used to approximate the trochoidal tooth path and θ' is assumed to be equal to θ . Based on this, the time delay is found to be a constant for a constant spindle speed milling process and of the form

$$\tau_0 = \frac{2\pi}{N\Omega} \quad (2.4)$$

where N is the number of tooth and Ω is the spindle speed in rad/second.

In Figure 2.2(b), an ideal situation is illustrated and in this situation, the vibration between work piece and tool can be ignored. Then, equations (2.2) and (2.3) can be simplified to

$$\overline{o_1 o_2} = \tau f \quad (2.5)$$

$$\alpha = \frac{\pi}{2} - \theta' \quad (2.6)$$

Then, from equations (2.1), (2.5) and (2.6), it follows that

$$\frac{\tau f}{\sin(\theta' - \theta)} = \frac{R}{\sin(\frac{\pi}{2} + \theta)} = \frac{R - \overline{AB}}{\cos \theta'} \quad (2.7)$$

Furthermore, in practical milling operations, since τf is usually much smaller than R , one can obtain

$$\sin(\theta' - \theta) \approx \theta' - \theta \quad (2.8)$$

From the definition of time delay, it follows that

$$\tau = t - t' = \frac{2\pi}{N\Omega} + \frac{\theta - \theta'}{\Omega} \quad (2.9)$$

where t' is the time at which the immediate previous cutter tooth arrives at the angular position θ' and t is the time when the current cutter tooth arrives at the angular position θ . After combining equations (2.7)-(2.9), one can obtain

$$\tau(\theta) = \frac{2\pi R}{N(\Omega R + f \cos \theta)} \quad (2.10)$$

The delay given by equation (2.10) is referred to as the variable time delay. Since the relationships shown in Figure 2.2(c) are identical to those shown in Figure 2.2(b), one can also get the same expression as equation (2.10) for the time delay associated with the quasi-static tool path case. In Figure 2.3, the normalized time delays are shown for different feed rates. For a given tool radius, the difference between the variable delay and the constant delay increases along with the increase of the feed rate.

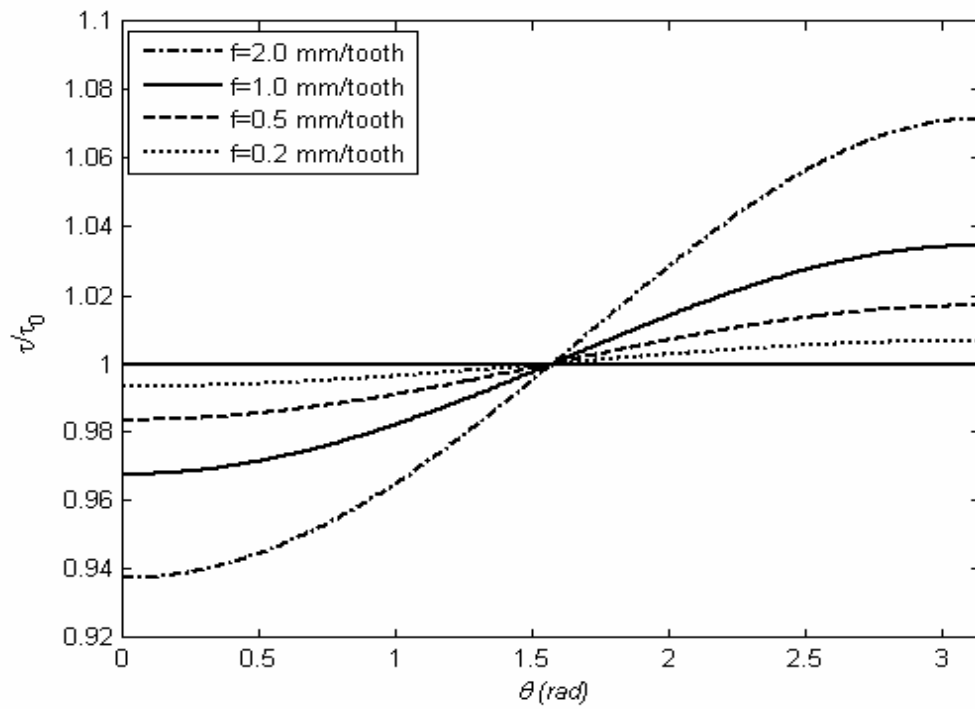


Figure 2.3: Variable time delays for $\Omega=5000$ rpm, $R=9.53$ mm, and $N=2$.

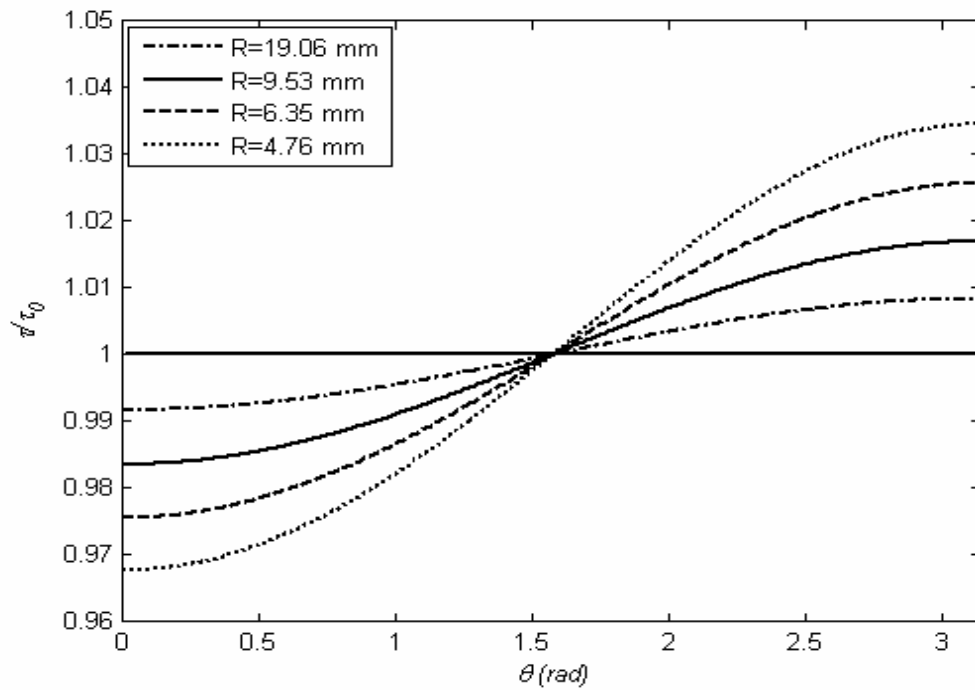


Figure 2.4: Variable time delays for $\Omega=5000$ rpm, $f=0.5$ mm/tooth, and $N=2$.

When $f=2.00$ mm/tooth, the maximum difference between variable time delay and constant time delay is up to 7% and when $f=0.2$ mm/tooth and maximum difference is less than 1%. For the given radius of tool, the difference between variable delay and constant delay increases with increase in the feed rate. In Figure 2.4, the normalized delays are shown for different tool radius and the same feed rate. In this figure, the feed-rate effects on time delay is largest when the radius $R=4.76$ mm and smallest when the radius $R=19.06$ mm. The effects of feed rate on time delay decrease with the increase of the radius of the tool.

It is mentioned that unlike in the previous models, the inclusion of feed rate allows for a trochoidal tool path without the oscillatory dynamics. Also, that along with the work reported in references (Long and Balachandran, 2004), this is the first time that it has been pointed out that a variable time delay can occur in the model of a constant, spindle speed milling process.

2.2. Feed Motion Effect on the Static Cutting Entry Angle and Exit Angle

The feed rate not only influences the time delay, but also influences the cutting entry angle and exit angle. Refer to Figure 2.5, one has

$$\Delta\theta \approx \sin \Delta\theta = \frac{\tau f}{2R} \quad (2.11)$$

where $\Delta\theta$ is the angle through which one either advances the cutting entry angle for up-milling or delays the exit angle for down-milling due to feed motion. It is

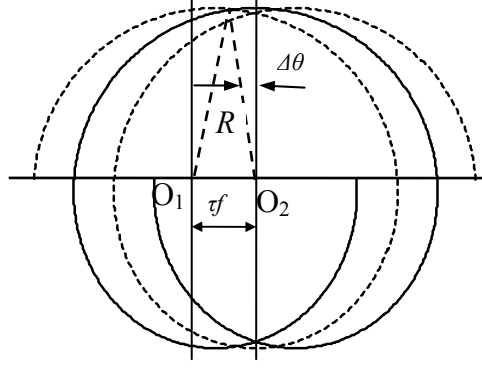


Figure 2.5: Schematic diagram for cutting entry angle and exit angle.

remarked that Balachandran and Zhao (2001) got the following expression based on a quasi-static tooth path:

$$\Delta\theta \approx \sin \Delta\theta = \frac{\tau_1 f}{2R} \quad (2.12)$$

In equation (2.12), the delay τ_1 along x-direction is a constant. By contrast, in equation (2.11), the delay τ is not a constant.

2.3. Feed Motion Effect on the Static Uncut Chip Thickness

From equation (2.7), referring to Figure 2.2b, one can obtain the static uncut chip thickness as follows

$$h_{sv} = \overline{AB} = R - \frac{R \cos \theta'}{\cos \theta} \quad (2.13)$$

By using Taylor series expansion, it can be determined that

$$\cos \theta' = \cos \theta - (\theta' - \theta) \sin \theta - \frac{1}{2} \cos \theta [(\theta' - \theta)^2] + O[(\theta' - \theta)^3] \quad (2.14)$$

Combining equations (2.9-2.10), (2.13), and (2.14), one can find that

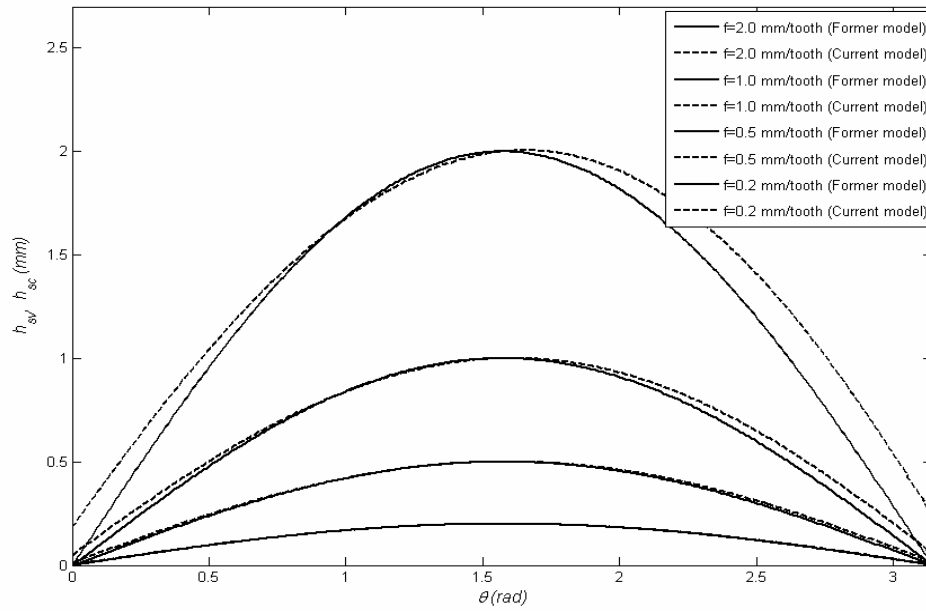


Figure 2.6: Static uncut chip thickness for $R=9.53$ mm and $N=2$.

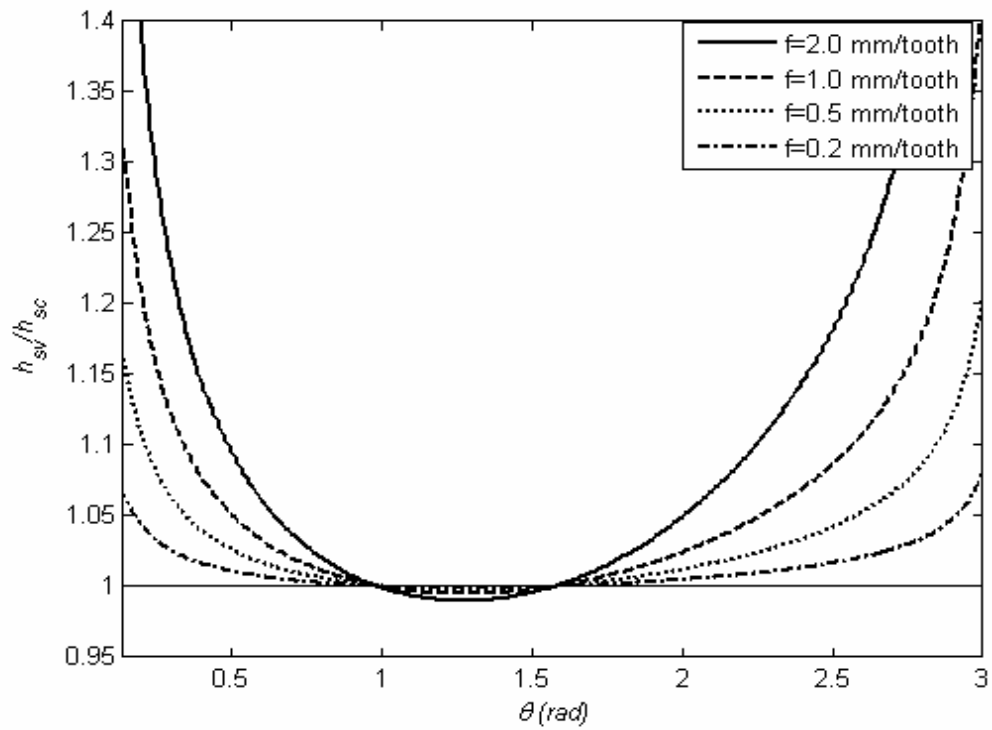


Figure 2.7: Normalized static uncut chip thickness for $R=9.53$ mm and $N=2$.

$$h_{sv} = \tau f \sin \theta + \frac{1}{2} R (\theta' - \theta)^2 = \tau f \sin \theta + \frac{1}{2} R \left(\tau \Omega - \frac{2\pi}{N} \right)^2 \quad (2.15)$$

Substituting equation (2.10) into (2.15), one can obtain

$$h_{sv} = \tau f \sin \theta + \frac{1}{2R} (\tau f \cos \theta)^2 \quad (2.16)$$

The static uncut chip thicknesses for different feed rate are presented in Figure 2.6. In this figure, the dashed curve representing, h_{sv} , is the static uncut chip thickness in current model which is obtained by using equation (2.16), and the solid curve representing, h_{sc} , is the static uncut chip thickness in the former model determined by equation (2.18). When the feed rate is small such as $f=0.2$ mm/tooth, the difference between h_{sv} and h_{sc} is very “small” in the angular range. However, the difference between h_{sv} and h_{sc} increases with the increase of feed rate. In Figure 2.7, the normalized chip thicknesses are presented for different feed rate. The deviation of h_{sv} from h_{sc} is obvious for the angular position $\theta \approx 0$ and $\theta \approx \pi$, where h_{sc} is very small. The deviation of h_{sv} from h_{sc} is small, when the angular position $\theta \approx 0.5\pi$. If one remains the first order term of $(\theta' - \theta)$ and ignores the higher order term in equation (2.14), then the result is

$$h_{sv} \approx \tau f \sin \theta \quad (2.17)$$

This formula is similar to the one that was used in former model, where

$$h_{sc} = \tau_0 f \sin \theta \quad (2.18)$$

2.4. Feed Motion Effect on the Amplitude of Feed Mark Wave

In Figure 2.8, the diagram for feed marks is shown, and here, h_s is the amplitude of feed mark wave. It is of the form

$$h_s = R - \sqrt{R^2 - \left(\frac{\tau f}{2}\right)^2} \quad (2.19)$$

For an up-milling operation,

$$\theta'_s = -\Delta\theta \square 1 \quad (2.20)$$

Then, from equation (2.10), it follows that

$$\tau = \frac{2\pi R}{N(\Omega R + f \cos \Delta\theta)} \approx \frac{2\pi R}{N(\Omega R + f)} \quad (2.21)$$

After substituting equation (2.21) into (2.19), one can obtain

$$h_s = R \left[1 - \sqrt{1 - \left(\frac{\pi f}{N(\Omega R + f)}\right)^2} \right] \approx \frac{R}{2} \left(\frac{\pi f}{N(\Omega R + f)}\right)^2 \quad (2.22)$$

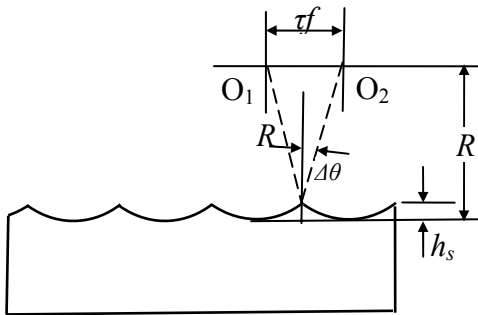


Figure 2.8: Schematic diagram for feed marks on the workpiece.

Considering an up-milling operation for one of the cases of Figure 2.3 with $f = 1.0$ mm/tooth, $R = 9.53$ mm, $N = 2$, and a spindle speed of 5000 rpm, the amplitude of feed-mark wave obtained from equation (2.22) is $h_s = 0.0123$ mm. This matches the result obtained on the basis of the expression given by Martellotti (1941); that is

$$h_s = \frac{(\pi f)^2}{2N^2\Omega(\Omega R + 2f)} = 0.0123\text{mm} \quad (2.23)$$

For a down-milling operation,

$$\theta'_e = \pi + \Delta\theta \quad (2.24)$$

Then, from equation (2.10), it follows that

$$\tau = \frac{2\pi R}{N(\Omega R - f \cos \Delta\theta)} \approx \frac{2\pi R}{N(\Omega R - f)} \quad (2.25)$$

After substituting equation (2.25) into equation (2.19), one can obtain

$$h_s = R \left[1 - \sqrt{1 - \left(\frac{\pi f}{N(\Omega R - f)} \right)^2} \right] \approx \frac{R}{2} \left(\frac{\pi f}{N(\Omega R - f)} \right)^2 \quad (2.26)$$

Now, considering a down-milling operation for one of the cases of Figure 2.3 with $f = 1.0$ mm/tooth, $R = 9.53$ mm, $N = 2$, and a spindle speed of 5000 rpm, the amplitude of feed-mark wave obtained from equation (2.26) is $h_s = 0.014$ mm. This matches the result obtained on the basis of the expression given by Martellotti (1945); that is

$$h_s = \frac{(\pi f)^2}{2N^2\Omega(\Omega R - 2f)} = 0.0141\text{mm} \quad (2.27)$$

For the given machining parameter values, the amplitudes of the feed-mark waves are different for the up-milling and down-milling operations. A flatter arc of trochoid is obtained in an up-milling operation compared to that obtained in a down-milling operation. If the machining operation is stable, then this would mean a better finished surface during an up-milling operation.

2.5. Modeling of Milling Process System

In Figure 2.9, a multi-degree-of-freedom configuration representative of a workpiece-tool system is illustrated for milling operations with a cylindrical end mill. The top configuration is for an up-milling operation, and the bottom one is for a down-milling operation. The cutting tool has a radius R , N flutes, and a helix angle η . For convenience, the X-direction is oriented along the feed direction of cutter. The vertical axis of the tool is oriented along the Z-direction. The spindle rotational speed in rad/second is represented by Ω and the angular position is represented by θ . The quantities θ'_s and θ'_e represent the entry cutting angle and exit cutting angle, respectively, and these angles define the static cutting zone. The forces F_x and F_y act on the cutter, and the forces F_u and F_v act on the workpiece. The resonance frequencies associated with the torsion modes and the Z-direction vibration modes are expected to be higher than those associated with the primary bending vibration modes along the X-direction and the Y-direction. For this reason, only the vibration modes in the horizontal plane are considered in the models presented in these systems. In developing these models, the modal properties of the tool and the workpiece are

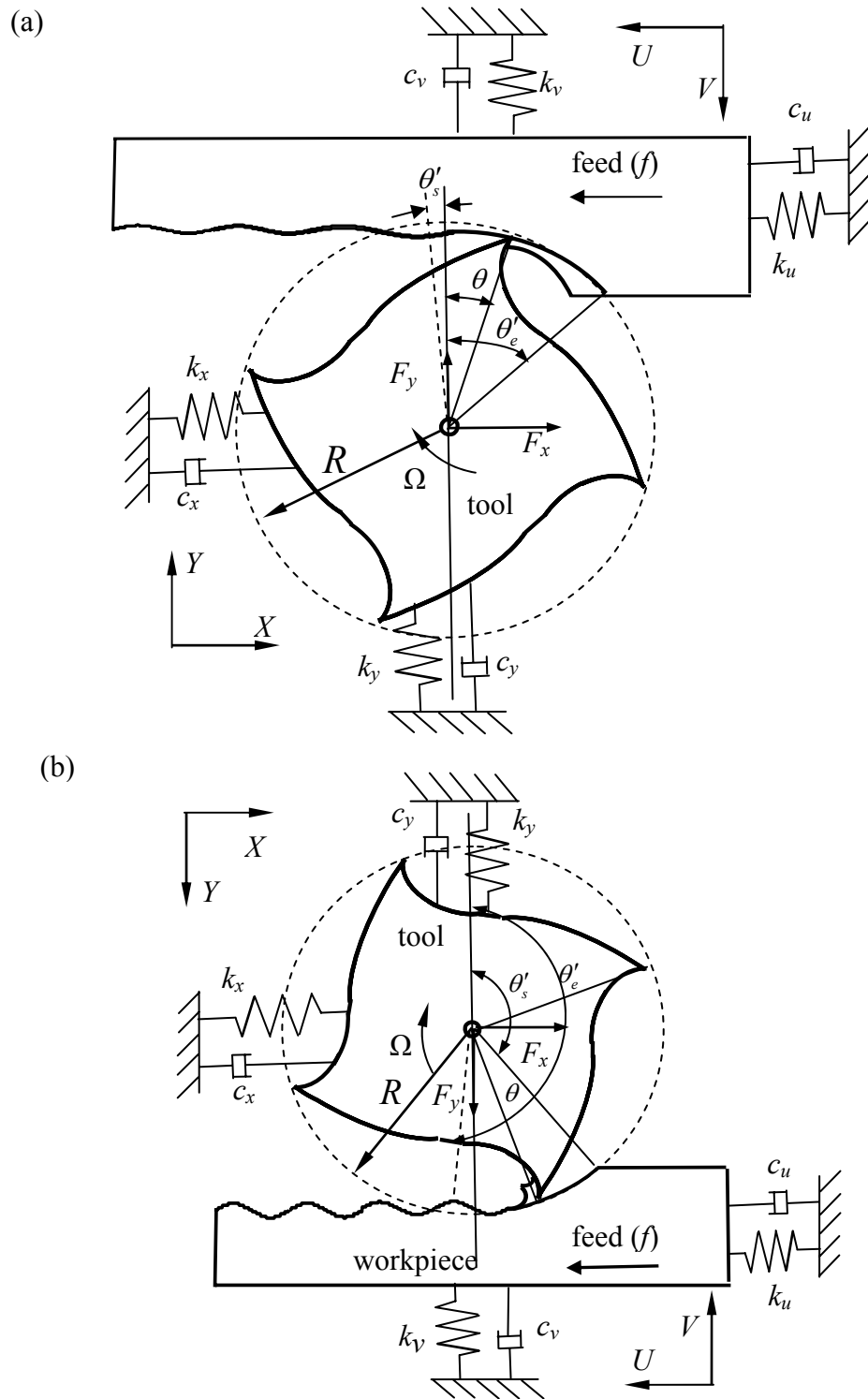


Figure 2.9: Workpiece-Tool system model: (a) up-milling operation and (b) down-milling operation.

assumed to be determined through experimental modal analysis and/or finite-element analyses. Thus, a system with a flexible tool and a flexible workpiece can be represented by an equivalent lumped parameter system. The governing equations are of the form

$$\left. \begin{aligned} m_x \ddot{q}_x + c_x \dot{q}_x + k_x q_x &= F_x(t; \tau(t, i, z)) \\ m_y \ddot{q}_y + c_y \dot{q}_y + k_y q_y &= F_y(t; \tau(t, i, z)) \\ m_u \ddot{q}_u + c_u \dot{q}_u + k_u q_u &= F_u(t; \tau(t, i, z)) \\ m_v \ddot{q}_v + c_v \dot{q}_v + k_v q_v &= F_v(t; \tau(t, i, z)) \end{aligned} \right\} \quad (2.28)$$

where the tool has two degrees of freedom and the workpiece has two degrees of freedom. The variables q_x and q_y respectively represent the tool dynamic displacements measured along the X and the Y directions in a reference frame, whose origin is located on the tool center and shares the rigid-body translation of the tool due to a constant feed rate. The variables q_u and q_v represent the workpiece displacements measured respectively along the U and V directions in a fixed reference frame. The quantities m_x, m_y, m_u , and m_v are the modal masses, the quantities c_x, c_y, c_u , and c_v are the modal damping coefficients, and the quantities k_x, k_y, k_u , and k_v are the modal stiffness coefficients associated with motions along the X, Y, U, and V directions, respectively. The cutting-force components, which appear on the right-hand side of the equations, are time-periodic functions. Furthermore, the variable time delay $\tau(t, i, z)$ is introduced in the governing equations through the cutting-force components. As discussed later in this section, the variable time delay depends on the feed rate, the radius of tool, the spatial location along the Z-direction, and the

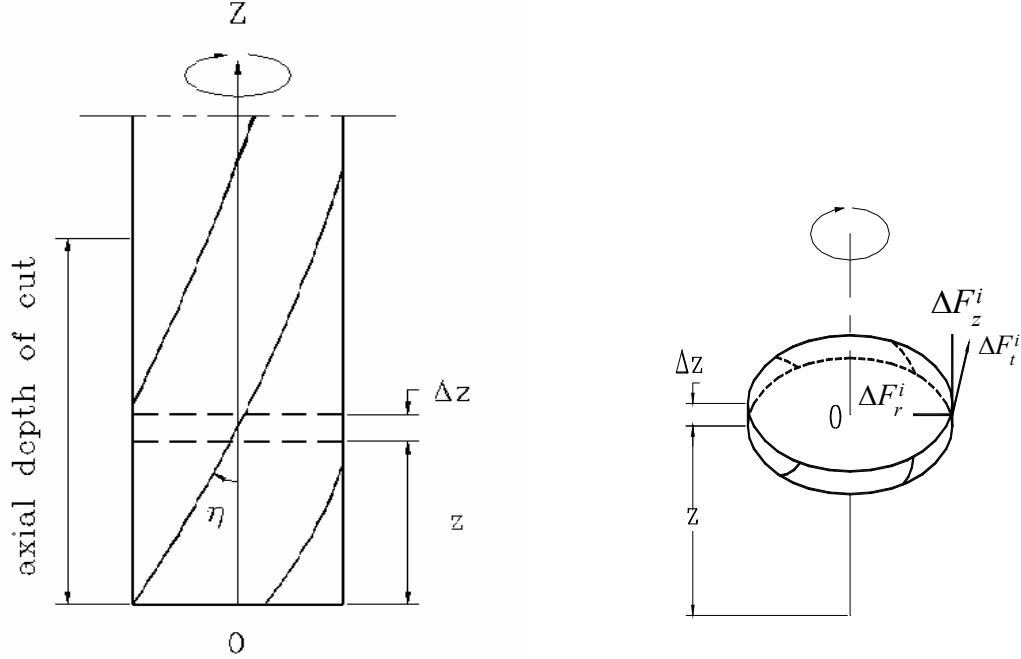


Figure 2.10: Cylindrical end mill with helical flutes and thin disk element.

spindle rotation speed. The dependence of the cutting forces on the system states is not explicitly shown in equations (2.28).

The cutter is modeled as a stack of infinitesimal disk elements. In Figure 2.10, a cylindrical end mill with helix flutes and one of the end mill elements located at an axial distance z along the tool where $0 \leq z_1(i, t) \leq z \leq z_2(i, t) \leq ADOC$ is shown. For the i th tooth, the cutting-force components associated with this disk element are represented by ΔF_r^i for the radial direction, ΔF_t^i for the tangential direction, and ΔF_z^i for the axial direction. To determine the cutting-force component along the radial direction, the dynamic uncut chip thickness for the i th flute of the cutter at time t and height z is determined from

$$h(t, i, z) = A(t, i, z) \sin \theta(t, i, z) + B(t, i, z) \cos \theta(t, i, z) + h_{sv} \quad (2.29)$$

where h_{sv} is given by equation (2.16) and the relative displacements are given by

$$\begin{aligned} A(t, i, z) &= q_x(t) - q_x(t - \tau(t, i, z)) + q_u(t) - q_u(t - \tau(t, i, z)) \\ B(t, i, z) &= q_y(t) - q_y(t - \tau(t, i, z)) + q_v(t) - q_v(t - \tau(t, i, z)) \end{aligned} \quad (2.30)$$

The variable $\theta(t, i, z)$, which is the angular position of tooth i at axial location z and time t , is determined by

$$\theta(t, i, z) = \Omega t - (i-1) \frac{2\pi}{N} - \frac{\tan \eta}{R} z + \theta_0 \quad (2.31)$$

For the infinitesimal disk element shown in Figure 2.10, the cutting forces take the form

$$\begin{Bmatrix} \Delta F_r^i \\ \Delta F_t^i \\ \Delta F_z^i \end{Bmatrix} = \begin{bmatrix} 1 & 0 & 0 \\ 0 & \cos \eta & \sin \eta \\ 0 & -\sin \eta & \cos \eta \end{bmatrix} \begin{bmatrix} k_t \\ k_n k_t \\ \mu k_t (\cos \varphi_n - k_n \sin \varphi_n) \end{bmatrix} \times h(t, i, z) \frac{\Delta z}{\cos \eta} \quad (2.32)$$

where k_t is the specific cutting energy, φ_n is the normal rake angle, k_n is a proportionality constant, and μ is the friction coefficient for the sliding motion between the inner surface of chip and the front rake face of the tooth respectively. They are related to the cutting geometry, the material properties, and the cutting conditions.

Transforming the cutting forces from the local cylinder coordinates to the global Cartesian coordinates, one can obtain

$$\begin{Bmatrix} \Delta F_x^i \\ \Delta F_y^i \\ \Delta F_z^i \end{Bmatrix} = \begin{bmatrix} -\sin \theta(t, i, z) & -\cos \theta(t, i, z) & 0 \\ -\cos \theta(t, i, z) & \sin \theta(t, i, z) & 0 \\ 0 & 0 & 1 \end{bmatrix} \begin{Bmatrix} \Delta F_r^i \\ \Delta F_t^i \\ \Delta F_z^i \end{Bmatrix} \quad (2.33)$$

On substituting equation (2.32) into equation (2.33), the cutting forces act on the thin disk element of every tooth are obtained in the following matrix form in terms of the dynamic uncut chip thickness h . Ignoring the forces along the Z-direction, one has

$$\begin{Bmatrix} \Delta F_x^i(t) \\ \Delta F_y^i(t) \end{Bmatrix} = \begin{bmatrix} \hat{k}_{11}^i(t, z) & \hat{k}_{12}^i(t, z) \\ \hat{k}_{21}^i(t, z) & \hat{k}_{22}^i(t, z) \end{bmatrix} \begin{Bmatrix} A(t, i, z) \\ B(t, i, z) \end{Bmatrix} + \begin{bmatrix} \hat{c}_1^i(t, z) \\ \hat{c}_2^i(t, z) \end{bmatrix} \left[\tau f \sin \theta(t, i, z) + \frac{1}{2R} (\tau f \cos \theta(t, i, z))^2 \right] \quad (2.34)$$

In equations (2.34), the time-periodic coefficient matrices are given by

$$\begin{bmatrix} \hat{k}_{11}^i(t, z) & \hat{k}_{12}^i(t, z) \\ \hat{k}_{21}^i(t, z) & \hat{k}_{22}^i(t, z) \end{bmatrix} = \begin{bmatrix} -\sin \theta(t, i, z) & -\cos \theta(t, i, z) \\ -\cos \theta(t, i, z) & \sin \theta(t, i, z) \end{bmatrix} \begin{bmatrix} k_1 k_t \\ k_2 k_t \end{bmatrix} \begin{bmatrix} -\sin \theta(t, i, z) & \cos \theta(t, i, z) \end{bmatrix} \quad (2.35)$$

$$\begin{bmatrix} \hat{c}_1^i(t, z) \\ \hat{c}_2^i(t, z) \end{bmatrix} = \begin{bmatrix} -\sin \theta(t, i, z) & -\cos \theta(t, i, z) \\ -\cos \theta(t, i, z) & \sin \theta(t, i, z) \end{bmatrix} \begin{bmatrix} k_1 k_t \\ k_2 k_t \end{bmatrix} \quad (2.36)$$

where

$$\begin{aligned} k_1 &= \frac{k_n}{\cos \eta} \\ k_2 &= 1 + \tan \eta [\mu (\cos \varphi_n - k_n \sin \varphi_n)] \end{aligned} \quad (2.37)$$

In the cutting zone $\theta_s^i < \theta(i, t, z) < \theta_e^i$, when the i th cutting tooth is in contact with workpiece, the corresponding cutting force components along the X-direction and the Y-direction can be derived by integrating equations (2.34) along the Z-direction; this

leads to

$$\begin{aligned} \begin{Bmatrix} F_x^i(t) \\ F_y^i(t) \end{Bmatrix} &= \int_{z_1(t,i)}^{z_2(t,i)} \begin{bmatrix} \hat{k}_{11}^i(t,z) & \hat{k}_{12}^i(t,z) \\ \hat{k}_{21}^i(t,z) & \hat{k}_{22}^i(t,z) \end{bmatrix} \begin{Bmatrix} A(t,i,z) \\ B(t,i,z) \end{Bmatrix} + \\ &\begin{bmatrix} \hat{c}_1^i(t,z) \\ \hat{c}_2^i(t,z) \end{bmatrix} \left[\tau f \sin \theta(t,i,z) + \frac{1}{2R} (\tau f \cos \theta(t,i,z))^2 \right] dz \end{aligned} \quad (2.38)$$

When a cutting flute is outside the cutting zone or the dynamic uncut chip thickness associated with this flute is zero, there is loss of contact, then, the cutting force components associated with this flute are zero; that is,

$$\begin{Bmatrix} F_x^i(t) \\ F_y^i(t) \end{Bmatrix} = \mathbf{0} \quad (2.39)$$

Summing the cutting forces that act on the N cutting flutes, one can obtain the net cutting force acting on the tool; this takes the form

$$\begin{Bmatrix} F_x(t) \\ F_y(t) \end{Bmatrix} = \sum_{i=1}^N \begin{Bmatrix} F_x^i(t) \\ F_y^i(t) \end{Bmatrix} \quad (2.40)$$

In addition, from Newton's third law of motion, the forces acting on the workpiece (see Figure 2.9) can be determined as

$$\begin{Bmatrix} F_u(t; \tau(t,i,z)) \\ F_v(t; \tau(t,i,z)) \end{Bmatrix} = \begin{Bmatrix} F_x(t; \tau(t,i,z)) \\ F_y(t; \tau(t,i,z)) \end{Bmatrix} \quad (2.41)$$

After substituting equations (2.30), (2.38), (2.40) and (2.41) into equations (2.28) and writing them in compact form, one can arrive at

$$\mathbf{M}\ddot{\mathbf{q}}(t) + \mathbf{C}\dot{\mathbf{q}}(t) + \mathbf{K}\mathbf{q}(t) = \hat{\mathbf{K}}(t)\mathbf{q}(t) - \sum_{i=1}^N \int_{z_1(t,i)}^{z_2(t,i)} \hat{\mathbf{K}}^i(t, z)\mathbf{q}(t - \tau(t, i, z))dz + \bar{\mathbf{K}}(t)f \quad (2.42)$$

where the vector $\mathbf{q}(t)$ is given by

$$\mathbf{q}(t) = \{q_x(t) \quad q_y(t) \quad q_u(t) \quad q_v(t)\}^T \quad (2.43)$$

and the matrices \mathbf{M} , \mathbf{C} , and \mathbf{K} are the mass matrix, the damping matrix, and the stiffness matrix, respectively. They are given by

$$\mathbf{M} = \begin{bmatrix} m_x & 0 & 0 & 0 \\ 0 & m_y & 0 & 0 \\ 0 & 0 & m_u & 0 \\ 0 & 0 & 0 & m_y \end{bmatrix}, \quad \mathbf{C} = \begin{bmatrix} c_x & 0 & 0 & 0 \\ 0 & c_y & 0 & 0 \\ 0 & 0 & c_u & 0 \\ 0 & 0 & 0 & c_v \end{bmatrix}, \quad \text{and} \quad \mathbf{K} = \begin{bmatrix} k_x & 0 & 0 & 0 \\ 0 & k_y & 0 & 0 \\ 0 & 0 & k_u & 0 \\ 0 & 0 & 0 & k_v \end{bmatrix} \quad (2.44)$$

The time-periodic matrices $\hat{\mathbf{K}}(t)$, $\bar{\mathbf{K}}(t)$, and $\hat{\mathbf{K}}^i(t, z)$ are of the form

$$\hat{\mathbf{K}}^i(t, z) = \begin{bmatrix} \hat{k}_{11}^i(t, z) & \hat{k}_{12}^i(t, z) & \hat{k}_{11}^i(t, z) & \hat{k}_{12}^i(t, z) \\ \hat{k}_{21}^i(t, z) & \hat{k}_{22}^i(t, z) & \hat{k}_{21}^i(t, z) & \hat{k}_{22}^i(t, z) \\ \hat{k}_{11}^i(t, z) & \hat{k}_{12}^i(t, z) & \hat{k}_{11}^i(t, z) & \hat{k}_{12}^i(t, z) \\ \hat{k}_{21}^i(t, z) & \hat{k}_{22}^i(t, z) & \hat{k}_{21}^i(t, z) & \hat{k}_{22}^i(t, z) \end{bmatrix}, \quad \hat{\mathbf{K}}(t) = \sum_{i=1}^N \int_{z_1(t,i)}^{z_2(t,i)} \hat{\mathbf{K}}^i(t, z) dz, \quad \text{and}$$

$$\bar{\mathbf{K}}(t) = \sum_{i=1}^N \int_{z_1(t,i)}^{z_2(t,i)} \left(\begin{bmatrix} \hat{k}_{11}^i(t, z) \\ \hat{k}_{21}^i(t, z) \\ \hat{k}_{11}^i(t, z) \\ \hat{k}_{21}^i(t, z) \end{bmatrix} \tau(t, i, z) + \frac{f}{2R} \begin{bmatrix} \hat{c}_1^i(t, z) \\ \hat{c}_2^i(t, z) \\ \hat{c}_1^i(t, z) \\ \hat{c}_2^i(t, z) \end{bmatrix} \left[\tau^2(t, i, z) \cos^2 \theta(t, i, z) \right] \right) dz \quad (2.45)$$

Let $\mathbf{Q}(t) = \{\mathbf{q}^T(t) \quad \dot{\mathbf{q}}^T(t)\}^T$. Then, the system (2.42) can be put in the state-space form

$$\mathcal{Q}(t) = \begin{bmatrix} \mathbf{0} & \mathbf{I} \\ -\mathbf{M}^{-1}[\mathbf{K} - \hat{\mathbf{K}}(t)] & -\mathbf{M}^{-1}\mathbf{C} \end{bmatrix} \mathbf{Q}(t) + \begin{bmatrix} \mathbf{0} \\ \bar{\mathbf{K}}(t)f \end{bmatrix} + \sum_{i=1}^N \int_{z_1(t,i)}^{z_2(t,i)} \begin{bmatrix} \mathbf{0} & \mathbf{0} \\ -\mathbf{M}^{-1}\hat{\mathbf{K}}^i(t,z) & \mathbf{0} \end{bmatrix} \mathbf{Q}(t - \tau(t,i,z)) dz \quad (2.46)$$

In order to simplify the system (2.46), the distributed time varying delay along the z-direction is approximated by the following

$$\tau(t,i,z) = \frac{2\pi R}{N[\Omega R + f \cos \theta(t,i,z)]} \approx \frac{2\pi R}{N[\Omega R + f \cos \theta_i(t)]} = \tau_i(t) \quad (2.47)$$

where

$$\theta_i(t) = \Omega t - (i-1) \frac{2\pi}{N} - \frac{\tan \eta}{R} \cdot \frac{1}{2} [z_1(t,i) + z_2(t,i)] + \theta_0 \quad (2.48)$$

From equations (2.47) and (2.48), one can say time delay $\tau_i(t)$ are time periodic function and their range are determined by

$$\tau_{\min} = \frac{2\pi R}{N(\Omega R + f)} \leq \tau_i(t) \leq \frac{2\pi R}{N(\Omega R - f)} = \tau_{\max} \quad (2.49)$$

Then, the terms associated with the time varying delay can be approximated as

$$\int_{z_1(t,i)}^{z_2(t,i)} \begin{bmatrix} \mathbf{0} & \mathbf{0} \\ -\mathbf{M}^{-1}\hat{\mathbf{K}}^i(t,z) & \mathbf{0} \end{bmatrix} \mathbf{Q}(t - \tau(t,i,z)) dz \approx \int_{z_1(t,i)}^{z_2(t,i)} \begin{bmatrix} \mathbf{0} & \mathbf{0} \\ -\mathbf{M}^{-1}\hat{\mathbf{K}}^i(t,z) & \mathbf{0} \end{bmatrix} dz \mathbf{Q}(t - \tau_i(t)) \quad (2.50)$$

and the system (2.46) can be put in the form

$$\dot{\mathbf{Q}}(t) = \mathbf{W}_0(t)\mathbf{Q}(t) + \sum_{i=1}^N \mathbf{W}_i(t)\mathbf{Q}(t - \tau_i(t)) + \begin{bmatrix} \mathbf{0} \\ \bar{\mathbf{K}}(t)f \end{bmatrix} \quad (2.51)$$

where $\mathbf{W}_0(t)$ is the coefficient matrix associated with present states and $\mathbf{W}_i(t)$ are the coefficient matrix associated with delayed states. They are piecewise, periodic functions of time and given by

$$\mathbf{W}_0(t) = \begin{bmatrix} \mathbf{0} & \mathbf{I} \\ -\mathbf{M}^{-1}[\mathbf{K} - \hat{\mathbf{K}}(t)] & -\mathbf{M}^{-1}\mathbf{C} \end{bmatrix} \text{ and } \mathbf{W}_i(t) = \int_{z_1(t,i)}^{z_2(t,i)} \begin{bmatrix} \mathbf{0} & \mathbf{0} \\ -\mathbf{M}^{-1}\hat{\mathbf{K}}^i(t, z) & \mathbf{0} \end{bmatrix} dz \quad (2.52)$$

2.6. Model with Two Time Delays

Here, for reference, the two time delay model is also presented since a scheme for stability analysis for solution of this model has been developed in Chapter 3. For the model with two time delays, the governing equations of motion are of the form [Balachandran and Zhao (2000) and Zhao and Balachandran (2001)]

$$\left. \begin{aligned} m_x \ddot{q}_x + c_x \dot{q}_x + k_x q_x &= F_x(t; \tau_1, \tau_2) \\ m_y \ddot{q}_y + c_y \dot{q}_y + k_y q_y &= F_y(t; \tau_1, \tau_2) \\ m_u \ddot{q}_u + c_u \dot{q}_u + k_u q_u &= F_u(t; \tau_1, \tau_2) \\ m_v \ddot{q}_v + c_v \dot{q}_v + k_v q_v &= F_v(t; \tau_1, \tau_2) \end{aligned} \right\} \quad (2.53)$$

Referring to Figure 2.9, when $\theta'_s < \theta(i, t, z) < \theta'_e$, the i th cutting tooth is in contact with workpiece and the corresponding cutting force components are given by

$$\begin{Bmatrix} F_x^i(t) \\ F_y^i(t) \end{Bmatrix} = \begin{bmatrix} \hat{k}_{11}^i(t) & \hat{k}_{12}^i(t) \\ \hat{k}_{21}^i(t) & \hat{k}_{22}^i(t) \end{bmatrix} \begin{Bmatrix} A(t; \tau_1) \\ B(t; \tau_2) \end{Bmatrix} + \begin{bmatrix} \hat{c}_{11}^i(t) & \hat{c}_{12}^i(t) \\ \hat{c}_{21}^i(t) & \hat{c}_{22}^i(t) \end{bmatrix} \begin{Bmatrix} \dot{A}(t; \tau_1) \\ \dot{B}(t; \tau_2) \end{Bmatrix} \quad (2.54)$$

The relative displacements and velocities in equations (2.54) are given by

$$\begin{aligned} A(t; \tau_1) &= q_x(t) - q_x(t - \tau_1) + q_u(t) - q_u(t - \tau_1) + f\tau_1 \\ B(t; \tau_2) &= q_y(t) - q_y(t - \tau_2) + q_v(t) - q_v(t - \tau_2) \end{aligned} \quad (2.55)$$

$$\begin{aligned} \dot{A}(t; \tau_1) &= \dot{q}_x(t) - \dot{q}_x(t - \tau_1) + \dot{q}_u(t) - \dot{q}_u(t - \tau_1) \\ \dot{B}(t; \tau_2) &= \dot{q}_y(t) - \dot{q}_y(t - \tau_2) + \dot{q}_v(t) - \dot{q}_v(t - \tau_2) \end{aligned} \quad (2.56)$$

where τ_1 and τ_2 are one tooth pass periods along the X and Y directions, respectively.

They can be calculated from the following two equations:

$$\tau_1 = \frac{2\pi}{N\Omega} \quad (2.57)$$

$$\tau_2 = \frac{4\pi R}{N(2\Omega R + f)} \quad (2.58)$$

The difference between τ_1 and τ_2 is due to the feed motion, and τ_2 can be derived as follows under a static approximation. Referring to Figure 2.11, one can obtain the following equation

$$\sin \Delta\theta = \frac{\tau_2 f}{2R} \quad (2.59)$$

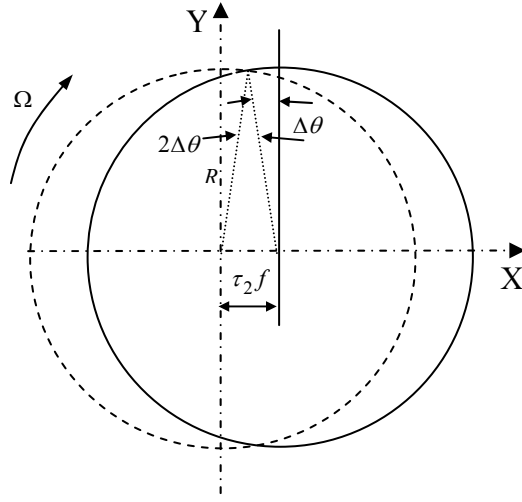


Figure 2.11: Static deviation of entry or exit angle in cutting zone.

where τ_2 can be calculated from the following equation

$$\tau_2 = \frac{\frac{2\pi}{N} - \Delta\theta}{\Omega} \quad (2.60)$$

In practical milling operations, $\tau_2 f \ll R$, and this leads to

$$\sin \Delta\theta \approx \Delta\theta \quad (2.61)$$

After combining equations (2.59)-(2.61), one can obtain the time delay τ_2 shown in equation (2.58).

The corresponding cutting force components are zero when there is loss of contact workpiece and tool; that is

$$\begin{cases} F_x^i(t; \tau_1, \tau_2) \\ F_y^i(t; \tau_1, \tau_2) \end{cases} = \mathbf{0} \quad (2.62)$$

Carrying out a summation over the N cutting flutes, the cutting forces are determined to be

$$\begin{Bmatrix} F_x(t; \tau_1, \tau_2) \\ F_y(t; \tau_1, \tau_2) \end{Bmatrix} = \sum_{i=1}^N \begin{Bmatrix} F_x^i(t; \tau_1, \tau_2) \\ F_y^i(t; \tau_1, \tau_2) \end{Bmatrix} = \begin{bmatrix} \hat{k}_{11}(t) & \hat{k}_{12}(t) \\ \hat{k}_{21}(t) & \hat{k}_{22}(t) \end{bmatrix} \begin{Bmatrix} A(t; \tau_1) \\ B(t; \tau_2) \end{Bmatrix} + \begin{bmatrix} \hat{c}_{11}(t) & \hat{c}_{12}(t) \\ \hat{c}_{21}(t) & \hat{c}_{22}(t) \end{bmatrix} \begin{Bmatrix} \dot{A}(t; \tau_1) \\ \dot{B}(t; \tau_2) \end{Bmatrix} \quad (2.63)$$

On substituting equations (2.54) to (2.63) into equations (2.53), the resulting system is

$$\begin{aligned} \mathbf{M}\ddot{\mathbf{q}}(t) + [\mathbf{C} - \hat{\mathbf{C}}(t)]\dot{\mathbf{q}}(t) + [\mathbf{K} - \hat{\mathbf{K}}(t)]\mathbf{q}(t) = -\hat{\mathbf{C}}_1(t)\dot{\mathbf{q}}(t - \tau_1) \\ -\hat{\mathbf{C}}_2(t)\dot{\mathbf{q}}(t - \tau_2) - \hat{\mathbf{K}}_1(t)\mathbf{q}(t - \tau_1) - \hat{\mathbf{K}}_2(t)\mathbf{q}(t - \tau_2) + \hat{\mathbf{k}}_3(t)\tau_1 f \end{aligned} \quad (2.64)$$

where

$$\hat{\mathbf{C}}(t) = \hat{\mathbf{C}}_1(t) + \hat{\mathbf{C}}_2(t)$$

$$\hat{\mathbf{C}}_1(t) = \begin{bmatrix} \hat{c}_{11}(t) & 0 & \hat{c}_{11}(t) & 0 \\ \hat{c}_{21}(t) & 0 & \hat{c}_{21}(t) & 0 \\ \hat{c}_{11}(t) & 0 & \hat{c}_{11}(t) & 0 \\ \hat{c}_{21}(t) & 0 & \hat{c}_{21}(t) & 0 \end{bmatrix}, \quad \hat{\mathbf{C}}_2(t) = \begin{bmatrix} 0 & \hat{c}_{12}(t) & 0 & \hat{c}_{12}(t) \\ 0 & \hat{c}_{22}(t) & 0 & \hat{c}_{22}(t) \\ 0 & \hat{c}_{12}(t) & 0 & \hat{c}_{12}(t) \\ 0 & \hat{c}_{22}(t) & 0 & \hat{c}_{22}(t) \end{bmatrix} \quad (2.65)$$

$$\hat{\mathbf{K}}(t) = \hat{\mathbf{K}}_1(t) + \hat{\mathbf{K}}_2(t)$$

$$\hat{\mathbf{K}}_1(t) = \begin{bmatrix} \hat{k}_{11}(t) & 0 & \hat{k}_{11}(t) & 0 \\ \hat{k}_{21}(t) & 0 & \hat{k}_{21}(t) & 0 \\ \hat{k}_{11}(t) & 0 & \hat{k}_{11}(t) & 0 \\ \hat{k}_{21}(t) & 0 & \hat{k}_{21}(t) & 0 \end{bmatrix}, \quad \hat{\mathbf{K}}_2(t) = \begin{bmatrix} 0 & \hat{k}_{12}(t) & 0 & \hat{k}_{12}(t) \\ 0 & \hat{k}_{22}(t) & 0 & \hat{k}_{22}(t) \\ 0 & \hat{k}_{12}(t) & 0 & \hat{k}_{12}(t) \\ 0 & \hat{k}_{22}(t) & 0 & \hat{k}_{22}(t) \end{bmatrix}, \quad \text{and } \hat{\mathbf{k}}_3(t) = \begin{Bmatrix} \hat{k}_{11}(t) \\ \hat{k}_{21}(t) \\ \hat{k}_{11}(t) \\ \hat{k}_{21}(t) \end{Bmatrix} \quad (2.66)$$

In state-space form, equations (2.64) can be written as

$$\dot{\mathbf{Q}}(t) = \mathbf{W}_0(t)\mathbf{Q}(t) + \mathbf{W}_1(t)\mathbf{Q}(t - \tau_1) + \mathbf{W}_2(t)\mathbf{Q}(t - \tau_2) + \left\{ \begin{array}{c} \mathbf{0} \\ \hat{\mathbf{k}}_3(t) \end{array} \right\} f \tau_1 \quad (2.67)$$

where $\mathbf{W}_0(t)$ is the coefficient matrix for the vector of present states

$$\mathbf{W}_0(t) = \begin{bmatrix} \mathbf{0} & \mathbf{I} \\ -\mathbf{M}^{-1}(\mathbf{K} - \hat{\mathbf{K}}(t)) & -\mathbf{M}^{-1}(\mathbf{C} - \hat{\mathbf{C}}(t)) \end{bmatrix} \quad (2.68)$$

and $\mathbf{W}_1(t)$ and $\mathbf{W}_2(t)$ are the coefficient matrices associated with vectors of delayed states. These matrices are given by

$$\mathbf{W}_1(t) = \begin{bmatrix} \mathbf{0} & \mathbf{0} \\ -\mathbf{M}^{-1}\hat{\mathbf{K}}_1(t) & -\mathbf{M}^{-1}\hat{\mathbf{C}}_1(t) \end{bmatrix} \quad (2.69)$$

$$\mathbf{W}_2(t) = \begin{bmatrix} \mathbf{0} & \mathbf{0} \\ -\mathbf{M}^{-1}\hat{\mathbf{K}}_2(t) & -\mathbf{M}^{-1}\hat{\mathbf{C}}_2(t) \end{bmatrix} \quad (2.70)$$

Chapter 3

Stability Analysis

Equations (2.51) and (2.67) are nonlinear, non-homogeneous, delay-differential systems with time-periodic coefficients. In a nonlinear dynamic system, there exist several different types of motions associated with different solutions, which include the stationary solution (the equilibrium solution) and dynamic solutions, for example, periodic, quasi-periodic, and chaotic solutions (Nayfeh and Balachandran, 1995). As the system control parameters go through a critical value, the motion of the system can change from one type of motion to a qualitatively different one, and a bifurcation may occur. In this chapter, the difficulty to examine the stability of periodic motions of the delay differential equation with time-periodic coefficients is discussed. Following that, a refined version of the semi-discretization scheme (Insperger and Stépán 2001, 2002), which is used to analyze the stability of systems (2.51) and (2.67), is presented. Numerical results obtained by using the semi-discretization scheme are compared with the corresponding experimental results, the results obtained by using time-domain simulations and the average coefficient method, and the accuracy and efficiency of semi-discretization scheme are also discussed.

Numerical investigations were performed to compare the predictions from the model with a variable time delay presented in the previous chapter with available experimental data and the predictions from the model with constant time delay. The feed-rate effects are examined by comparing the prediction results obtained for milling operations with different feed rate.

3.1. *Periodic Motions of Delay Differential System with Time-Periodic Coefficients*

In order to explain the difficulty associated with carrying out stability analysis of periodic motions of delay differential equations with time-periodic coefficients, here, the basic concepts pertaining to periodic solution of ordinary differential systems are briefly reviewed first. The general form of an n -dimensional ordinary differential system can be written as

$$\dot{\mathbf{X}}(t) = \mathbf{F}(\mathbf{X}, t; \mathbf{P}) \quad (3.1)$$

where \mathbf{X} is an n -dimensional state vector and \mathbf{P} is a p -dimensional parameter vector. Let $\mathbf{X}_0(t)$ denote the periodic solution of equations (3.1) at $\mathbf{P} = \mathbf{P}_0$ and let this solution have a minimal period T . Then, a disturbance $\mathbf{y}(t)$ is superimposed on $\mathbf{X}_0(t)$, resulting in

$$\mathbf{X}(t) = \mathbf{X}_0(t) + \mathbf{y}(t) \quad (3.2)$$

After substituting equations (3.2) into (3.1), assuming that \mathbf{F} is at least twice continuously differentiable, expanding \mathbf{F} in a Taylor series about $\mathbf{X}_0(t)$ and retaining only linear terms in the disturbance leads to

$$\dot{\mathbf{y}}(t) = \mathbf{A}(t)\mathbf{y}(t) \quad (3.3)$$

where $\mathbf{A}(t)$ is the matrix of first partial derivatives of \mathbf{F} . If \mathbf{F} is a linear function of state vector \mathbf{X} , $\mathbf{A}(t)$ is a constant matrix and equation (3.3) is a linear autonomous ordinary differential system. The stability properties of the trivial solution of linear autonomous system of ordinary differential equations can be determined from the roots of the associated characteristic polynomial. The periodic solution, $\mathbf{X}_0(t)$, is

stable if and only if all the characteristic roots have negative real parts. If \mathbf{F} is a nonlinear function of state vector \mathbf{X} , then

$$\mathbf{A}(t+T) = \mathbf{A}(t) \quad (3.4)$$

Floquet theory can be used to study the stability of zero solution of the period system (3.3) [Nayfeh and Mook (1979) and Nayfeh and Balachandran (1995)]. For the system (3.3), there have n linearly independent solutions, which can be used to construct the so-called fundamental set of solutions $\mathbf{Y}(t) = [\mathbf{y}_1(t) \ \mathbf{y}_2(t) \ \cdots \ \mathbf{y}_n(t)]$.

Next, the $\Phi(T)$ can be defined so that

$$\mathbf{Y}(T+t) = \Phi(T)\mathbf{Y}(t) \quad (3.5)$$

The $\Phi(T)$, which is an $n \times n$ constant matrix, depends on the chosen fundamental matrix solution and is not unique. If the initial condition is specified as $\mathbf{Y}(0) = \mathbf{I}$, then $\Phi(T) = \mathbf{Y}(T)$ is called the monodromy matrix. The eigenvalues of the monodromy matrix $\Phi(T)$ are called the Floquet or characteristic multipliers. The periodic solution, $\mathbf{X}_0(t)$, is stable, if and only if all the Floquet multipliers have a modulus less than one. Note for autonomous system, this is not true. One of the multipliers is always one in modulus.

The difference between a delay differential system and an ordinary differential system is that the future states of the system are not only determined by the present but also by the past states. For example, a linear periodic delay differential system can be written as (Hale and Lunel, 1993 and Kolmanovskii and Myshkis, 1999)

$$\mathbf{y}(t) = L(t)\mathbf{y}_t = \int_{-\tau}^0 d\boldsymbol{\mu}(t, \boldsymbol{\theta})\mathbf{y}(t + \boldsymbol{\theta}) \quad (3.6)$$

where $\mu(t, \mathcal{G})$ is a function of bounded matrix and $L(T+t) = L(t)$. The extended Floquet theorem can be used for system (3.6) (Hahn, 1961, and Farkas, 1994). Due to the time delay effect, infinite dimensional linear operators are used here instead of the finite dimensional operator used in the system (3.5). Let $\phi(t)$ be an initial history function in the space of continuous functions on $[-\tau, 0]$. One can define this linear operator as

$$(U\phi)(s) = \mathbf{y}(s+T)\phi \quad (3.7)$$

where the notation $\mathbf{y}(t; \phi)$ indicates the solution of (3.6) with the initial history function on the interval $[-\tau, 0]$. If there is a non-trivial solution $\mathbf{y}(t; \phi)$ of (3.6) such that $\mathbf{y}(t+T; \phi) = \rho \mathbf{y}(t; \phi)$ for all t then ρ is a characteristic multiplier of (3.6). The characteristic (Floquet) multipliers of (3.6) are then the eigenvalues of the operator U defined in (3.7). For more information on periodic delay differential equations, please see the reference of Hale and Lunel (1993).

3.2. Semi-Discretization Method for System with Two Time Delays

The system of equations (2.67) are nonlinear, non-homogeneous and non-autonomous delay-differential equation with time-periodic coefficients. The difficulty is that the operator U has no closed form for a system such as (2.67). So, the stability conditions can't be determined in closed form. Hence, approximations are needed. In this section, the semi-discretization scheme presented by Insperger and Stépán (2001, 2002) is used to determine the local stability of a periodic motion. This scheme is

extended here to handle systems with two discrete time delays, and further, this scheme is applied to a system with loss of contact nonlinearities.

Let the nominal periodic solution of equations (2.67) be represented by $\mathbf{Q}_0(t)$. Then, a perturbation $\mathbf{X}(t)$ is provided to this nominal solution resulting in

$$\mathbf{Q}(t) = \mathbf{Q}_0(t) + \mathbf{X}(t) \quad (3.8)$$

After substituting equations (3.8) into (2.67), the resulting system governing the perturbation is given by

$$\dot{\mathbf{X}}(t) = \mathbf{W}_0(t)\mathbf{X}(t) + \mathbf{W}_1(t)\mathbf{X}(t - \tau_1) + \mathbf{W}_2(t)\mathbf{X}(t - \tau_2) \quad (3.9)$$

In the following part of this section, the formulation of the semi-discretization method is presented to examine the stability of non-trivial solution of equation (3.9). In this formulation, the time period T of the periodic orbit is first broken up into $k+1$ equal intervals each of length Δt , and in each interval, the non-autonomous delay-differential system (3.9) is replaced by an autonomous ordinary differential system. This piecewise linear system of ordinary differential equations is solved to obtain a high-dimensional linear map, which is examined for determining stability of $\mathbf{X}(t) = \mathbf{0}$ of the system (3.9).

As illustrated in Figure 3.1, the time interval Δt is chosen as

$$\Delta t = \frac{\tau_1}{k+1} \quad (3.10)$$

The relationship between Δt and the other discrete time delay τ_2 is given by

$$\tau_2 = (N2 + 1/2 + yr) \times \Delta t \quad (3.11)$$

where yr is given by

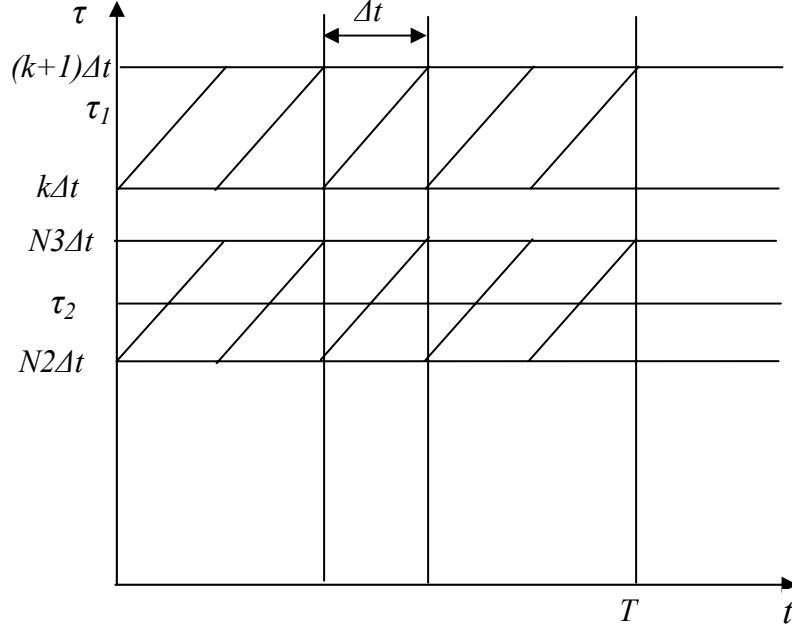


Figure 3.1: Discretization scheme for two delays.

$$yr = \text{mod}\left(\frac{\tau_2 - 1/2\Delta t}{\Delta t}\right) \quad (3.12)$$

and

$$N2 = \frac{\tau_2}{\Delta t} - yr - \frac{1}{2} \quad (3.13)$$

For $t \in [t_i, t_{i+1}]$, the delayed states are approximated as

$$\mathbf{X}(t - \tau_1) \square \mathbf{X}(t_i + 1/2\Delta t - (k+1)\Delta t) = 0.5[\mathbf{X}(t_{i-k}) + \mathbf{X}(t_{i-k-1})] \quad (3.14)$$

$$\mathbf{X}(t - \tau_2) \square \mathbf{X}(t_i + 1/2\Delta t - \tau_2) = \mathbf{X}(t_{i-N2-yr}) \square (1-yr)\mathbf{X}(t_{i-N2}) + yr \cdot \mathbf{X}(t_{i-N3}) \quad (3.15)$$

and $N3 = N2 + 1$

The time-periodic terms in equations (3.9) are approximated as

$$\mathbf{W}_{i,0} = \mathbf{W}_0(t_i) = \frac{1}{\Delta t} \int_{t_i}^{t_{i+1}} \mathbf{W}_0(t) dt \quad (3.16)$$

$$\mathbf{W}_{i,k} = \mathbf{W}_{i,k+1} = \frac{0.5}{\Delta t} \int_{t_i}^{t_{i+1}} \mathbf{W}_1(t) dt \quad (3.17)$$

$$\mathbf{W}_{i,N2} = \mathbf{W}_{N2}(t_i) = \frac{1-yr}{\Delta t} \int_{t_i}^{t_{i+1}} \mathbf{W}_2(t) dt \quad (3.18)$$

$$\mathbf{W}_{i,N3} = \mathbf{W}_{N3}(t_i) = \frac{yr}{\Delta t} \int_{t_i}^{t_{i+1}} \mathbf{W}_2(t) dt \quad (3.19)$$

Then, over each time interval $t \in [t_i, t_{i+1}]$ for $i = 0, 1, 2, \dots, k$, equations (3.9) can be approximated as

$$\dot{\mathbf{X}}(t) = \mathbf{W}_{i,0}(t_i) \mathbf{X}(t) + \mathbf{W}_{i,k} \mathbf{X}_{i-k} + \mathbf{W}_{i,k+1} \mathbf{X}_{i-k-1} + \mathbf{W}_{i,N2} \mathbf{X}_{i-N2} + \mathbf{W}_{i,N3} \mathbf{X}_{i-N3} \quad (3.20)$$

where $\mathbf{X}(t_i)$ has been written as \mathbf{X}_i . Thus, the infinite-dimensional system (3.9) has been replaced by a piecewise system of ordinary differential equations with constant coefficients in the time period $t \in [t_0, t_0 + T]$. Note that in each interval, the autonomous system has a constant excitation or forcing term that arises due to the delay effects.

To proceed further, it is assumed that $\mathbf{W}_{i,0}$ is invertible for all i . Then, the solution of equations (3.20) takes the form

$$\mathbf{X}(t) = e^{\mathbf{W}_{i,0}(t-t_i)} \left[\mathbf{X}_i + \mathbf{W}_{i,0}^{-1} \sum_{j=1}^{N1} \mathbf{W}_{i,j} \mathbf{X}_{i-j} \right] - \mathbf{W}_{i,0}^{-1} \sum_{j=1}^{N1} \mathbf{W}_{i,j} \mathbf{X}_{i-j} \quad (3.21)$$

where $\mathbf{W}_{i,j} = 0$ for $j \neq k, k+1, N2$, and $N3$. When $t = t_{i+1}$, equation (3.21) leads to

$$\mathbf{X}_{i+1} = \mathbf{M}_{i,0} \mathbf{X}_i + \sum_{j=1}^{k+1} \mathbf{M}_{i,j} \mathbf{X}_{i-j} \quad (3.22)$$

where the associated matrices are given by

$$\mathbf{M}_{i,0} = \exp(\mathbf{W}_{i,0} \Delta t) + \exp(\mathbf{W}_{i,0} \Delta t - \mathbf{I}) \mathbf{W}_{i,0}^{-1} \mathbf{W}_{i,1} \quad (3.23)$$

and for $j > 0$

$$\mathbf{M}_{i,j} = \begin{cases} \exp(\mathbf{W}_{i,0}\Delta t - \mathbf{I})\mathbf{W}_{i,0}^{-1}\mathbf{W}_{i,j} & \text{if } j = k, k+1, N2, N3 \\ 0 & \text{otherwise} \end{cases} \quad (3.24)$$

The system (3.22) can be used to construct the state vector

$$\mathbf{Y}_i = (\mathbf{X}_i^T, \mathbf{X}_{i-1}^T, \dots, \mathbf{X}_{i-k-1}^T)^T \quad (3.25)$$

and the linear discrete map

$$\mathbf{Y}_{i+1} = \mathbf{B}_i \mathbf{Y}_i \quad (3.26)$$

where each \mathbf{B}_i matrix is given by

$$\mathbf{B}_i = \begin{bmatrix} \mathbf{M}_{i,0} & \mathbf{0} & \dots & \mathbf{M}_{i,N2} & \mathbf{M}_{i,N3} & \dots & \mathbf{M}_{i,k} & \mathbf{M}_{i,k+1} \\ \mathbf{I} & \mathbf{0} & \dots & \mathbf{0} & \mathbf{0} & \dots & \mathbf{0} & \mathbf{0} \\ \mathbf{0} & \mathbf{I} & \dots & \mathbf{0} & \mathbf{0} & \dots & \mathbf{0} & \mathbf{0} \\ \vdots & \vdots & \ddots & \vdots & \vdots & \ddots & \vdots & \vdots \\ \mathbf{0} & \mathbf{0} & \dots & \mathbf{I} & \mathbf{0} & \dots & \mathbf{0} & \mathbf{0} \\ \mathbf{0} & \mathbf{0} & \dots & \mathbf{0} & \mathbf{I} & \dots & \mathbf{0} & \mathbf{0} \\ \vdots & \vdots & \ddots & \vdots & \vdots & \ddots & \vdots & \vdots \\ \mathbf{0} & \mathbf{0} & \dots & \mathbf{0} & \mathbf{0} & \dots & \mathbf{I} & \mathbf{0} \end{bmatrix} \quad (3.27)$$

For a “small” feed rate, $\tau_1 \leq \tau_2 + 0.5\Delta t$, and hence, $k+1 = N3$. In this case, the matrix

\mathbf{B}_i can be shown to be

$$\mathbf{B}_i = \begin{bmatrix} \mathbf{M}_{i,0} & \mathbf{0} & \dots & \mathbf{M}_{i,N2} + \mathbf{M}_{i,k} & \mathbf{M}_{i,N3} + \mathbf{M}_{i,k+1} \\ \mathbf{I} & \mathbf{0} & \dots & \mathbf{0} & \mathbf{0} \\ \mathbf{0} & \mathbf{I} & \dots & \mathbf{0} & \mathbf{0} \\ \vdots & \vdots & \ddots & \vdots & \vdots \\ \mathbf{0} & \mathbf{0} & \dots & \mathbf{I} & \mathbf{0} \end{bmatrix} \quad (3.28)$$

From the system (3.26), it follows that

$$\mathbf{Y}_{k+1} = \mathbf{B}_k \cdots \mathbf{B}_1 \mathbf{B}_0 \mathbf{Y}_0 \quad (3.29)$$

from which the transition matrix can be identified as

$$\Phi = \mathbf{B}_k \cdots \mathbf{B}_1 \mathbf{B}_0 \quad (3.30)$$

This matrix Φ represents a finite-dimensional approximation of the “monodromy matrix” associated with the periodic orbit $\mathbf{Q}_0(t)$ of (2.67) and the trivial solution $\mathbf{X}(t) = \mathbf{0}$ of (3.9). If the eigenvalues of this matrix are all within the unit circle, then the trivial fixed point of (3.9) is stable, and hence, the associated periodic orbit of (2.67) is stable. At a bifurcation point, one or more of the eigenvalues of the transition matrix will be on the unit circle. Here, this information is used to determine when a period-doubling bifurcation or a secondary Hopf-bifurcation is imminent.

3.3. Numerical Results for System with Two Time Delays

In this section, results obtained for two time delay model are obtained through numerical investigations are presented. The results for single-degree-of-freedom system are compared with available experimental data and the results for four-degree-of-freedom system are compared with corresponding results obtained by time-domain simulations and average coefficients method (Altintas and Budak, 1995).

3.3.1. Single-degree-of-freedom system

The workpiece-tool system modal parameters for the chosen system are given in Table 3.1, and the tool and cutting parameters are provided in Table 3.2. The feed rate is fixed at 0.1016 mm/tooth for both the up-milling and down-milling operations. For comparison, experimental results (Mann, Insperger, Bayly, and Stépán, 2003) are used. In Figure 3.2, the experimental arrangement used by Mann *et al.* (2003) is shown. In this milling test, a monolithic, unidirectional flexure was designed to mimic a single-degree-of-freedom system. The workpiece material is aluminum and a non-

contact displacement sensor is used to measure the dynamic displacement of workpiece.

Table 3.1. Modal parameters of single-degree-of-freedom milling system (Mann *et al.*, 2003)

mode	frequency (Hz)	Damping (%)	modal stiffness (N/m)	modal mass (kg)
workpiece (X)	146.6	0.32	2.18×10^6	2.573

Table 3.2. Machining parameters of single-degree-of-freedom milling system (Mann *et al.*, 2003)

normal rake angle (ϕ_n)	helix angle (η)	tool number	Radius (mm)	K_t (Mpa)	k_n	cutting friction coefficient (μ)
120	0^0	1	9.53	550	0.364	0.2

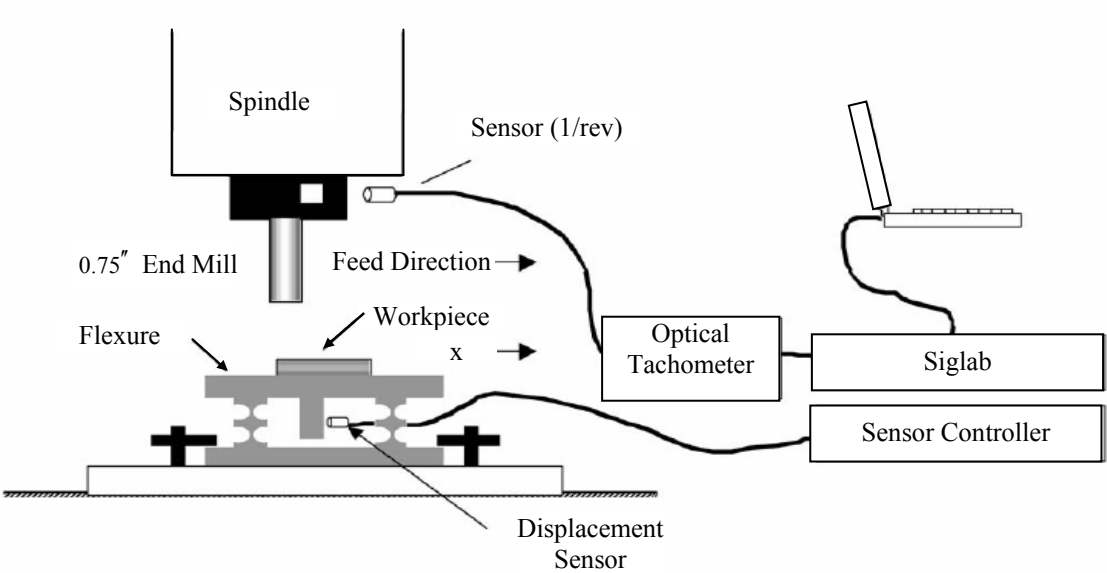


Figure 3.2: Schematic diagram of experimental arrangement (Mann *et al.*, 2003).

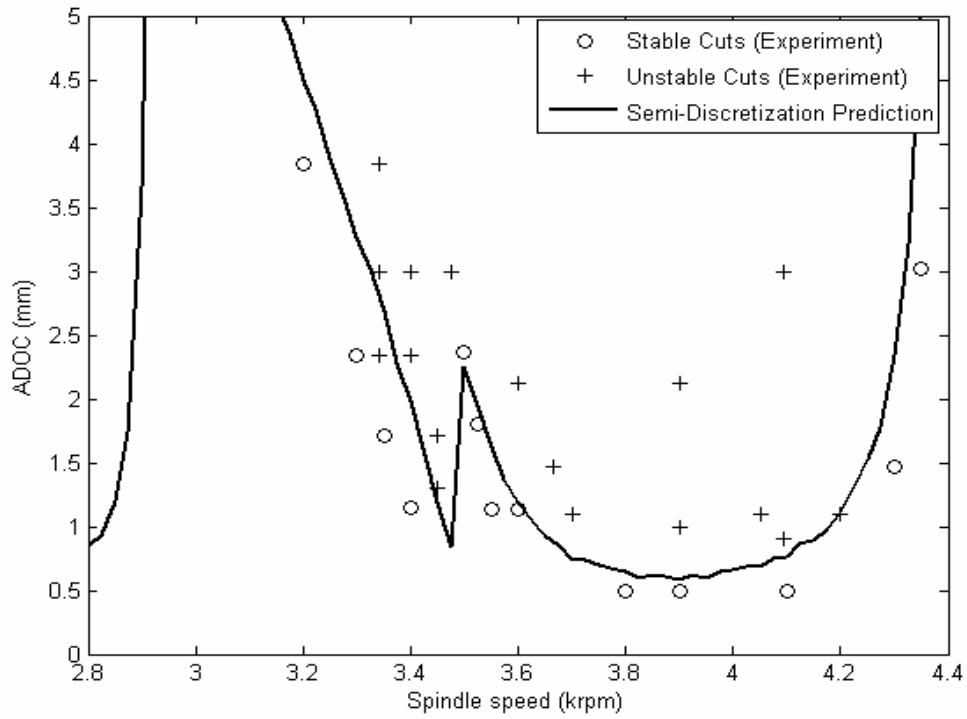


Figure 3.3: Stability predictions for 25% immersion down-milling operations.

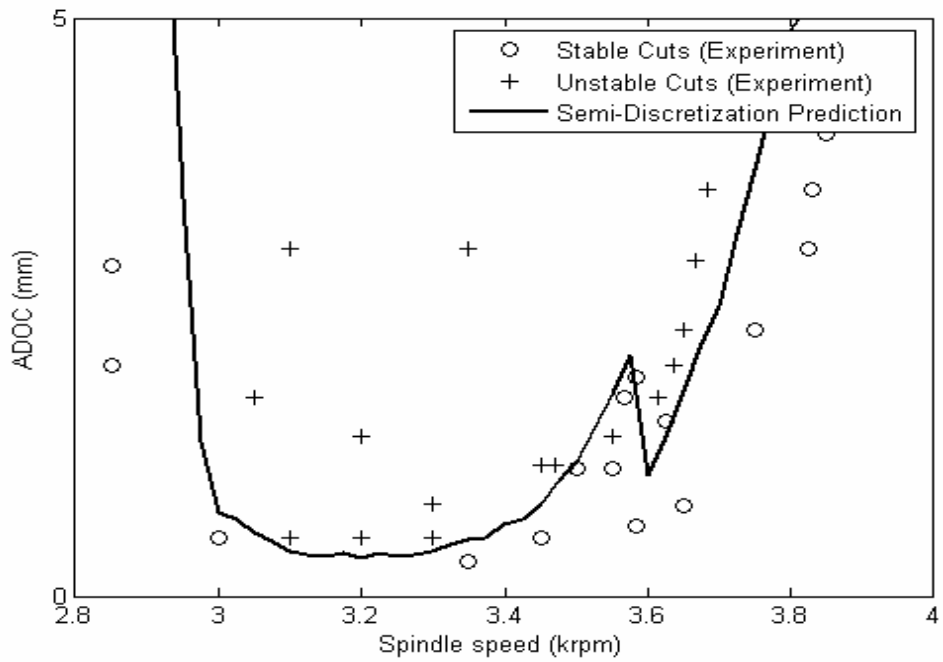


Figure 3.4: Stability predictions for 25% immersion up-milling operations.

In Figures 3.3 and 3.4, the stability charts are presented for single-degree-of-freedom system, 25% immersion down-milling and up-milling operations. It can be seen that the stability charts are different for the up-milling and down-milling operations. This is expected based on the earlier work of Zhao and Balachandran (2001). The legend, “semi-discretization” denotes that the stability lobe obtained by semi-discretization scheme discussed in Section 3.2. The system modal parameters, which are given in Table 3.1, and the machining parameters, which are given in Table 3.2, are used in this semi-discretization treatment. Since only the deformation of workpiece in the X-direction is considered, there is only one time delay, τ_1 , in this system. For the semi-discretization treatment, the integer k is increased until the stability results converge. For a fixed value of spindle speed, the axial depth of cut is increased gradually in a quasi-static manner. The corresponding pseudo-monodromy matrix Φ is determined for each pair of values of the chosen spindle speed and the axial depth of cut. As discussed in the earlier section, if one of the Floquet multipliers of Φ is close to one in the magnitude, while all the other multipliers are less than one in modulus, one can say that this axial depth of cut is a critical value that determines a point on the stability lobe. In the experiment, a stable cutting condition is denoted by “o” and the milling process is stable for the chosen values of the control parameters, namely, the axial depth of cut and the spindle speed. Similar, an unstable cutting condition is denoted by “+” and the milling process is unstable for the corresponding control parameter values. The experimental results were obtained from Mann *et al.* (2003). It is seen that the stability charts determined by the semi-discretization method are in good agreement with the experimental results. The agreement between predictions and

experimental results indicates that semi-discretization method is an efficient method to analyze the stability of periodic solutions of nonlinear, non-autonomous delay differential equations with time-periodic coefficients, which includes the loss of contact effects.

3.3.2. Four-degree-of-freedom system

For the multi-degree-of-freedom system (2.67), beside the regenerative effect and loss of contact nonlinearities, mode coupling is also a mechanism that can result in chatter. Considering the feed-rate effects, the time delay along the X-direction is different from the time delay along the Y-direction. In a recent effort (Long and Balachandran, 2006), the semi-discretization method is extended to handle systems with two discrete time delays, and further, this scheme is applied to a system with loss of

Table 3.3. Modal parameters of four-degree-of-freedom milling system

Mode	frequency (Hz)	damping (%)	modal stiffness (N/m)	modal mass (kg)
tool (X)	1006.58	1.0	8.0×10^5	2.0×10^{-2}
tool (Y)	1027.34	1.5	1.0×10^6	2.4×10^{-2}
workpiece (U)	503.29	1.0	1.0×10^6	1.0×10^{-1}
workpiece (V)	711.76	1.0	3.0×10^6	1.5×10^{-1}

Table 3.4. Machining parameters of four-degree-of-freedom milling system

normal rake angle (ϕ_n)	helix angle (η)	tool number	Radius (mm)	K_t (Mpa)	k_n	cutting friction coefficient (μ)
15^0	30^0	2	6.35	600	0.3	0.2

contact nonlinearities. Referring Figure 2.1, the workpiece-tool system modal parameters and the tool and cutting parameters are shown in Tables 3.3 and 3.4, respectively. The feed rate is fixed at 0.1024 mm/tooth for both the up-milling and down-milling operations. For comparisons, the stability charts generated by using time-domain simulations [Zhao and Balachandran (2001), and Balachandran (2001)] and the averaged coefficients method are presented. The legend, “Averaged coefficients” denotes the stability lobes obtained by averaged coefficients. In formulating the averaged coefficients method, the periodic coefficients in system (2.67) are averaged over one period of the orbit, as commonly carried out in prior studies, for example, the work of Altintas and Budak (1995).

In Figure 3.5, the stability charts are presented for a 25% immersion up-milling operation. The stability lobes determined by time-domain simulations mark the transition from periodic motion to quasi-periodic or period-doubling motions of the system (2.53). The stability lobes determined by the averaged coefficients method are the loci of Hopf-bifurcation points of the time-averaged autonomous system derived from (2.53). The stability lobes determined through the semi-discretization method are the loci of secondary Hopf-bifurcation points or period-doubling points. The period-doubling bifurcation points are marked by stars in the figures. At the other locations on the stability lobes, it is numerically ascertained that secondary Hopf-bifurcations occur. The stability chart determined by the semi-discretization method is close to the stability chart generated through time-domain simulations, while the stability chart generated by the averaged coefficients method is not close to these stability charts, especially at high spindle speeds.

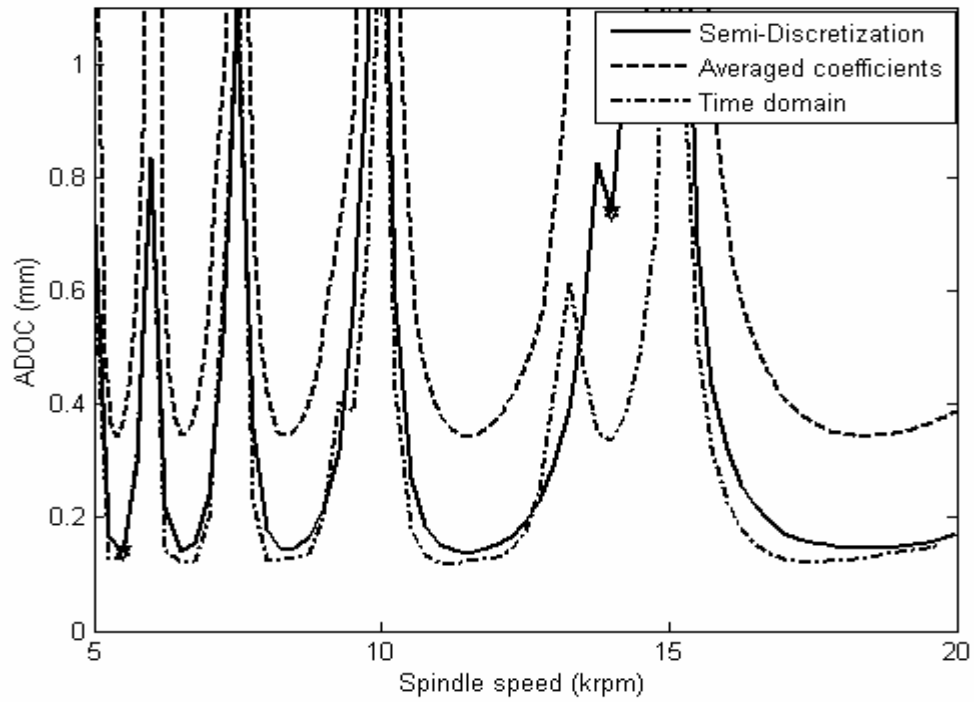


Figure 3.5: Stability predictions for 25% immersion up-milling operations.

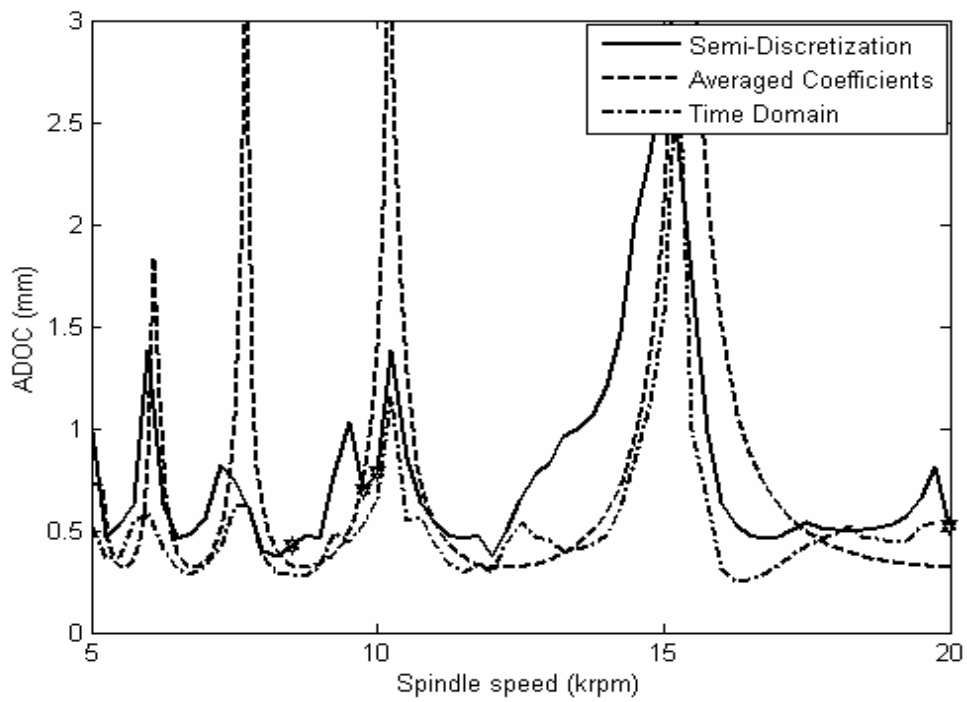


Figure 3.6: Stability predictions for 25% immersion down-milling operations.

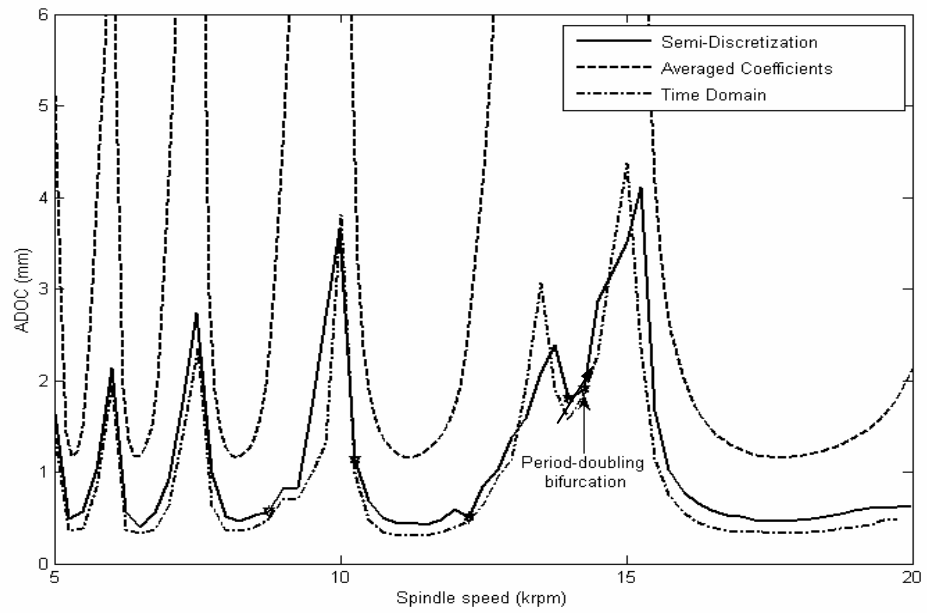


Figure 3.7: Stability predictions for 10% immersion up-milling operations.

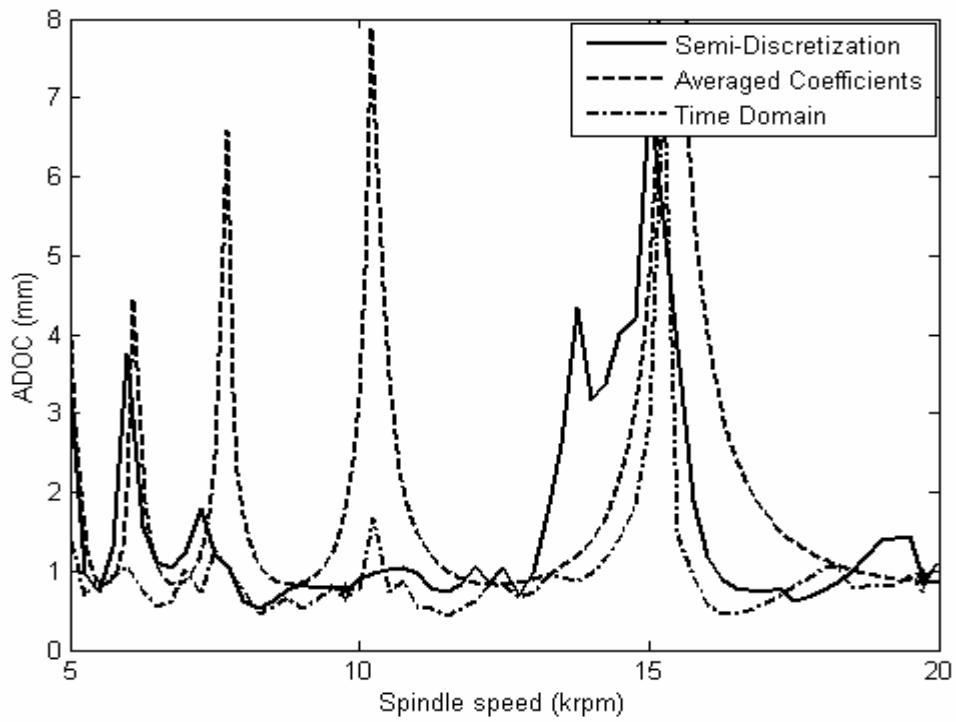


Figure 3.8: Stability predictions for 10% immersion down-milling operations.

In Figure 3.6, the stability charts are presented for a 25% immersion down-milling operation. A down-milling operation has the opposite direction of spindle rotation than that for an up-milling operation. Figures 3.7 and 3.8 represent a similar pair of results obtained for up-milling and down-milling operations with 10% immersion. As the immersion percentage of the tool into the workpiece decreases, the loss of contact effects become more prominent in the workpiece-tool system dynamics. As first reported by Zhao and Balachandran (2001), the stability charts generated for up-milling operations and down-milling operations can be different and this is confirmed by the results presented in Figures 3.5 to 3.8. In addition, the occurrence of a period-doubling bifurcation is indicated by the time-domain simulations and confirmed by the results of the semi-discretization analysis. Due to the nature of the formulation of the averaged coefficient method, period-doubling bifurcations cannot be picked up by this method. In addition, as indicated in the charts for up-milling operations, the stable regions predicted by the averaged coefficient methods is much larger than that predicted by both time-domain simulations and the stability analysis based on semi-discretization.

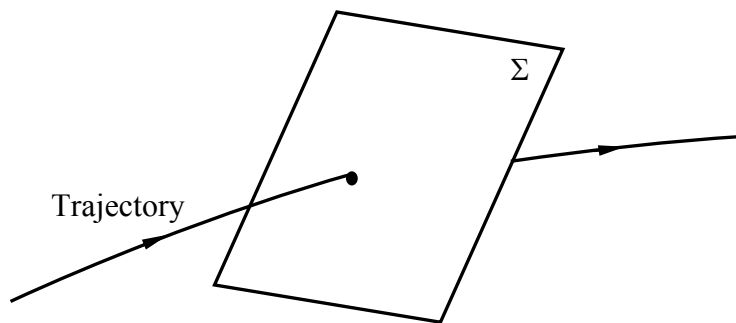


Figure 3.9: Poincaré section and trajectory.

In order to explore the possibilities for bifurcation further, time-domain simulations are used. The Poincaré sections used for this bifurcation diagram are constructed by using the period of the orbit as the clock period. A Poincaré section is a hypersurface in the state space that is transverse to the flow of a given system. In an n -dimensional space, a Poincaré section is a surface whose dimension is less than n . In Figure 3.9, an example of a Poincaré section that intersects a trajectory is illustrated. Here, this trajectory corresponds to an orbit of tool displacement. One can observe different characteristics in a Poincaré section, which can be used to observe the occurrence of the bifurcation in time-domain simulations.

In Figure 3.10, three different Poincaré sections that are associated with three different type of solutions are shown. When the system dynamics changes from a periodic motion to a period-doubled motion, a period-doubling bifurcation is said to have occurred. When the system dynamics changes from a periodic motion to a quasiperiodic motion, a Neimark or a secondary Hopf-bifurcation is said to have occurred. In Figure 3.11, for a fixed spindle speed, the numerically generated bifurcation diagram is shown when the axial depth of cut is used as a control parameter. The Poincaré section is transverse to flow of the tool displacement along the X-direction. The first period-doubling bifurcation occurs at ADOC=1.87 mm as pointed out in Figure 3.7. This result agrees with the prediction of semi-discretization method, shown in Figure 3.7.

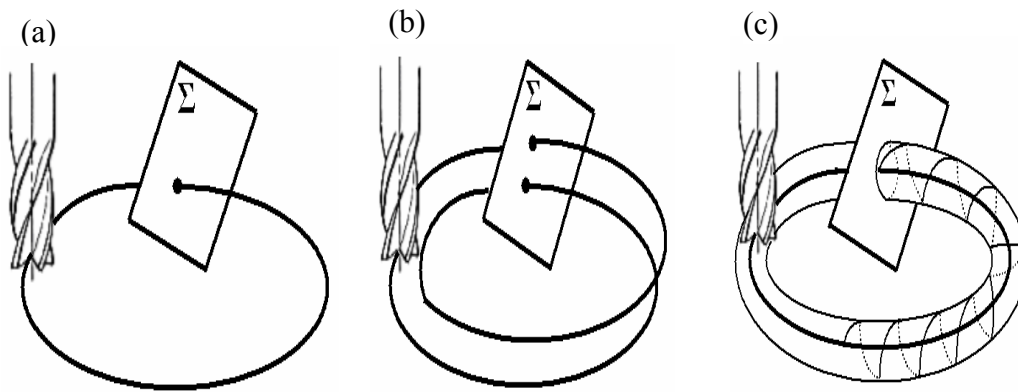


Figure 3.10: (a) Poincaré section of periodic orbit, (b) Poincaré section of period-two orbit, and (c) Poincaré section of quasi-periodic orbit.

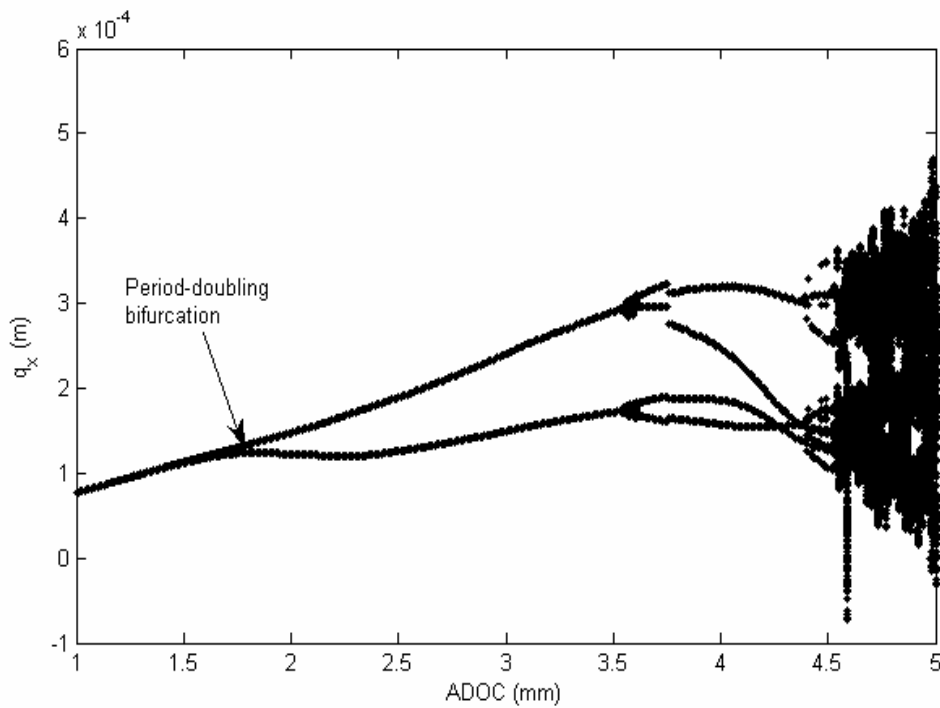


Figure 3.11: Bifurcation diagram for 10% immersion up-milling operation at spindle speed 14200 rpm.

3.4. *Semi-Discretization Method for System with Variable Time Delay*

The stability analysis for systems with a variable time delay is similar to the stability analysis of system with two time delays carried out by using the semi-discretization method. Let the nominal periodic solution of equations (2.51) be represented by $\mathbf{Q}_0(t)$. Then, a perturbation $\mathbf{X}(t)$ is provided to this nominal solution resulting in

$$\mathbf{Q}(t) = \mathbf{Q}_0(t) + \mathbf{X}(t) \quad (3.31)$$

After substituting equations (3.31) into (2.51), the resulting system governing the perturbation is given by

$$\dot{\mathbf{X}}(t) = \mathbf{W}_0(t)\mathbf{X}(t) + \sum_{i=1}^N \mathbf{W}_i(t)\mathbf{X}(t - \tau_i(t)) \quad (3.32)$$

The time period T of the periodic orbit is first divided into $k + 1$ equal intervals with a length Δt and the time interval Δt is chosen as

$$\Delta t = \frac{T}{k + 1} \quad (3.33)$$

For $t \in [t_j, t_{j+1}]$, the time-periodic coefficient matrices in equation (2.51) are approximated as

$$\mathbf{W}_{j,0} \approx \frac{1}{\Delta t} \int_{t_j}^{t_{j+1}} \mathbf{W}_0(t) dt \quad (3.34)$$

$$\mathbf{W}_{j,i} \approx \frac{1}{\Delta t} \int_{t_j}^{t_{j+1}} \mathbf{W}_i(t) dt \quad (3.35)$$

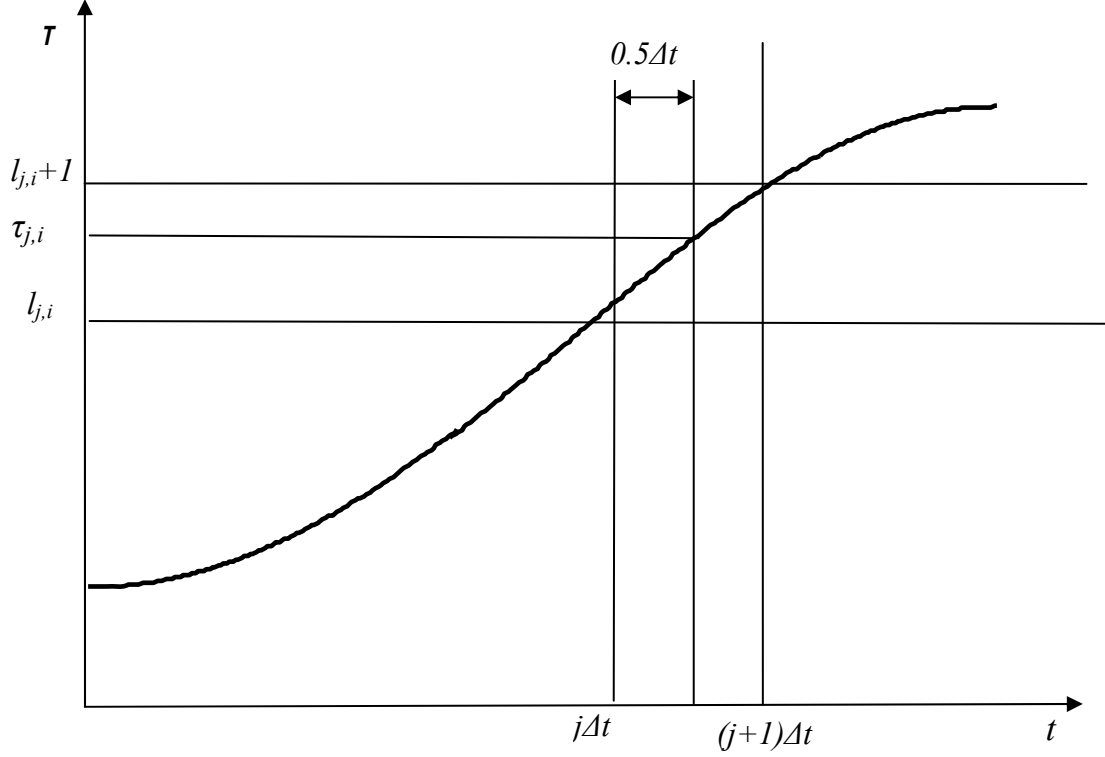


Figure 3.12: Discretization scheme for variable time delay.

Referring to Figure 3.12, the time delays are approximated as

$$\tau_{j,i} = \frac{2\pi R}{N[\Omega R + f \cos \theta_i(t_j + 0.5\Delta t)]} \quad (3.36)$$

The relationship between Δt and the time delay $\tau_{j,i}$ is given by

$$\tau_{j,i} = (l_{j,i} + lr_{j,i} + 0.5)\Delta t \quad (3.37)$$

where $lr_{j,i}$ is given by

$$lr_{j,i} = \text{mod}\left(\frac{\tau_{j,i} - 0.5\Delta t}{\Delta t}\right) \quad (3.38)$$

and

$$l_{j,i} = \frac{\tau_{j,i}}{\Delta t} - lr_{j,i} - 0.5 \quad (3.39)$$

The delayed states are approximated as

$$\mathbf{X}(t - \tau_{j,i}) \approx \mathbf{X}(t_j + 1/2\Delta t - \tau_{j,i}) = \mathbf{X}(t_{j-l_{j,i}-l_{r_{j,i}}}) \approx (1 - l_{r_{j,i}}) \cdot \mathbf{X}(t_{j-l_{j,i}}) + l_{r_{j,i}} \cdot \mathbf{X}(t_{j-l_{j,i}-1}) \quad (3.40)$$

Then, over each time interval $t \in [t_j, t_{j+1}]$ for $j = 0, 1, 2, \dots, k$, writing $\mathbf{X}(t_j)$ as \mathbf{X}_j , the system (3.32) can be approximated as

$$\dot{\mathbf{X}}(t) = \mathbf{W}_{j,0} \mathbf{X}(t) + \sum_{i=1}^N \mathbf{W}_{j,i} \left[(1 - l_{r_{j,i}}) \cdot \mathbf{X}(t_{j-l_{j,i}}) + l_{r_{j,i}} \cdot \mathbf{X}(t_{j-l_{j,i}-1}) \right] \quad (3.41)$$

The solution of equations (3.41) takes the form

$$\mathbf{X}(t) = e^{\mathbf{W}_{j,0}(t-t_j)} \mathbf{X}_j + \left(e^{\mathbf{W}_{j,0}(t-t_j)} - \mathbf{I} \right) \sum_{i=1}^N \mathbf{W}_{j,0}^{-1} \mathbf{W}_{j,i} \left[(1 - l_{r_{j,i}}) \cdot \mathbf{X}(t_{j-l_{j,i}}) + l_{r_{j,i}} \cdot \mathbf{X}(t_{j-l_{j,i}-1}) \right] \quad (3.42)$$

When $t = t_{j+1}$, equation (3.42) leads to

$$\mathbf{X}_{j+1} = \mathbf{M}_{j,0} \mathbf{X}_j + \sum_{i=1}^N \left(\mathbf{M}_{j,l_{j,i}} \mathbf{X}_{j-l_{j,i}} + \mathbf{M}_{j,l_{j,i}+1} \mathbf{X}_{j-l_{j,i}-1} \right) \quad (3.43)$$

where the associated matrices are given by

$$\mathbf{M}_{j,0} = e^{\mathbf{W}_{j,0}\Delta t} \quad (3.44)$$

$$\mathbf{M}_{j,l_{j,i}} = \left(e^{\mathbf{W}_{j,0}\Delta t} - \mathbf{I} \right) \mathbf{W}_{j,0}^{-1} \mathbf{W}_{j,i} (1 - l_{r_{j,i}}) \quad (3.45)$$

$$\mathbf{M}_{j,l_{j,i}+1} = \left(e^{\mathbf{W}_{j,0}\Delta t} - \mathbf{I} \right) \mathbf{W}_{j,0}^{-1} \mathbf{W}_{j,i} \cdot l_{r_{j,i}} \quad (3.46)$$

Let

$$\mathbf{Y}_j = (\mathbf{X}_j^T, \mathbf{X}_{j-1}^T, \dots, \mathbf{X}_{j-l_{\max}}^T)^T \quad (3.47)$$

where

$$l_{\max} = \frac{\tau_{\max}}{\Delta t} - \text{mod} \left(\frac{\tau_{\max}}{\Delta t} \right) + 1 \quad (3.48)$$

Combining equations (3.43) to (3.47), one can construct the linear discrete map

$$\mathbf{Y}_{j+1} = \mathbf{B}_j \mathbf{Y}_j \quad (3.49)$$

where each \mathbf{B}_j matrix is given by

$$\mathbf{B}_j = \begin{bmatrix} \mathbf{M}_{j,0} & \mathbf{0} & \cdots & \mathbf{0} & \mathbf{0} & \mathbf{0} \\ \mathbf{I} & \mathbf{0} & \cdots & \mathbf{0} & \mathbf{0} & \mathbf{0} \\ \mathbf{0} & \mathbf{I} & \cdots & \mathbf{0} & \mathbf{0} & \mathbf{0} \\ \vdots & \vdots & \ddots & \vdots & \vdots & \vdots \\ \mathbf{0} & \mathbf{0} & \cdots & \mathbf{I} & \mathbf{0} & \mathbf{0} \\ \mathbf{0} & \mathbf{0} & \cdots & \mathbf{0} & \mathbf{I} & \mathbf{0} \end{bmatrix} + \sum_{i=1}^N \begin{bmatrix} \mathbf{0} & \cdots & \mathbf{M}_{j,l_{j,i}} & \mathbf{M}_{j,l_{j,i}+1} & \cdots & \mathbf{0} \\ \mathbf{0} & \cdots & \mathbf{0} & \mathbf{0} & \cdots & \mathbf{0} \\ \mathbf{0} & \cdots & \mathbf{0} & \mathbf{0} & \cdots & \mathbf{0} \\ \vdots & \vdots & \vdots & \vdots & \vdots & \vdots \\ \mathbf{0} & \cdots & \mathbf{0} & \mathbf{0} & \cdots & \mathbf{0} \\ \mathbf{0} & \cdots & \mathbf{0} & \mathbf{0} & \cdots & \mathbf{0} \end{bmatrix} \quad (3.50)$$

From equations (3.49), one can obtain

$$\mathbf{Y}_{k+1} = \mathbf{B}_k \cdots \mathbf{B}_1 \mathbf{B}_0 \mathbf{Y}_0 \quad (3.51)$$

and from equations (3.51), the transition matrix over the principal period

$T = (k+1)\Delta t$ can be identified as

$$\mathbf{\Phi} = \mathbf{B}_k \cdots \mathbf{B}_1 \mathbf{B}_0 \quad (3.52)$$

The dimension of the finite size matrix $\mathbf{\Phi}$ is determined by the integer l_{\max} .

As shown by Insperger *et al.* (2003a, 2003b), one can also determine the chatter frequencies of an unstable milling process by using the eigenvalues of $\mathbf{\Phi}$. For the case of Hopf bifurcations, there are a complex pair eigenvalues $\mu = e^{\pm i\omega T}$ located on the unit circle; the chatter frequencies that arise in this cutting process are given by

$$f_H = \left\{ \pm \frac{\omega}{2\pi} + n \frac{N\Omega}{2\pi} \right\} \text{Hz}, \quad n = \dots, -1, 0, 1, \dots, \quad (3.53)$$

where the index H refers to Hopf bifurcation. In the case of a period doubling bifurcation, there is one eigenvalue $\mu = e^{\pm i\omega T} = -1$. The chatter frequencies that arise in this cutting process are given by

$$f_{PD} = \left(\frac{1}{2} + n \right) \frac{N\Omega}{2\pi} \text{Hz}, \quad n = \dots, -1, 0, 1, \dots, \quad (3.54)$$

where the index PD refers to n period-doubling bifurcation. The tooth-pass excitation frequencies are of the form

$$f_{TP} = n \frac{N\Omega}{2\pi} (\text{Hz}), \quad n = \dots, -1, 0, 1, \dots, \quad (3.55)$$

where the index TP refers to the tooth-pass excitation.

3.5. Results for Systems with Variable Time Delay

In this section, results obtained through numerical investigations for two different systems are presented. These results are also compared with experimental data obtained in experiments similar to those reported by Mann *et al.* (2003). The first system considered is a two degree-of-freedom system and the corresponding workpiece-tool system modal parameters are given in Table 3.5. The tool and cutting parameters are provided in Table 3.6.

Table 3.5. Modal parameters of a two-degree-of-freedom milling system.

Mode	Frequency (Hz)	Modal mass (kg)	Damping (%)	modal stiffness (N/m)
Workpiece (X)	729	0.0436	1.07	9.1397×10^5
Workpiece (Y)	729	0.0478	0.9949	1.002×10^6

Table 3.6. Machining parameters for a two-degree-of-freedom milling system.

normal rake angle (φ_n)	helix angle (η)	Tooth number	Radius (mm)	K_t (Mpa)	k_n	cutting friction coefficient (μ)
15^0	40^0	2	6.35	600	0.417	0.2

The stability charts are presented for 5% immersion down-milling operations in Figure 3.13. The feed rate that has been used through out the numerical investigation and during the corresponding experiments is $f = 0.127$ mm/tooth. The legend, “constant delay” denotes that the stability lobes obtained by using the semi-discretization method discussed in the previous section for the system with constant time delay. The legend, “variable time delay” denotes the stability lobes determined for the system with a variable delay. In Figure 3.13, the stable cuts observed in the experiments are identified by using the open circles “o”, the unstable cuts observed in the experiments are identified by using the symbol “∇”, and the suspected borderline cases between stable and unstable cuts are identified by using the symbol “+”. The stability charts obtained for the system with the constant time delay and the system with the variable time delay are close to each other and they agree well with the experimental results. For the chosen feed rate, it is clear that the stability charts obtained for the system with the variable time delay is “closer” to the experiments results than those obtained for the system with the constant delay. It is seen that the stability lobes obtained for system with variable time delay have a slight shift to the right from the stability lobes obtained for system with constant delay. This is due to the variable time delay is larger than the constant time delay, as shown in Figures 2.3 and 2.4, in the cutting zone of 5% immersion down-milling operations, which starts at $\theta'_s = 2.691$ and ends at $\theta'_e \approx \pi$. One also can find the peaks of the stability lobes obtained for system with variable time delay shift down-ward as a result of the changed of time delay. In Figure 3.14, the normalized stability lobes are presented for

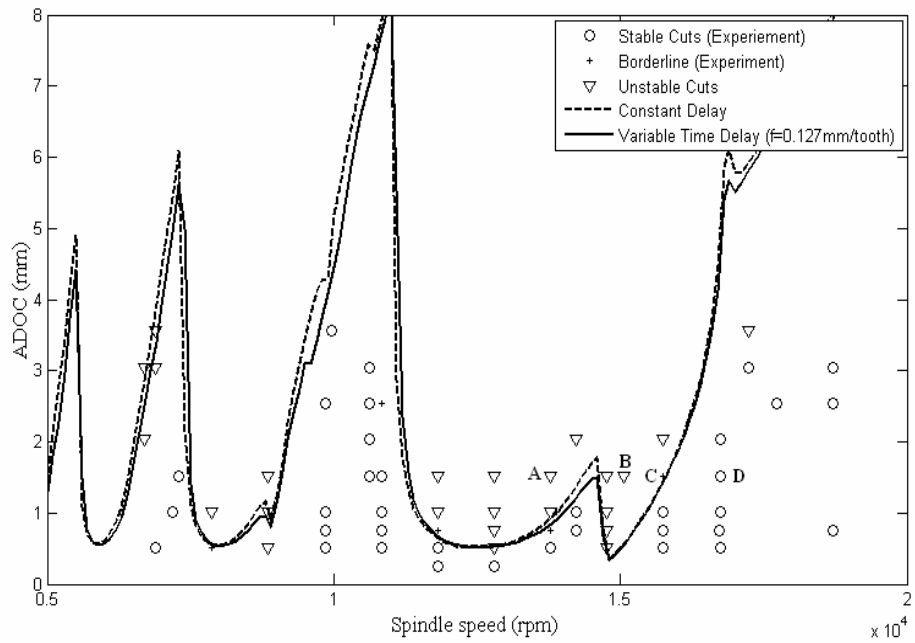


Figure 3.13: Stability charts for 5% immersion down-milling operations.

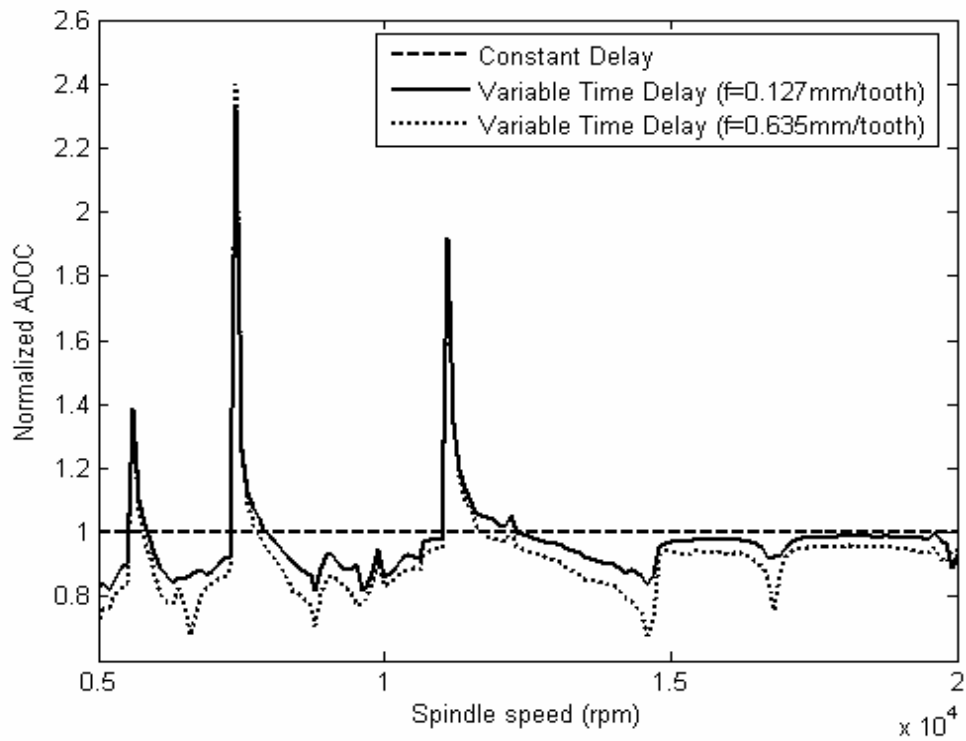


Figure 3.14: Normalized stability limit for 5% immersion down-milling operations.

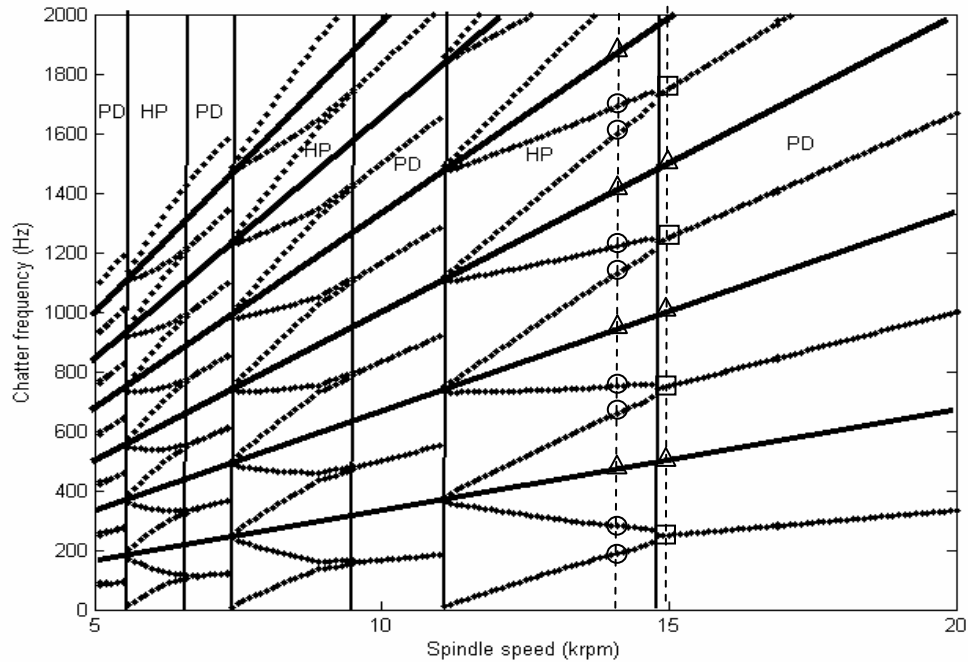


Figure 3.15: Chatter frequencies for 5% immersion down-milling operations. The labels “PD” and “Hopf” are used to mark the period-doubling and Hopf bifurcation windows, respectively.

different feed rates. The normalization is done so that the normalized ADOC is one for the constant time delay case. The deviations of stability lobes obtained for a system with variable time delay from the stability lobes obtained for a system with constant delay are clear and this deviation increases with increase in the feed rate.

The chatter frequencies associated with the unstable cutting cases are shown in Figure 3.15. There are two types of instabilities of periodic solutions that can lead to chatter. One of them is related to a secondary Hopf bifurcation, and the other is related to a period-doubling bifurcation. From Figure 3.15, one can see that the Hopf-bifurcation windows and period-doubling windows alternate. Since a pair of complex eigenvalues of Φ crosses the unit circle in the case of a Hopf bifurcation, the chatter frequencies occur in duplicates.

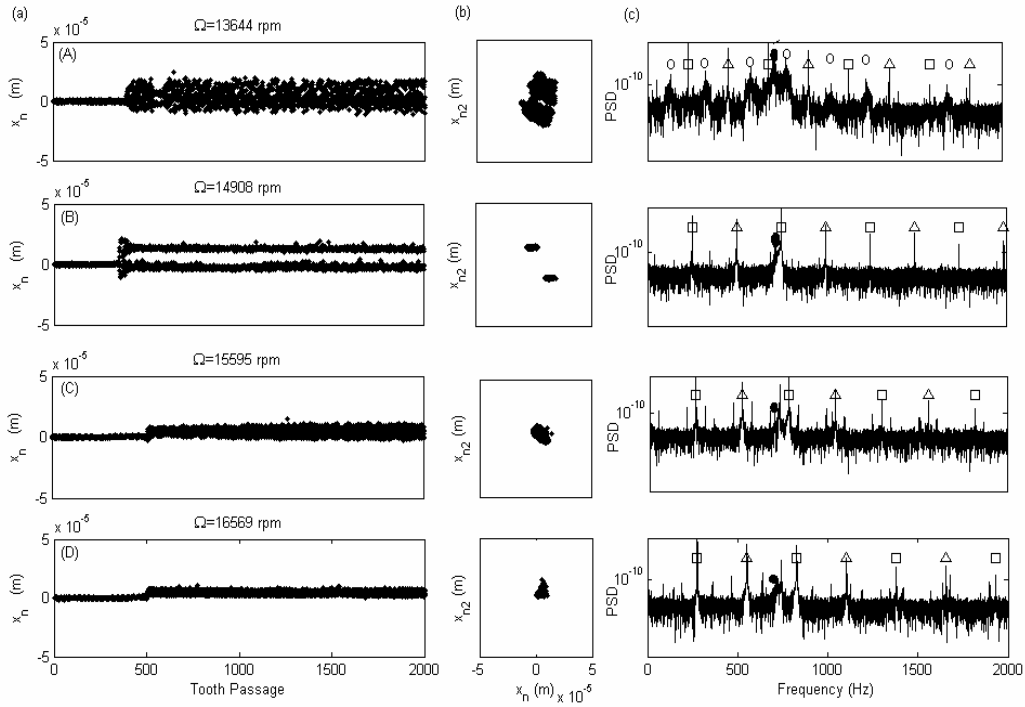


Figure 3.16: Experimental results obtained for a 5% immersion down-milling case: (a) 1/rev sampled signals; (b) Poincaré sections; and (c) power spectra. The cases A, B, C, and D shown here correspond to cases A, B, C, and D of Figure 3.13. The symbols \circ , \square , Δ , and \bullet , are used to mark the Hopf chatter frequencies f_H , the period-doubling chatter frequencies f_{PD} , the tooth-passing frequencies f_{TP} , and the damped natural frequency, respectively.

In Figure 3.16, the experimental results corresponding to locations A, B, C, and D on the stability charts of Figure 3.13 are shown. The results of case A correspond to a post-bifurcation motion following a secondary Hopf bifurcation, and the dominant frequencies are the Hopf chatter frequencies f_H . In the present case, these frequencies are not synchronized with f_{TP} . The results of Case B correspond a post-bifurcation motion following a period-doubling bifurcation. Case C corresponds to a critical case, and Case D corresponds to stable cutting. In the power spectra shown for all the cases, it is believed that multiples of one half of the tooth pass frequency may be due to “dynamic” run out in the tool.

In Figure 3.17, the stability charts are presented for 5% immersion up-milling operations. The results show that the stability chart obtained for the system with the constant delay is different from the stability charts obtained for variable time delays with different feed rate. There is a shift between the stability chart obtained for system with the constant delay and the stability charts obtained for system with a variable time delay. The shift increases as the feed rate is increased. The feed-rate effects depend on the ratio f/R . As the feed rate is increased, the differences between the stability charts obtained for the system with a constant delay and for the system with a variable delay become more pronounced. Other effects such as loss of contact effects may also be dominant in the dynamics of low-immersion milling operation. This is confirmed by comparing the feed-rate effects on the stability charts for low-immersion milling operations and the feed-rate effects in the stability charts for high-immersion and full-immersion milling operations.

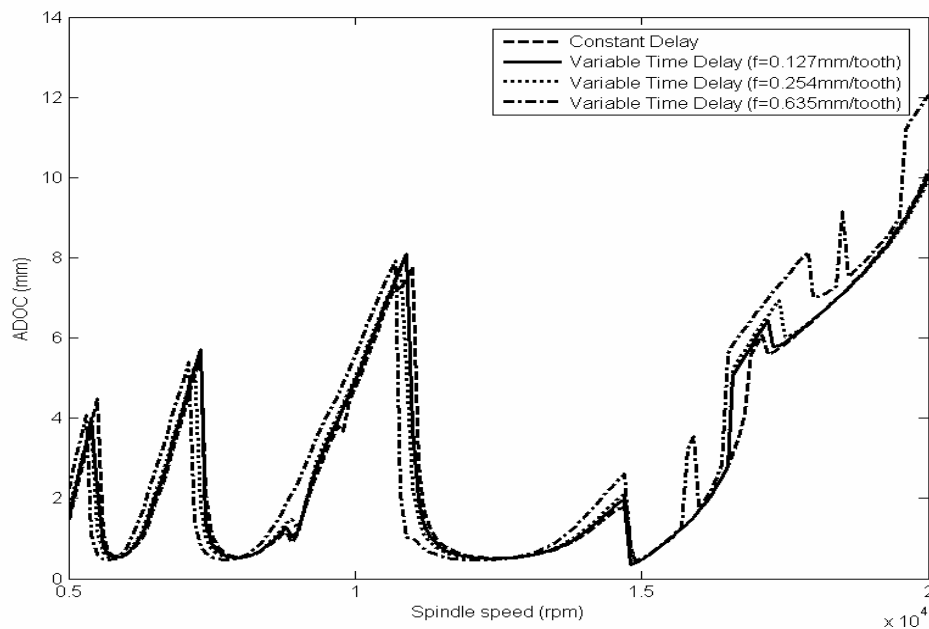


Figure 3.17: Stability charts for 5% immersion up-milling operations.

To examine the feed-rate effects for different immersion ratios, the immersion ratio is increased up to 25%, 50%, and 75% and the corresponding stability charts are shown in Figure 3.18, 3.19, and 3.20. In these Figures, the difference between the stability charts obtained for the system with constant delay and the stability lobes obtained for the system with a variable delay is not as noticeable as that seen in Figure 3.17. This difference decreases with the increase in the immersion rate. In Figure 3.21, the stability charts for full-immersion milling operations are shown. Observing Figure 3.21, the stability charts obtained for the system with constant delay and stability charts obtained for system with a variable time delay are close each other, even when the ratio f/R goes up to 0.1. The feed-rate effects on the stability charts is pronounced in low-immersion milling operations, and can be ignored in the case of full or high-immersion milling operations. In Figure 3.22, the chatter frequencies associated with the unstable cutting cases are shown. There is only one type of instability of a periodic solution that leads to chatter, namely, the secondary Hopf bifurcation. This is different with the case of low-immersion milling operations, where two types of instabilities can lead to chatter, a secondary Hopf bifurcation, and a period-doubling bifurcation. It is believed that the chatter due to period-doubling bifurcation is a result of the loss of contact effects that become prominent as the immersion ratio is reduced.

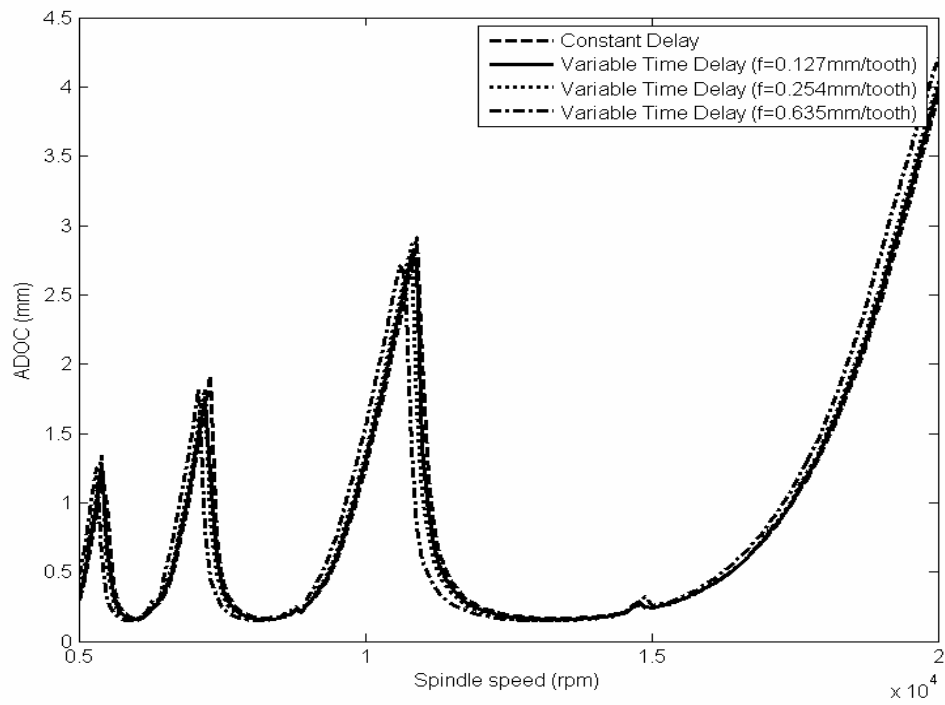
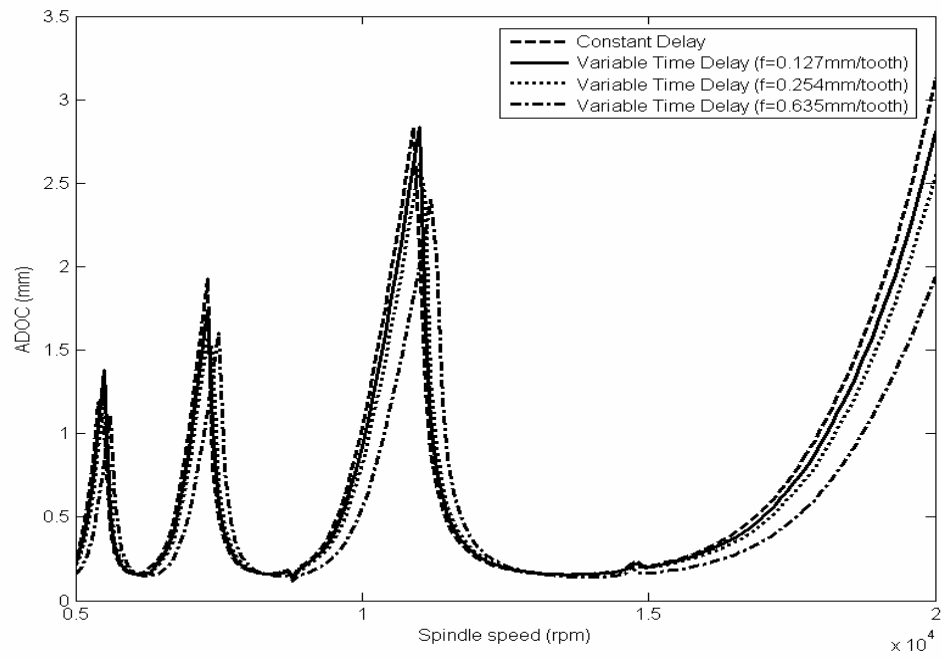


Figure 3.18: Stability charts for 25% immersion: (a) down-milling operation and (b) up-milling operations

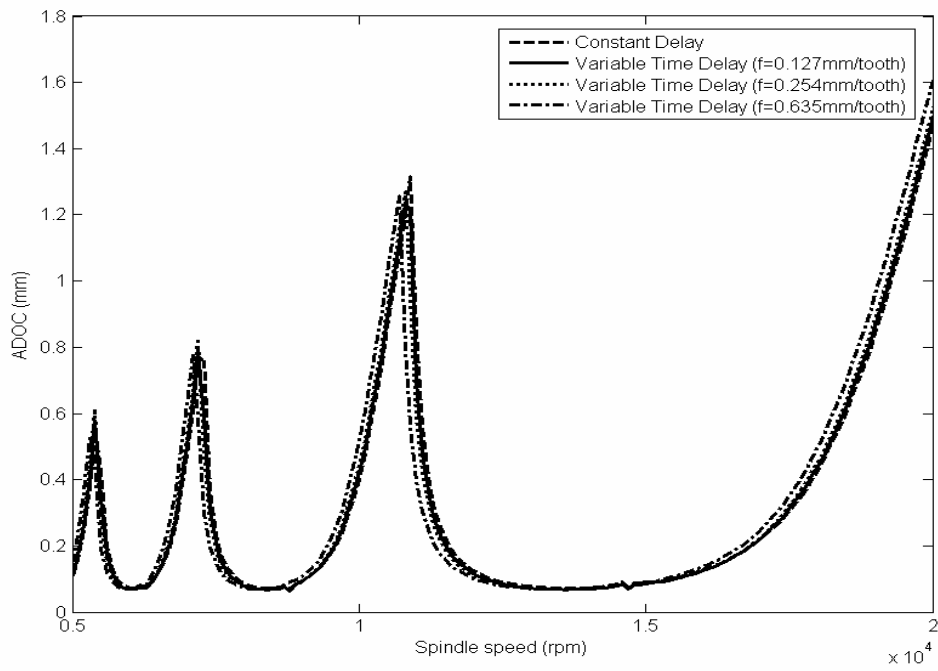
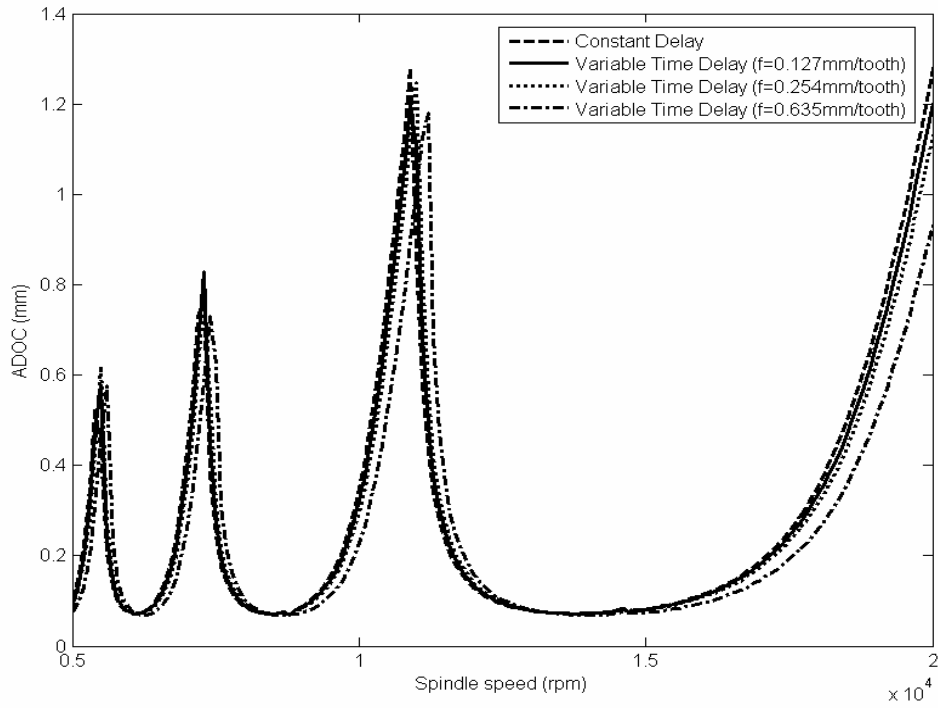


Figure 3.19: Stability charts for 50% immersion: (a) down-milling operation and (b) up-milling operations

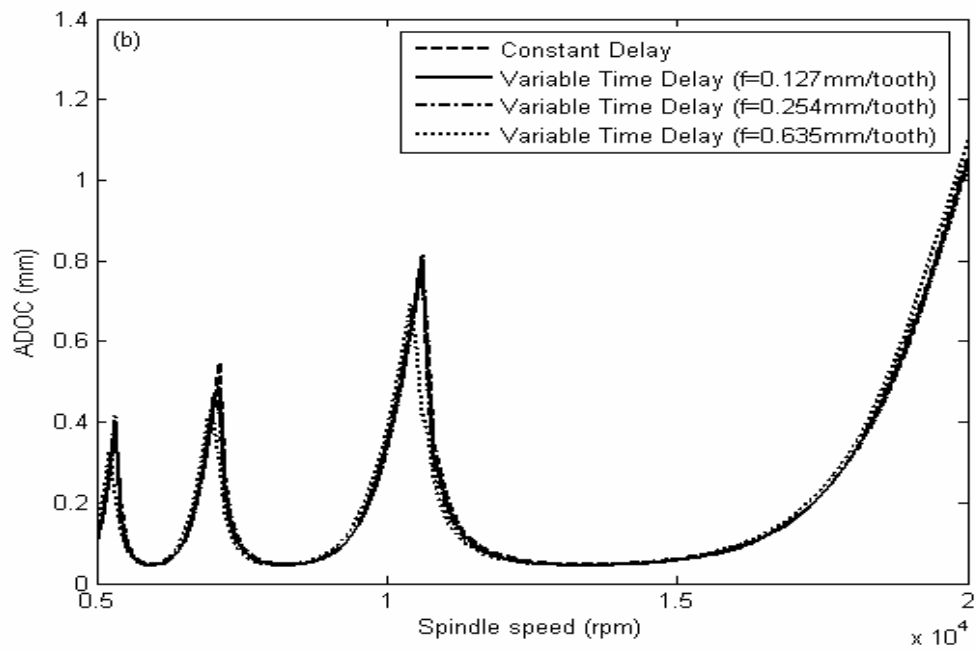
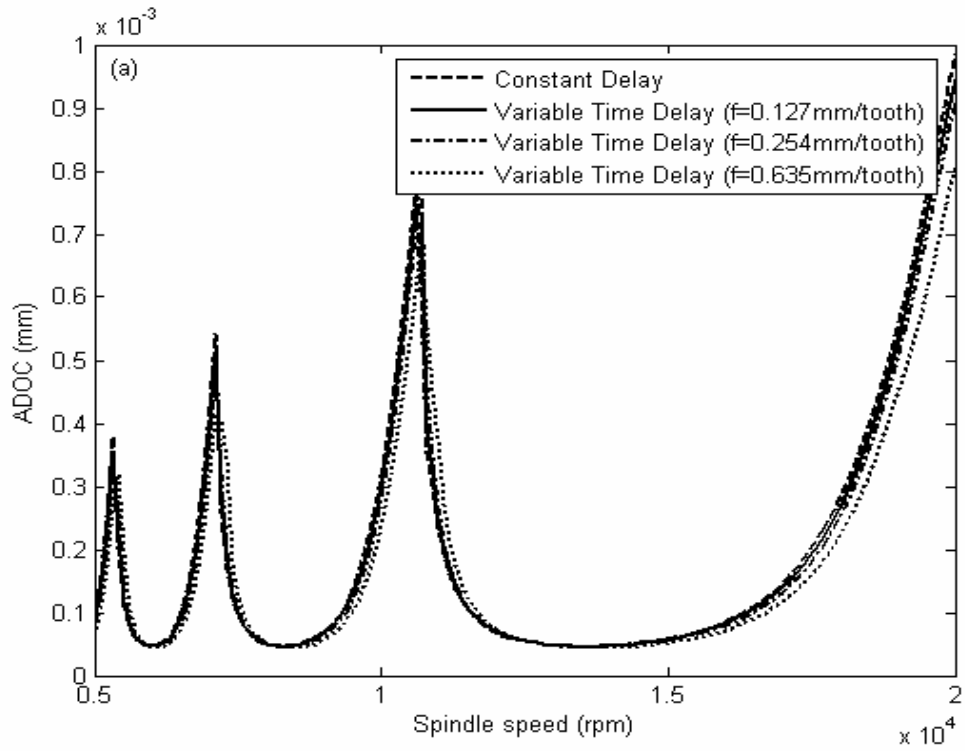


Figure 3.20: Stability charts for 75% immersion: (a) down-milling operation and (b) up-milling operations.

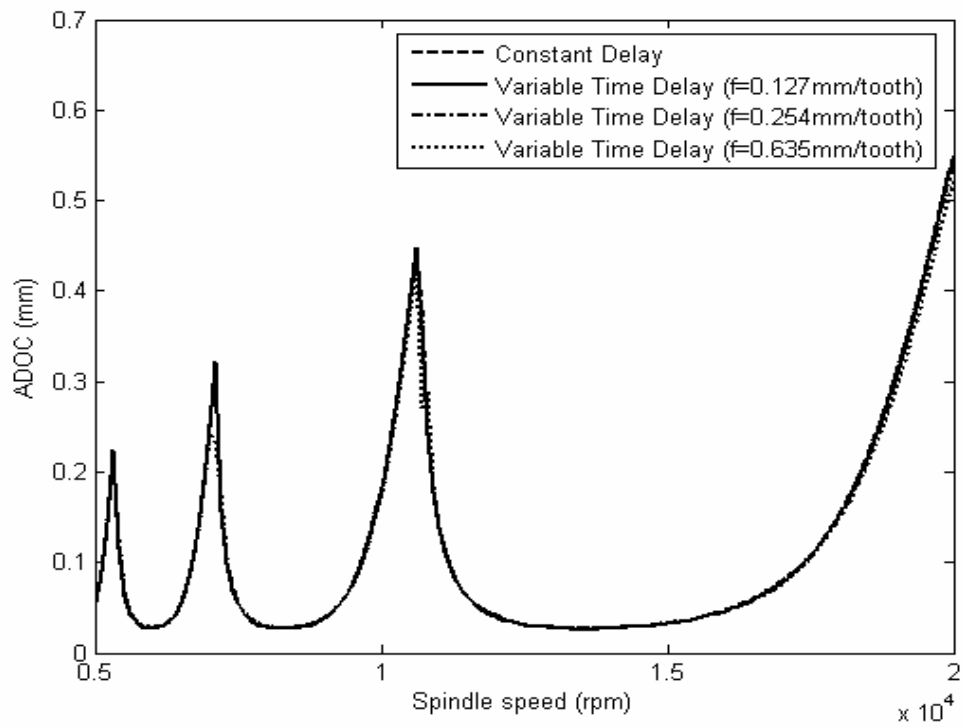


Figure 3.21: Stability charts for full-immersion milling operations.

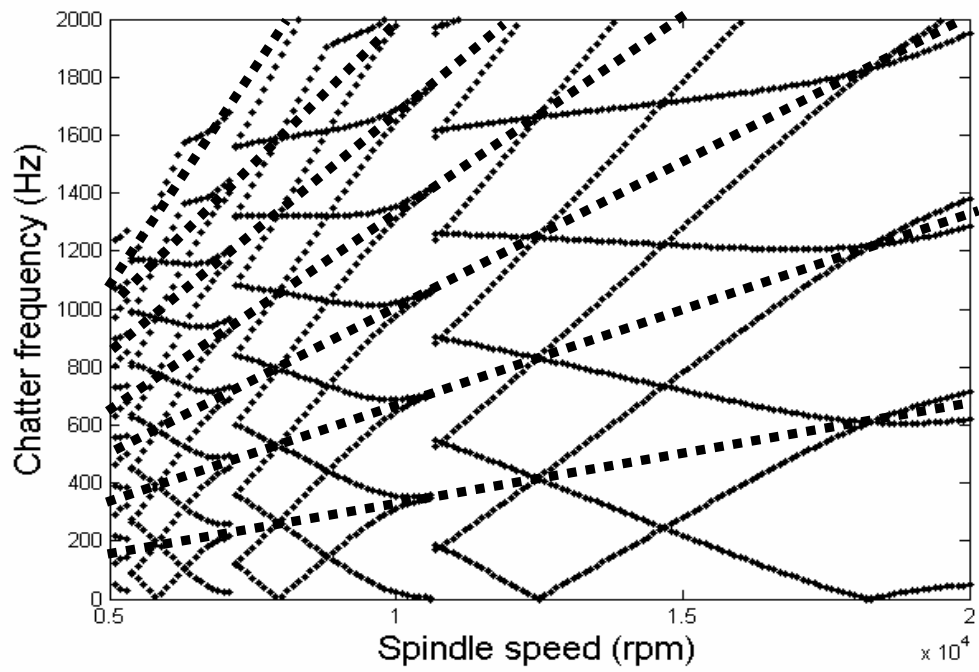


Figure 3.22: Chatter frequencies for full-immersion milling operations with $f=0.127$ mm/tooth.

For another case study, the workpiece-tool system modal parameters and the tool and cutting parameters are chosen as shown in Tables 3.3 and 3.4. Figures 3.23 and 3.24 represent a pair of results obtained for up-milling and down-milling operations for 10% immersion value. Similar to the results show in Figure 3.16, there is a shift between the stability charts obtained for system with the constant delay and the stability charts obtained for system with variable time delay. The shift increases as the feed rate is increased. The feed-rate effects depends on the ratio f/R .

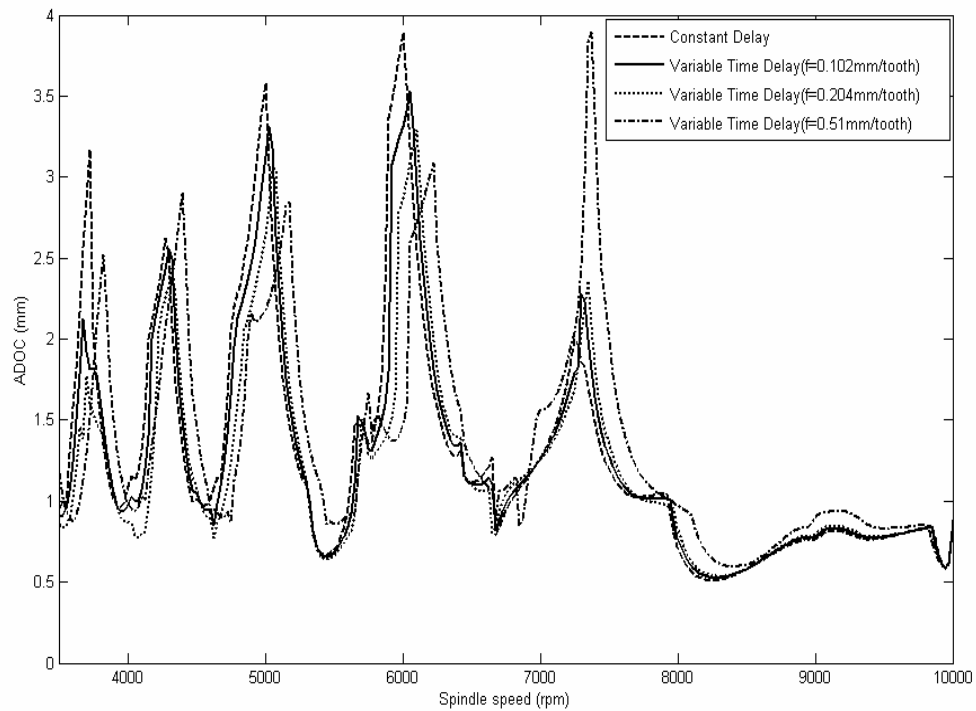


Figure 3.23: Stability predictions for 10% immersion down-milling operations.

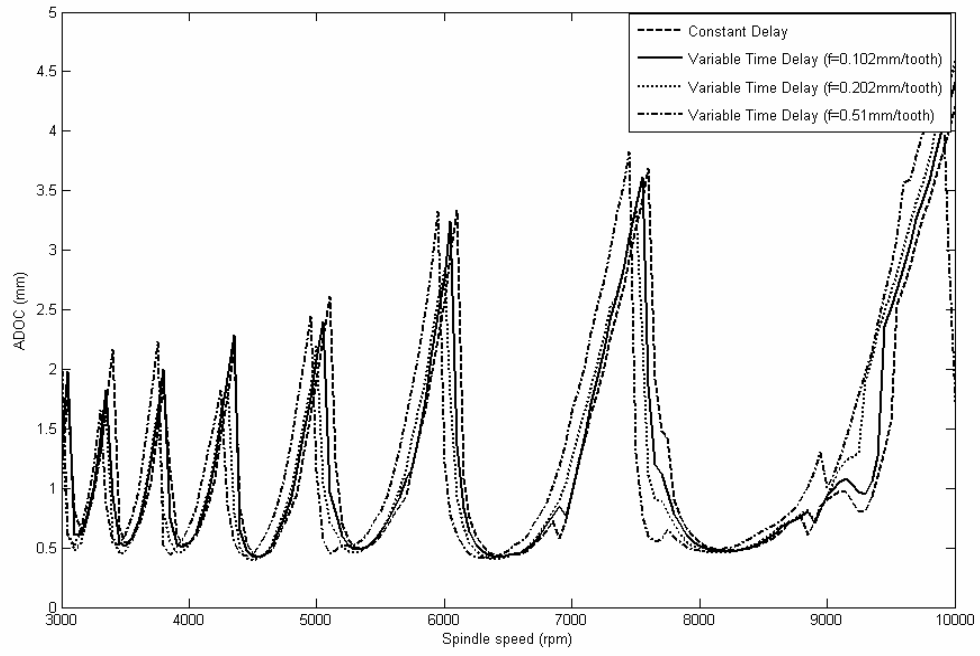


Figure 3.24: Stability predictions for 10% immersion up-milling operations.

Chapter 4

Dynamics of Variable Spindle Speed (VSS) Milling

Processes

Continuous variation of the cutting speed could help suppress the chatter that develops during conventional, constant speed machining. Similar to the modeling of constant spindle speed milling processes, a mechanics based model is presented for the variable spindle speed (VSS) machining. The dynamics of VSS milling processes is described by a set of DDEs with periodic coefficients and a time varying delay. This variation is caused by superimposing a sinusoidal modulation on a nominal spindle speed. The semi-discretization scheme is refined to study the stability of DDEs with time varying periodic coefficients and time varying delay and the stability charts are constructed as discussed the previous chapter. The benefits of VSS milling operations are discussed by comparing the stability charts of VSS milling operations with those obtained for constant spindle speed (CSS) milling operations.

4.1. Milling Model with Variable Spindle Speed

Referring to Figure 2.9, the governing equation of motion of VSS milling processes is written as

$$\left. \begin{aligned} m_x \ddot{q}_x + c_x \dot{q}_x + k_x q_x &= F_x(t; \tau(t)) \\ m_y \ddot{q}_y + c_y \dot{q}_y + k_y q_y &= F_y(t; \tau(t)) \\ m_u \ddot{q}_u + c_u \dot{q}_u + k_u q_u &= F_u(t; \tau(t)) \\ m_v \ddot{q}_v + c_v \dot{q}_v + k_v q_v &= F_v(t; \tau(t)) \end{aligned} \right\} \quad (4.1)$$

Similar to the derivation of cutting force discussed in chapter 2, one can write the governing equation of motion as follows

$$\dot{\mathbf{Q}}(t) = \mathbf{W}_0(t)\mathbf{Q}(t) + \mathbf{W}_1(t)\mathbf{Q}(t - \tau(t)) + \begin{bmatrix} \mathbf{0} \\ \bar{\mathbf{K}}(t)f \end{bmatrix} \quad (4.2)$$

where $\mathbf{W}_0(t)$ is the coefficient matrix associated with present states and $\mathbf{W}_1(t)$ is the coefficient matrix associated with delayed states and they are given by

$$\mathbf{W}_0(t) = \begin{bmatrix} \mathbf{0} & \mathbf{I} \\ -\mathbf{M}^{-1}[\mathbf{K} - \hat{\mathbf{K}}(t)] & -\mathbf{M}^{-1}\mathbf{C} \end{bmatrix} \quad \text{and} \quad \mathbf{W}_1(t) = \begin{bmatrix} \mathbf{0} & \mathbf{0} \\ -\mathbf{M}^{-1}\hat{\mathbf{K}}(t) & \mathbf{0} \end{bmatrix} \quad (4.3)$$

The time-periodic matrices $\hat{\mathbf{K}}(t)$, $\bar{\mathbf{K}}(t)$, and $\hat{\mathbf{K}}^i(t, z)$ are of the form

$$\hat{\mathbf{K}}(t) = \sum_{i=1}^N \int_{z_i(t,i)}^{z_{i+1}(t,i)} \hat{\mathbf{K}}^i(t, z) dz, \quad \bar{\mathbf{K}}(t) = \tau(t) \begin{bmatrix} \hat{k}_{11}(t) \\ \hat{k}_{21}(t) \\ \hat{k}_{11}(t) \\ \hat{k}_{21}(t) \end{bmatrix}, \quad \text{and}$$

$$\hat{\mathbf{K}}^i(t, z) = \begin{bmatrix} \hat{k}_{11}^i(t, z) & \hat{k}_{12}^i(t, z) & \hat{k}_{11}^i(t, z) & \hat{k}_{12}^i(t, z) \\ \hat{k}_{21}^i(t, z) & \hat{k}_{22}^i(t, z) & \hat{k}_{21}^i(t, z) & \hat{k}_{22}^i(t, z) \\ \hat{k}_{11}^i(t, z) & \hat{k}_{12}^i(t, z) & \hat{k}_{11}^i(t, z) & \hat{k}_{12}^i(t, z) \\ \hat{k}_{21}^i(t, z) & \hat{k}_{22}^i(t, z) & \hat{k}_{21}^i(t, z) & \hat{k}_{22}^i(t, z) \end{bmatrix} \quad (4.4)$$

The coefficient matrix $\mathbf{W}_0(t)$, $\mathbf{W}_1(t)$, and $\bar{\mathbf{K}}(t)$ are piecewise, periodic functions of time with period T . For CSS milling processes, $T = 2\pi/N\Omega_0$, and for VSS milling processes, T is determined by the nominal spindle speed Ω_0 , the number of tooth N , and the modulation frequency ω_m .

Noting that the spindle speed is time varying, in equation (2.35), the variable $\theta(t, i, z)$ is determined as

$$\theta(t, i, z) = \int_0^t \Omega(s) ds - (i-1) \frac{2\pi}{N} - \frac{\tan \eta}{R} z + \theta_0 \quad (4.5)$$

where $\Omega(t)$ is the spindle speed. In this effort, the sinusoidal modulation of the spindle speed is considered as

$$\Omega(t) = \Omega_0 + \Omega_1 \sin(\omega_m t) = \Omega_0 \left[1 + RVA \sin(RVF \cdot \Omega_0 t) \right] \quad (4.6)$$

Where Ω_0 is the nominal spindle speed, Ω_1 is the amplitude of speed variation, ω_m is the frequency of speed variation, $RVA = \Omega_1/\Omega_0$ is the ratio of speed variation amplitude to the nominal spindle speed, and $RVF = \omega_m/\Omega_0$ is the ratio of the speed variation frequency to the nominal spindle speed, respectively. After substituting (4.6) into (4.5), one can obtain

$$\theta(t, i, z) = \Omega_0 t + \frac{RVA}{RVF} \left[1 - \cos(\omega_m t) \right] - (i-1) \frac{2\pi}{N} - \frac{\tan \eta}{R} z + \theta_0 \quad (4.7)$$

This delay in equation (4.2) is determined as follows

$$\int_{t-\tau(t)}^t \Omega(s) ds = \frac{2\pi}{N} \quad (4.8)$$

After substituting (4.6) into (4.8) and integrating (4.8), one can obtain

$$\Omega_0 \tau(t) + \frac{\Omega_1}{\omega_m} \cos(\omega_m (t - \tau(t))) - \frac{\Omega_1}{\omega_m} \cos(\omega_m t) = \frac{2\pi}{N} \quad (4.9)$$

One can't get a closed form solution for $\tau(t)$ from equation (4.9). For “small” RVA and “small” RVF , $\tau(t)$ can be approximated as

$$\tau(t) \approx \tau_0 \left[1 - \left(1 - RVA \sin(\omega_m t - \phi) \right) RVA \sin(\omega_m t - \phi) \right] \quad (4.10)$$

where

$$\tau_0 = \frac{2\pi}{N\Omega_0} \quad \text{and} \quad \phi = \frac{2\pi \cdot RVF}{N} \quad (4.11)$$

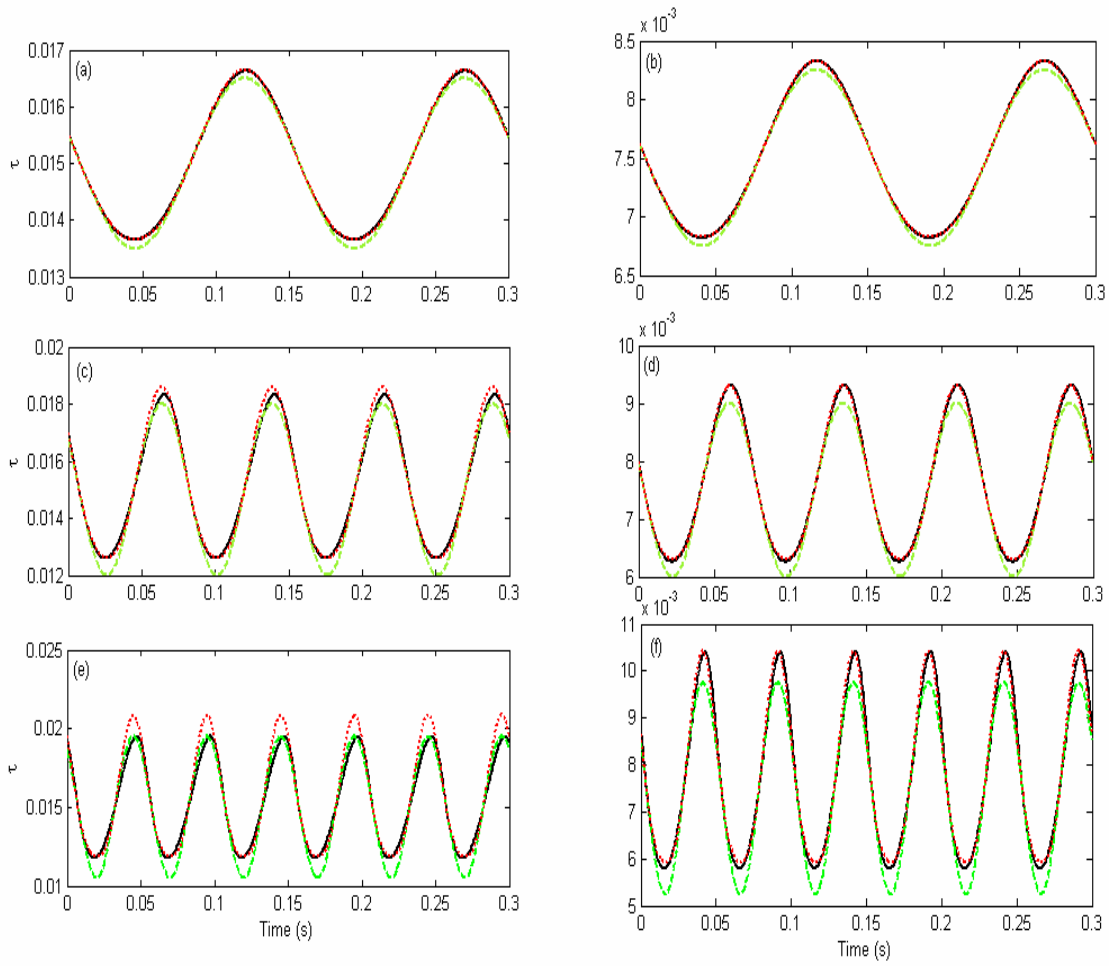


Figure 4.1: Exact and approximated delays for $\Omega_0 = 4000$ rpm: (a,b) $N=1, 2, RVA=0.1, RVF=0.1$, (c,d) $N=1, 2, RVA=0.2, RVF=0.2$, and (e,f) $N=1, 2, RVA=0.3, RVF=0.3$. (— Exact Delay; --- Approximated Delay (Current); Approximated Delay (Former)).

In Figure 4.1, the exact time delay and the approximated time delay obtained for the nominal spindle speed $\Omega_0 = 4000$ rpm and different number of cutting tooth, RVA , and RVF are presented. The numerical solution for $\tau(t)$, which is obtained by solving (4.9) is denoted by the legend “exact delay” (solid line) in these figures. The legend “Approximated Delay (Former)” (dashed line) denotes the approximation used in former research efforts (Sastry, etc. al, 2001, Insperger and Stépán, 2004). The legend

“Approximated Delay (Current)” denotes the time delay that has been determined by (4.10) (dotted line). From Figure 4.1, one can say the delay approximation, which is determined by (4.10), agree better with the exact delay compared to the delay approximation that was used in previous research efforts. The maximum deviation between the exact numerical solution and the delay approximation given by equation (4.10), are 0.28 % for one tooth with 0.1 modulation (4.1a), 0.09 % for two teeth with 0.1 modulation (4.1b), 2.6 % for one tooth with 0.2 modulation (4.1c), 0.85 % for two teeth with 0.2 modulation (4.1d), 9.3 % for one tooth with 0.3 modulation (4.1e), 3.2 % for two teeth with 0.3. modulation (4.1f). In further analysis, (4.10) is used to approximate the delay. From (4.10), one can determine

$$\tau(t) \leq \tau_{\max} = \tau_0 [1 + (1 + RVA) RVA] \quad (4.12)$$

4.2. Numerical Results for VSS Milling Processes

In this section, stability predictions obtained through the semi-discretization technique are presented for two different systems. The stability charts obtained for VSS milling processes are compared with those obtained for of CSS milling processes and the comparisons are discussed.

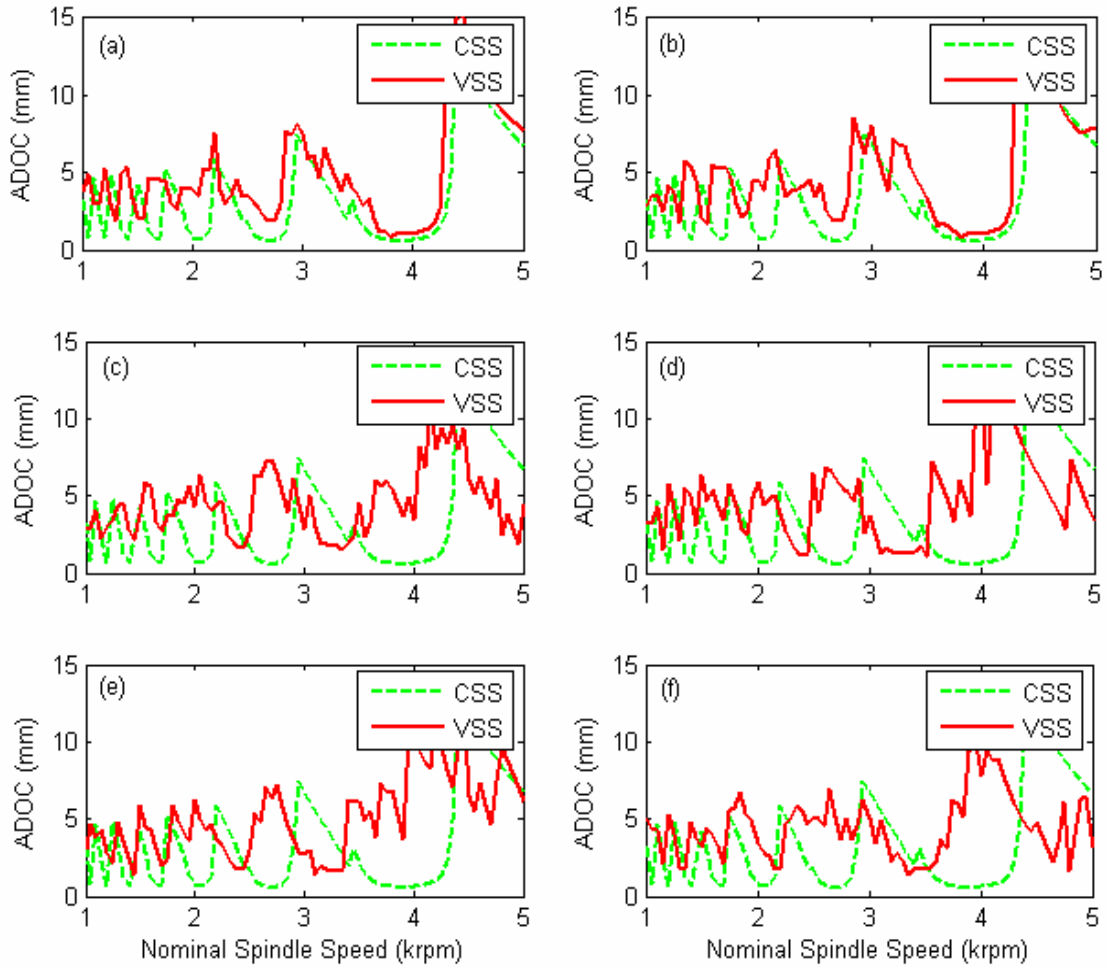


Figure 4.2: Stability predictions for 25% immersion down-milling operations: (a) $RVA=0.1$, $RVF=0.1$, (b) $RVA=0.1$, $RVF=0.2$, (c) $RVA=0.2$, $RVF=0.1$, (d) $RVA=0.2$, $RVF=0.2$, (e) $RVA=0.2$, $RVF=0.3$, and (f) $RVA=0.3$, $RVF=0.3$.

The first system considered is a single degree-of-freedom system; the corresponding workpiece-tool system modal parameters are given in Table 3.1. The tool and cutting parameters are provided in Table 3.2. Since, the tool helix angle is zero in this case, the cutting forces along the X-direction and the Y-direction do not depend on the normal rake angle and the friction coefficient, both of which are not provided in Table 3.2. In Figure 4.2, the stability charts are presented for 25% immersion down-milling

operations. Comparing the stability lobes for VSS milling processes with those obtained for CSS milling processes, one can observe the difference between these two different milling processes are obvious for low spindle speed operations such as in the range from those 500 rpm to 2500 rpm for all the selected RVA and RVF values. The stability lobes are quite flat in the low spindle speed range for VSS milling, and this suggests that the stability of VSS milling is robust with respect to variations in the natural frequency and the nominal spindle speed. With the increase of the nominal spindle speed value, the stability lobes for VSS milling are close to those obtained for the CSS milling in the high spindle speed range (2500 rpm to 5000 rpm) when $RVA=0.1$ (see Figures 4.2a,b). For $RVA=0.2, 0.3$, and $RVF=0.1, 0.2$, and 0.3 (see Figures 4.2c, d, e, and f), the VSS milling operations permit larger ADOC than that possible with CSS milling operations in some of the spindle speed ranges.

In order to investigate the effect of spindle speed variation on the different dominant modes of vibration of workpiece-tool structure system, a system with multiple degrees of freedom is studied. Referring to Figure 2.9, the workpiece-tool system modal parameters and the tool and cutting parameters are chosen as shown in Tables 4.1 and 4.2.

Table 4.1. Modal parameters of a two-degree-of-freedom workpiece-tool system.

Mode	frequency (Hz)	damping (%)	modal stiffness (N/m)	modal mass (kg)
tool (X)	729.07	1.07	9.14×10^5	4.36×10^{-2}
tool (Y)	728.83	1.0	1.0×10^6	4.78×10^{-2}

Table 4.2. Machining parameters for a two-degree-of-freedom workpiece-tool system.

normal rake angle (φ_n)	helix angle (η)	tooth number	Radius (mm)	$k_t(Mpa)$	k_n	cutting friction coefficient (μ)
6^0	40^0	2	6.35	600	0.42	0.2

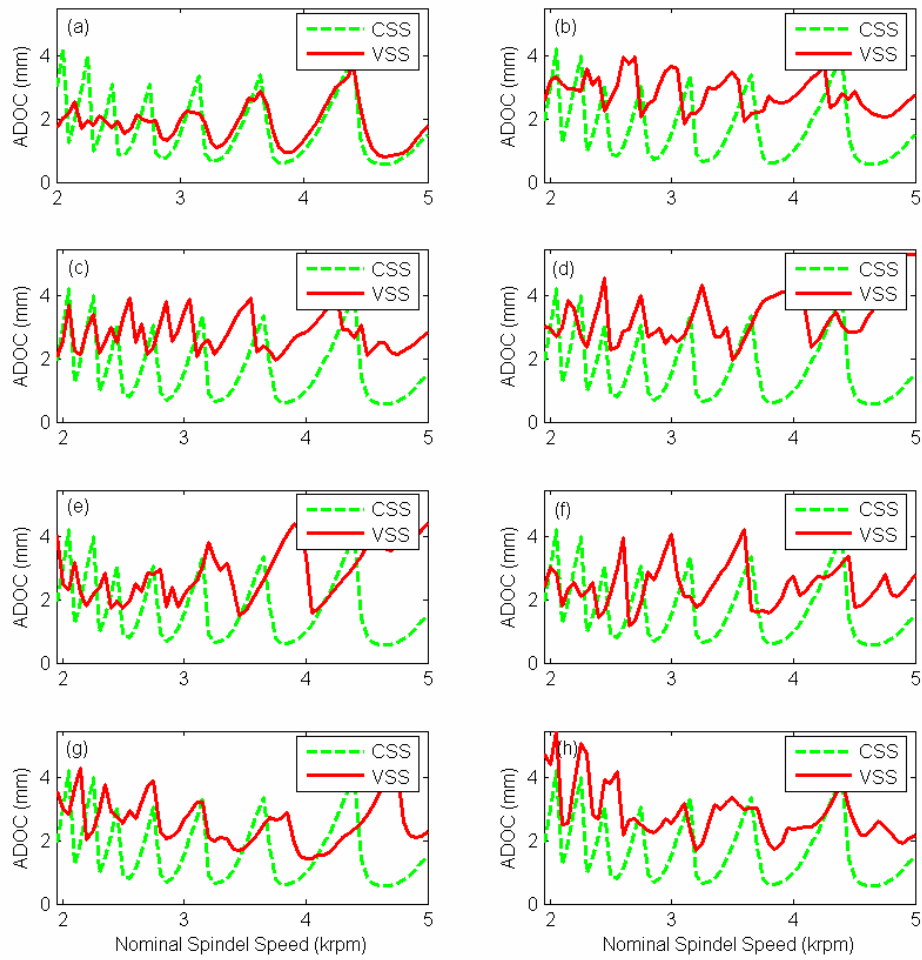


Figure 4.3: Stability predictions for 5% immersion up-milling operations: (a) $RVA=0.05$, $RVF=0.05$, (b) $RVA=0.1$, $RVF=0.1$, (c) $RVA=0.1$, $RVF=0.2$, (d) $RVA=0.2$, $RVF=0.1$, (e) $RVA=0.2$, $RVF=0.2$, (f) $RVA=0.3$, $RVF=0.2$, (g) $RVA=0.2$, $RVF=0.3$, and (h) $RVA=0.3$, $RVF=0.3$.

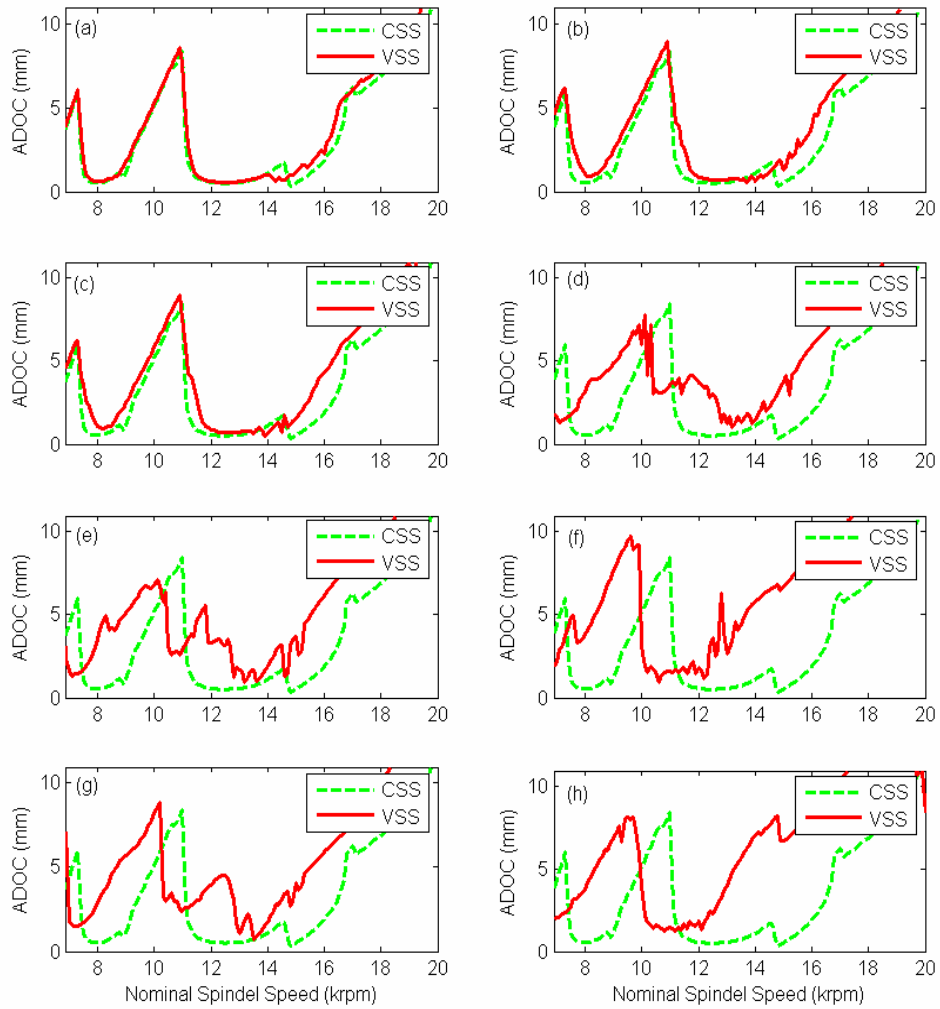


Figure 4.4: Stability predictions for 5% immersion up-milling operations: (a) $RVA=0.05$, $RVF=0.05$, (b) $RVA=0.1$, $RVF=0.1$, (c) $RVA=0.1$, $RVF=0.2$, (d) $RVA=0.2$, $RVF=0.1$, (e) $RVA=0.2$, $RVF=0.2$, (f) $RVA=0.3$, $RVF=0.2$, (g) $RVA=0.2$, $RVF=0.3$, and (h) $RVA=0.3$, $RVF=0.3$.

In Figure 4.3, the stability charts are presented for 5% immersion down-milling operations. From Figure 4.3a, one can say the permitted ADOC for VSS milling operations is different with that of CSS milling operations at low nominal spindle speed, such as in the range from those 2000 rpm to 3000 rpm when $RVA=0.05$ and $RVF=0.05$. The stability lobes are quite flat in the low spindle speed range for VSS

milling, and this suggests that the stability of VSS milling is robust with respect to variations in the natural frequency and the nominal spindle speed. This is similar with the results shown in Figure 4.2. When the $RVA \geq 0.1$ and $RVF \geq 0.1$, such as shown in Figure 4.3b, c, d, e, f, g, and h, throughout the considered spindle speed range, the permitted ADOC for VSS milling operations is larger than that obtained for the corresponding CSS milling operations. The results also show the robustness of the stability of VSS milling processes to the nominal spindle speed variation. One can discern the differences among the stability lobes of VSS and CSS for spindle speeds up to 5000 rpm, beyond which the stability lobes are close to each other. It is noted that the first natural frequency (728.83Hz) of this system is larger than that of the previous single degree-of- freedom system (146.6Hz). For higher spindle speeds, the results are shown in Figure 4.4. From this figure, one can say that the stability lobes for VSS milling are close to those obtained for CSS milling when $RVA \leq 0.1$ (Figures 4.4a, b, c). For higher values of RVA; that is, 0.2 and 0.3, the stability charts are shown in Figures 4.4d, e, f, g, and h. One can find that the stability range is improved and this improvement is extended to the high speed range. However, the permitted ADOC limit for VSS is lower than that obtained for the CSS in certain spindle speed ranges. This is similar to the results shown in Figure 4.2.

Chapter 5

Nonsmooth Dynamics

Due to the loss of contact between the workpiece and tool, the system of equations governing a milling process has a piecewise smooth right-hand side and this system is an example of a nonsmooth system. There are many bifurcations that occur in nonsmooth system, which are different from the conventional bifurcations that occur in a smooth system. In this chapter, the nonsmooth characteristics of milling operations are further examined. The dynamics of an elastic cantilever beam subjected to a repeated impact, which is similar to a simplified model of the milling process (Davies and Balachandran, 2000), is investigated by means of experiments and simulations. The test apparatus consisted of a stainless-steel cantilever beam with a tip mass, which is impacted by a shaker. The shaker excitation frequency and excitation amplitude are used as control parameters. Case of soft impact and hard impact between the impactor and the structure are considered, and the results are presented in the form of bifurcation diagrams, phase portraits, and contact forces. Considering the response of the system to be dominated by the beam's fundamental mode, a single-degree-of-freedom model is developed and numerical studies are conducted by using this model. This representative system is used to examine loss of contact dynamics in a milling process.

5.1. Nonsmooth Characteristics of Milling Processes

Revisiting equations (2.28), (2.53), and (4.1), the general form of governing equations of motion of milling processes can be put in the form

$$\left. \begin{aligned} m_x \ddot{q}_x + c_x \dot{q}_x + k_x q_x &= F_x(t; h) \\ m_y \ddot{q}_y + c_y \dot{q}_y + k_y q_y &= F_y(t; h) \\ m_u \ddot{q}_u + c_u \dot{q}_u + k_u q_u &= F_u(t; h) \\ m_v \ddot{q}_v + c_v \dot{q}_v + k_v q_v &= F_v(t; h) \end{aligned} \right\} \quad (5.1)$$

In these equations, the cutting forces, F_x, F_y, F_u , and F_v , are piecewise functions of time and the uncut chip thickness. Systems (2.28), (2.53), (4.1), and (5.1) can be referred to as nonsmooth systems.

In Figure 5.1, the simulated cutting forces are shown for the four-degree-of-freedom system during 10% immersion up-milling operations discussed previously. The forces are obtained in terms of the $F_r = \sqrt{F_x^2 + F_y^2}$ for different cutting condition. For stable cutting at $ADOC=1.2\text{mm}$ and $\Omega = 14200$ rpm, the cutting forces are periodic and the cutting forces are zeros, when there is loss of contact between tool and workpiece. For period-doubling cutting at $ADOC=2.4$ mm and $\Omega = 14200$ rpm, the cutting forces show a period-doubled character with two different peak values and the cutting force goes to zero when there is loss of contact between the tool and workpiece, which is due to the cutter rotation that results in the periodic engagement and disengagement. For unstable cutting at $ADOC=4.8$ mm and $\Omega = 14200$ rpm, the cutting forces have a chaotic character. There are two factors that lead to the loss of contact between tool and workpiece. One is low-immersion and the other is the jump out of workpiece. In case (d), when $ADOC=0.45$ mm and $\Omega = 12330$ rpm, the cutting forces have a period-doubled character with three different peak values and the loss of contact between tool and workpiece is due to the low-immersion operation and a jump out of workpiece. It is different from the results of case (b).

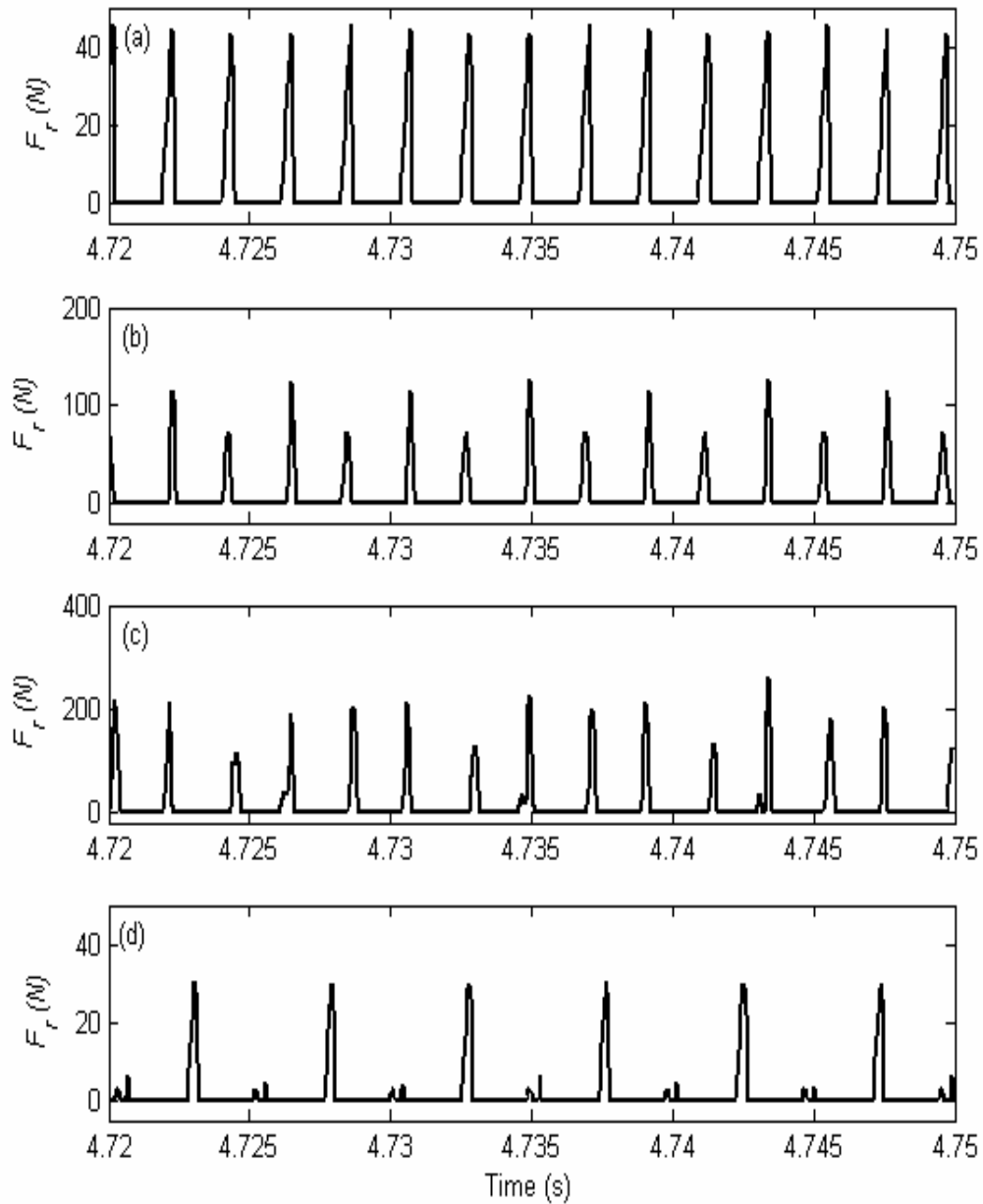


Figure 5.1: Simulated cutting forces for four degree-of-freedom system during 10% immersion up-milling operations: (a) cutting during periodic motions when $ADOC=1.2$ mm and $\Omega=14200$ rpm, (b) cutting during period-doubled motions when $ADOC=2.4$ mm and $\Omega=14200$ rpm, (c) cutting during chaotic motions when $ADOC=4.8$ mm and $\Omega=14200$ rpm, and (d) cutting during period-doubled motions (including jump of workpiece cutting) when $ADOC=0.45$ mm at $\Omega=12330$ rpm.

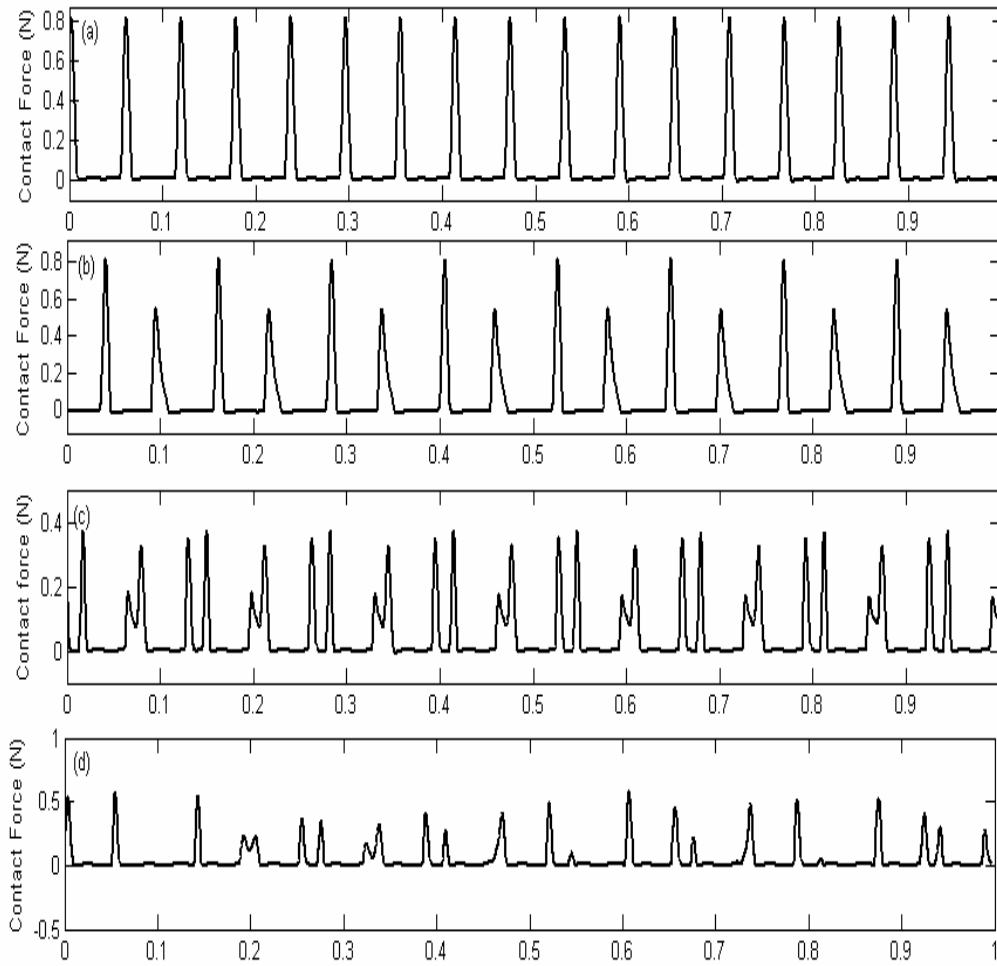


Figure 5.2: Experimental measurements of contact force in an impacted cantilever beam with a soft impact: (a) $\Omega/2\pi = 34.0$ Hz, periodic orbit, (b) $\Omega/2\pi = 33$ Hz, period-doubled orbit, (c) $\Omega/2\pi = 30.2$ Hz, period-doubled orbit, and (d) $\Omega/2\pi = 30.0$ Hz, chaotic orbit.

In Figure 5.2, the contact forces in an impacted cantilever beam with soft impact are shown. Comparing the cutting force as shown in Figure 5.1a with the contact force as shown in Figure 5.2a, one can find the cutting force in a periodic milling operation has the similar shape as that of the contact force in periodic motion of impacted cantilever beam. Similar results can be obtained by comparing Figure 5.1b with Figure 5.2b, Figure 5.1d with Figure 5.2c where both systems are in period-doubled motion, and Figure 5.1c with Figure 5.2d where both systems in chaotic motion. In

Figure 5.3, the phase plots for the cutting forces shown in Figure 5.1 are presented. In this figure, the space of (F_r, \dot{F}_r) is separated into two subspaces by the hypersurface $\Sigma_1 = \{(F_r, \dot{F}_r) \in (R^1 \times R^1) | F_r = 0\}$. If the orbit of cutting force, F_r , touches the hypersurface Σ_1 at a very low speed, that means $\dot{F}_r \rightarrow 0$. This case is referred to as a grazing or border collision. Grazing or border collisions can lead bifurcations different from the traditional bifurcations. In order to examine the bifurcations due to grazing or border collisions, the dynamics of an impacted cantilever beam is examined.

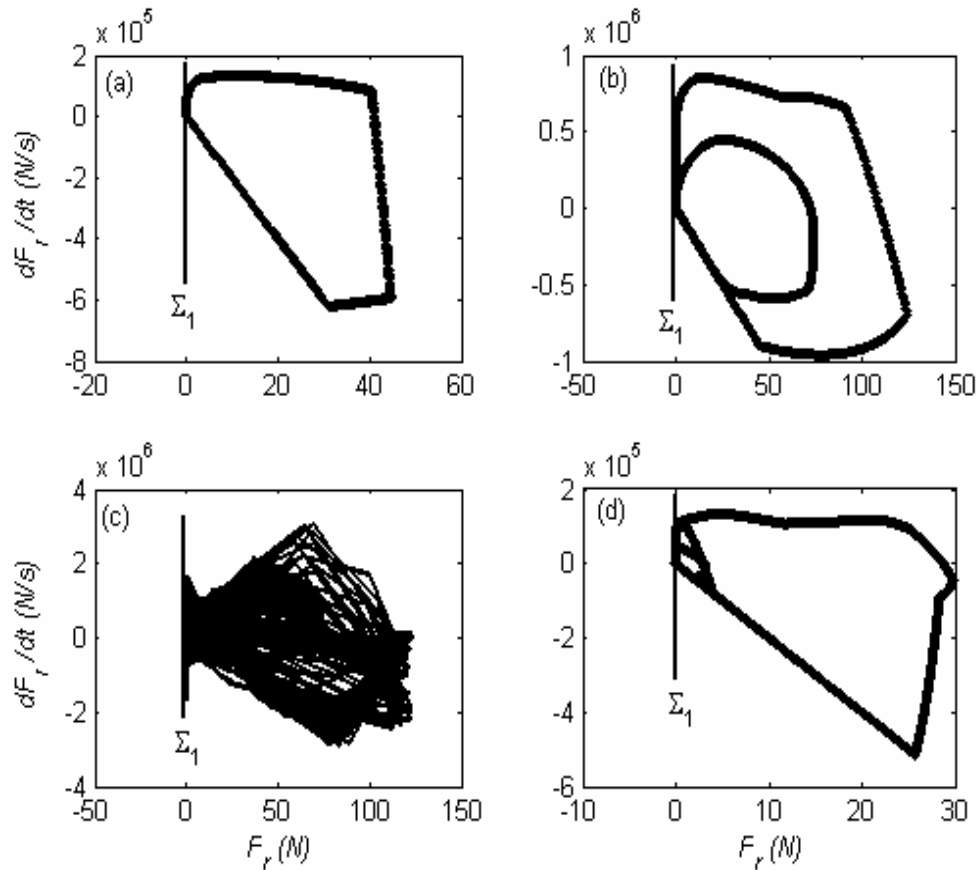


Figure 5.3: Cutting force phase plots for the four cases shown in Figure 5.1.

5.2. Model of Impacted Beam

In Figure 5.4, the schematic of an impacted cantilever beam with a tip mass is shown. Following earlier work (Balachandran 2003), the governing equation of motion for free oscillations is obtained as

$$\begin{aligned}
 0 = & \rho A \ddot{w} + EI w^{iv} - \rho Ag \left[w' + (s - \hat{l}) w'' \right] + mg w'' + \frac{3}{2} mg w'^2 w'' + EI \left[w' (w' w'')' \right]' \\
 & + \frac{1}{2} \rho A w' \frac{\partial}{\partial s} \left[\int_i^s \int_0^s \frac{\partial^2}{\partial t^2} (w'^2) d\hat{s} ds \right] - \rho Ag \left(\frac{1}{2} w'^3 + (s - \hat{l}) w'^2 w'' \right) ds \\
 & + \frac{1}{2} \rho A w'' \left[\int_i^s \int_0^s \frac{\partial^2}{\partial t^2} (w'^2) d\hat{s} ds \right] - \frac{1}{2} m w'' \int_0^i \frac{\partial^2}{\partial t^2} (w'^2)
 \end{aligned} \quad (5.2)$$

where ρ is the mass density of the elastic structure, A is the area of beam cross-section, EI is the flexural rigidity of the structure, m is the tip mass. The prime superscript represents a partial derivative with respect to the variable s , and the over-dot represents a time derivative. The boundary conditions without the nonlinear terms read as

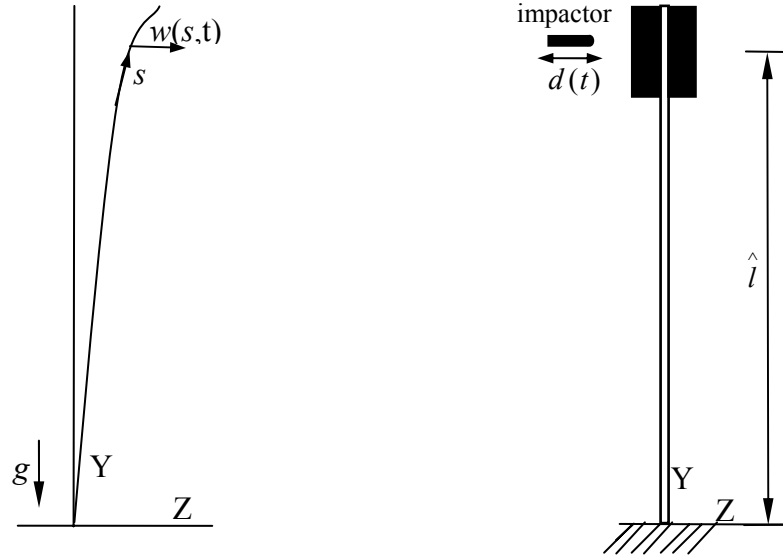


Figure 5.4: Model of an elastic cantilever beam subjected to impacts.

$$\begin{aligned}
w(s,t) &= 0 & \text{at } s = 0 \\
w'(s,t) &= 0 & \text{at } s = 0 \\
EIw'' + mgw' &= m\ddot{w} & \text{at } s = \hat{l} \\
EIw'' + J_m \ddot{w}' &= 0 & \text{at } s = \hat{l}
\end{aligned} \tag{5.3}$$

where J_m is the mass moment of inertia associated with the tip mass.

Equation (5.2) can be reduced to a series of ordinary differential equations by using the Galerkin approach. To this end, the solution for the transversal displacement $w(s,t)$ is written in the form

$$w(s,t) = \sum_{r=1}^{\infty} q_r(t) \phi_r(s) \tag{5.4}$$

where $q_r(t)$ is the temporal function associated with r th spatial function $\phi_r(s)$. This spatial function, which is given by the mode shape of a cantilever beam, has the form

$$\phi_r(s) = C_{1r} [\sin(\beta_r s) - \sinh(\beta_r s)] + C_{2r} [\cos(\beta_r s) - \cosh(\beta_r s)] \tag{5.5}$$

In equation (5.5), the ratios C_{2r}/C_{1r} and the eigenvalues β_r are to be determined from the characteristic equation. After substituting equation (5.4) into equation (5.2), taking advantage of the orthogonality of the modes, and retaining the first N modes, one obtains

$$\sum_{r=1}^N [m_r \ddot{q}_r + k_r q_r + c_r \dot{q}_r + a_{r1} q_r^3 + a_{r2} (\dot{q}_r^2 q_r + q_r^2 \ddot{q}_r)] = 0 \tag{5.6}$$

In this effort, the tip mass shown in Figure 5.4 is to be chosen, so that the first natural frequency of the structure is well separated from the second and higher frequencies. Hence, a single-mode approximation is used and the governing equation of motion is of the form

$$m_1 \ddot{q}_1 + k_1 q_1 + c_1 \dot{q}_1 + a_{11} q_1^3 + a_{12} [\dot{q}_1^2 q_1 + q_1^2 \ddot{q}_1] = 0 \quad (5.7)$$

where the cubic nonlinearities are geometric and inertia nonlinearities. The damping coefficient c_1 is determined from experiments. For completeness, the expressions for the coefficients that arise in equations (5.7) are shown in Appendix A.

In the experiments, as discussed in the next section, the impactor is driven by a harmonic excitation. During harmonic motions, the displacement of the impactor can be written as

$$d(t) = D \sin(\Omega t) \quad (5.8)$$

where D is the amplitude of the impactor's motion and Ω is the excitation frequency that is used as a control parameter for constructing the bifurcation diagram.

In the case of a hard impact, the impact is modeled by using an instantaneous coefficient of restitution and the impact is determined by the relative displacement

$$z(t) = w(s = \hat{l}, t) - d(t) \quad (5.9)$$

When only the first mode is considered, this relative displacement can be written as

$$z(t) = \phi_1(s = \hat{l}) q_1(t) - d(t) \quad (5.10)$$

The governing equations of beam subjected to an impact take the following form:

For $z(t) > z_c$

$$m_1 \ddot{q}_1 + k_1 q_1 + c_1 \dot{q}_1 + a_{11} q_1^3 + a_{12} [\dot{q}_1^2 q_1 + q_1^2 \ddot{q}_1] = 0 \quad (5.11)$$

and for $z(t) \leq z_c$

$$\dot{q}_1(t_k^+) = \left[-e \dot{q}_1(t_k^-) + (1+e) \dot{d}(t_k^-) / \phi_1(s = \hat{l}) + m_1/m_s \dot{q}_1(t_k^-) \right] \frac{1}{1 + m_1/m_s} \quad (5.12)$$

where z_c is the separation between the impactor and the center of tip mass, t^- and t^+ are the time instants before and after impacts, respectively, m_s is the mass of the impactor, and e is the coefficient of restitution.

In the case of a soft impact, the contact process can be divided into a compression phase and an expansion phase. In the compression phase, the contact condition is determined by

$$z(t) = w(s = \hat{l}, t) - d(t) \leq z_c \quad (5.13)$$

and in the expansion phase, the contact condition is determined by the contact force

$$F(z, \dot{z}) > 0 \quad (5.14)$$

Here, the contact force model is a piecewise linear model and this model takes the form

$$F(z, \dot{z}) = k_c (z - z_c) + c_c \dot{z} \quad (5.15)$$

where k_c and c_c are the contact stiffness and contact damping coefficients, respectively. When there is loss of contact between the beam and impactor, the equation of motion is given by

$$m_1 \ddot{q}_1 + k_1 q_1 + c_1 \dot{q}_1 + a_{11} q_1^3 + a_{12} [\dot{q}_1^2 q_1 + q_1^2 \ddot{q}_1] = 0 \quad (5.16)$$

When there is contact between the beam and impactor, the equation of motion is of the form

$$m_1 \ddot{q}_1 + k_1 q_1 + c_1 \dot{q}_1 + a_{11} q_1^3 + a_{12} [\dot{q}_1^2 q_1 + q_1^2 \ddot{q}_1] = \frac{F(z, \dot{z})}{\phi_1(s = \hat{l})} \quad (5.17)$$

5.3. Experimental Arrangement

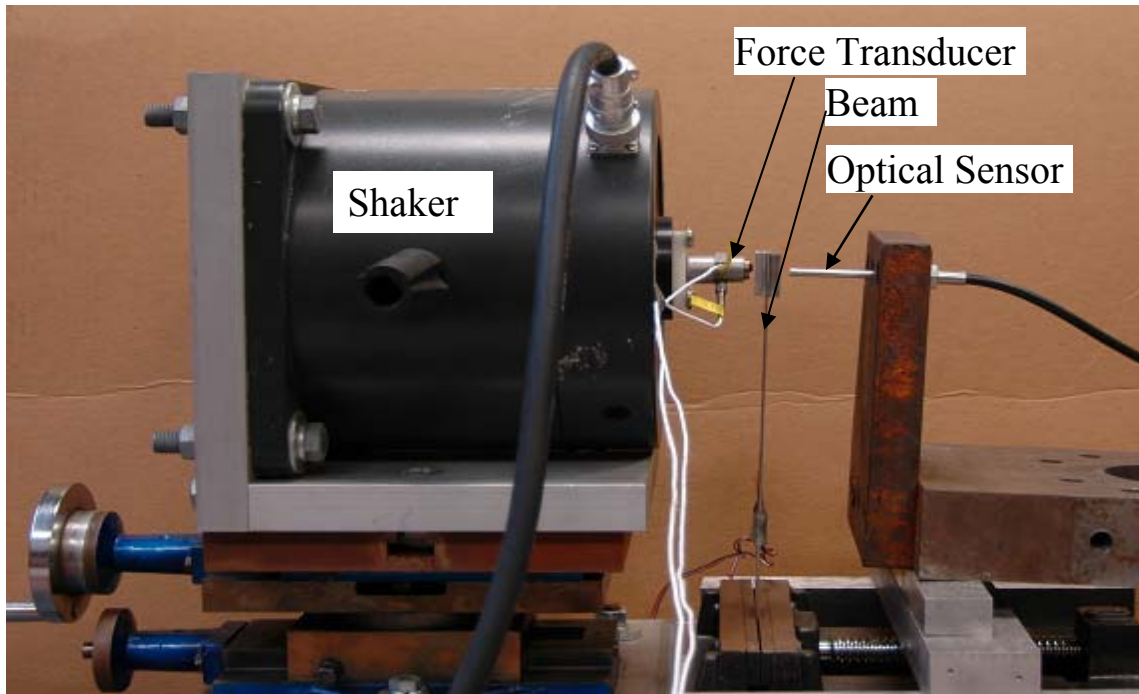


Figure 5.5: Photograph of experimental set up for impact studies.

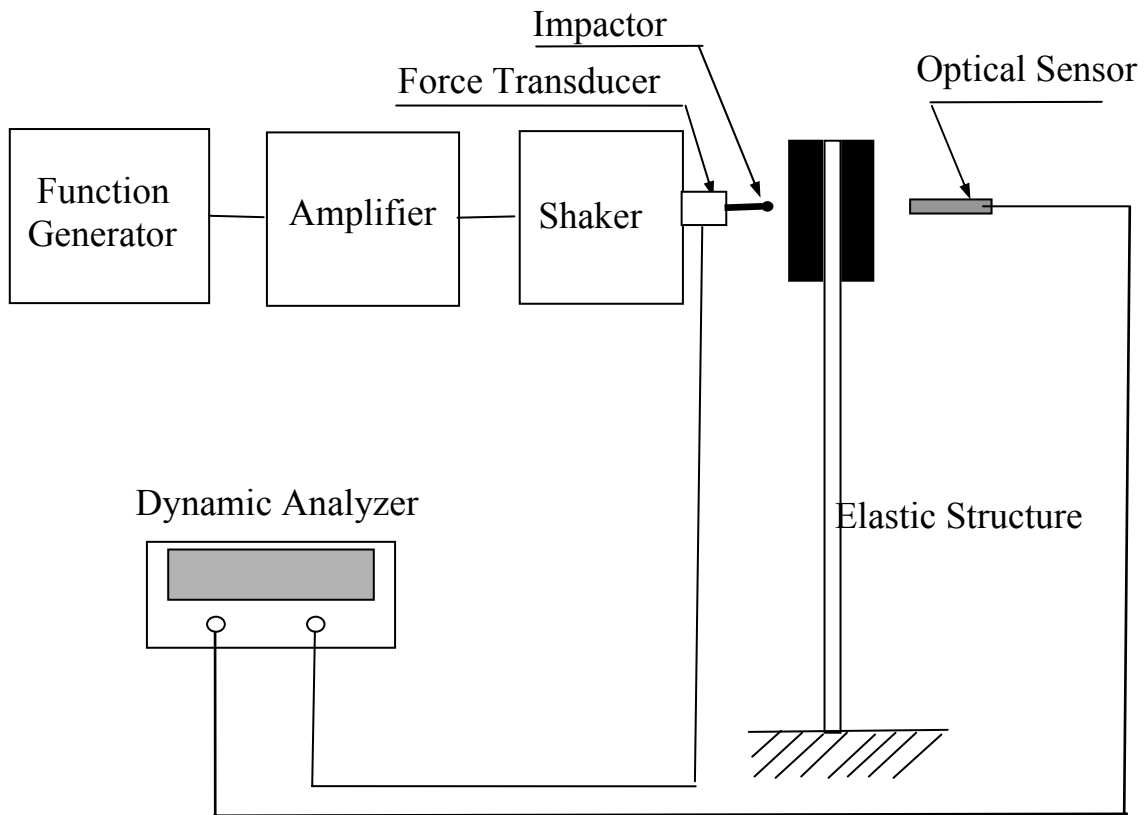


Figure 5.6: Schematic of experimental arrangement for impact studies.

In Figures 5.5 and 5.6, a photograph of the experimental set up and a schematic arrangement are shown, respectively. In this setup, a stainless-steel cantilever structure with a tip mass is considered. From the cantilevered end, the beam has a length of about 207.3 mm. The beam width and beam thickness are 25.4 mm and 1.6 mm, respectively. On each side of the beam, at the top, a stainless steel block with the dimensions of 25.4 mm x 25.4 mm x 5.9 mm is located. The center of the tip mass is impacted through a ball end contact by using a permanent magnet shaker, and the applied impact force is measured by using a piezoelectric force transducer. As shown in Figure 5.5, a non-contact fiber-optic sensor is used to measure the structure's displacement at the free end. This measurement allows us to ensure that there is no preloading on the structure. For the given geometry and material parameters, the analytical predictions for the first and second natural frequencies are about 12.75Hz and 131.2 Hz, respectively. The elastic system's first and second natural frequencies are experimentally determined to be about 12.8 Hz and 127 Hz, respectively. So, for disturbance frequencies less than 120 Hz, the elastic system can be modeled as a single degree-of-freedom system assuming that the nonlinear resonances are not active for the considered excitation levels.

5.4. Results and Discussion

In this section, the experimental and numerical bifurcation diagrams obtained for the different impact cases are presented and discussed. The grazing phenomenon and post-grazing (chaotic) motions are captured in the numerical simulations and experiments. Possible bifurcation control is also discussed.

The numerical values of the different coefficients in equation (5.7), (5.11), (5.16) and (5.17) are given by

$$m_1 = 1.75 \text{ kg}, \quad c_1 = 0.79 \text{ N/(m/s)}, \quad k_1 = 1.13 \times 10^4 \text{ N/m}, \quad a_{11} = -4.27 \times 10^6, \quad a_{12} = -45.8,$$

and $\phi(s = \hat{l}) = 4.5$.

5.4.1. Results for hard impact

In Figure 5.7, the experimentally obtained bifurcation diagram is shown. The amplitude of the motion of impactor D is chosen as 0.074 mm, the separation z_c between the impactor and the tip-mass center is fixed at 0 mm, and the excitation frequency is increased in a quasi-static fashion. The optical sensor is used to measure the displacement of the center of the tip mass and the Poincaré section is constructed according to

$$\Sigma = \left\{ (x, \dot{x}, t) \in (R^1 \times R^1 \times R^1) \mid \dot{x} = 0, \ddot{x} < 0 \right\} \quad (5.18)$$

where x is the displacement measured by the optical sensor. On examining Figure 5.7, one can find a rich variety of responses. All motions with one peak amplitude have been labeled as period-one motions, and motions with two different peak amplitudes have been labeled as period-two motions. Aperiodic motions have been labeled as chaos. This is confirmed by observations of a broadband spectral character. In the control parameter window, 50 Hz to 60 Hz, 110 Hz to 120 Hz, the results show the system can transit from periodic motions to chaotic motions and a period-doubling route is seen.

In Figure 5.8, the numerically obtained bifurcation diagram is shown. To generate this result, the coefficient of restitution is assumed to be 0.6, and the Poincaré section is

chosen as shown in equation (5.18). Period-one motions, period-doubling motions, and aperiodic motions are observed. The route from period-doubled motions to chaotic motions is also shown in this figure. By comparing with Figure 5.7, one can infer that the numerical results agree well with the experimental results in most ranges of the excitation frequency. The differences observed may be due to the form of the impact law used and simplification of the beam structure model to a single-degree-of-freedom system. Some discussion on the effect of multiple modes on the response of an impacted beam can be found in the work of Wagg and Bishop (2002).

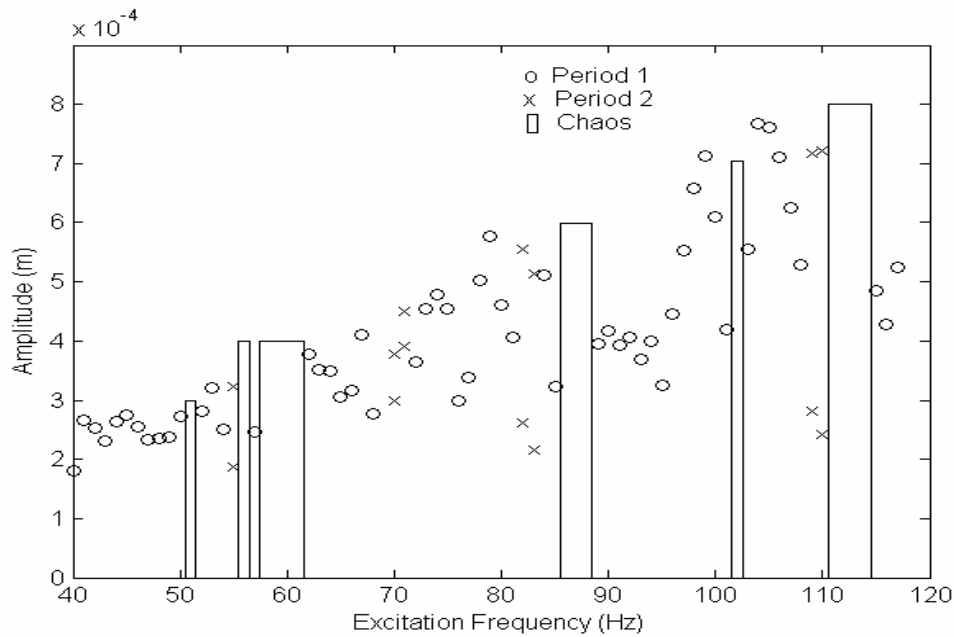


Figure 5.7: Experimentally obtained bifurcation diagram on a Poincaré section for $D=0.074$ mm.

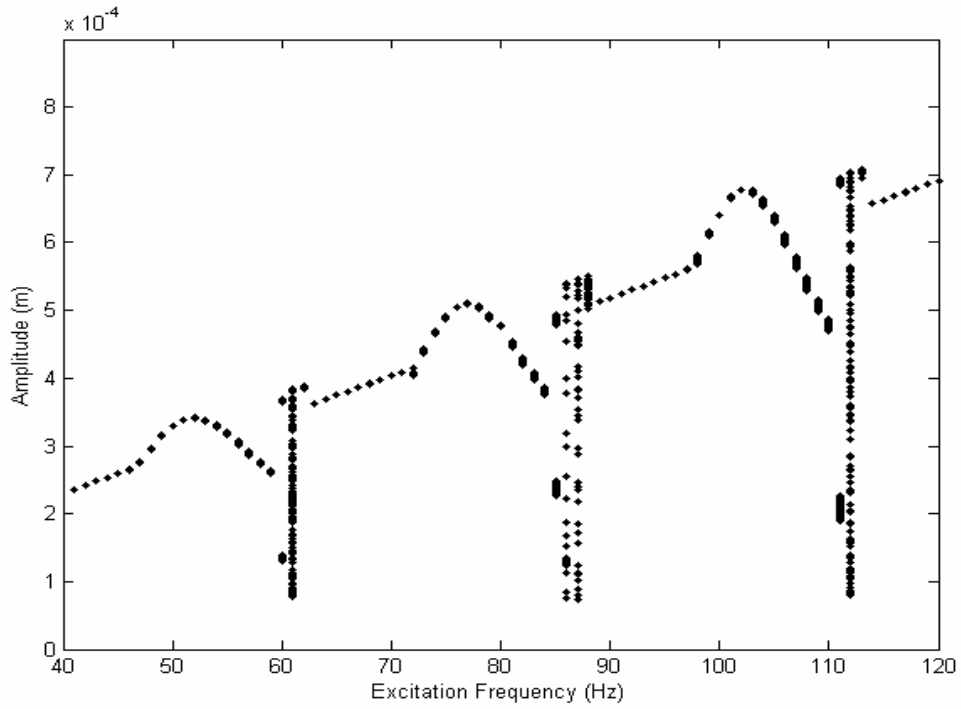


Figure 5.8: Numerically obtained bifurcation diagram on a Poincaré section for $D=0.074$ mm.

In Figures 5.9 and 5.10, the experimentally obtained phase plot and the numerically determined phase plot are shown for the excitation frequencies of 40 Hz and 112 Hz, respectively. The numerical results and the experimental results show reasonable agreement.

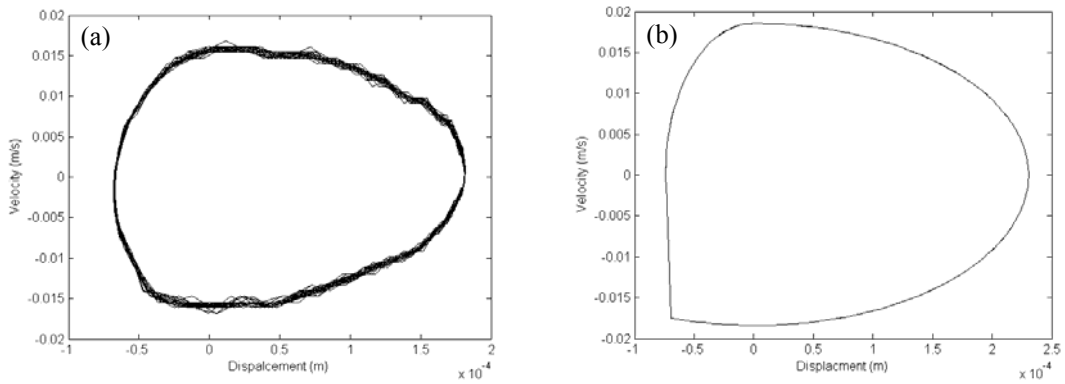


Figure 5.9: Phase plot for 40 Hz excitation frequency: (a) experimental result and (b) numerical result.

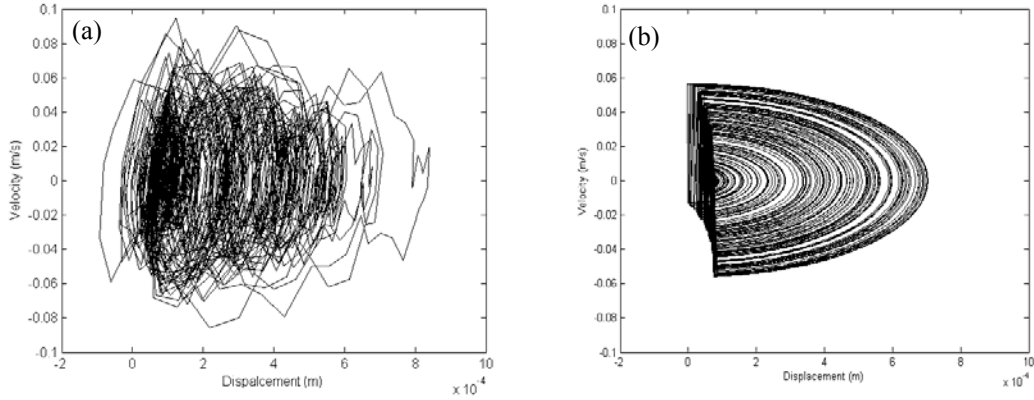


Figure 5.10: Phase plot for 112 Hz excitation frequency: (a) experimental result and (b) numerical result.

5.4.2. Grazing motions in systems with soft impacts

A grazing bifurcation is said to occur, when the system trajectory is tangent to a hyper surface, which separates the state space into different domains, and the system flow across the hyper surfaces is nonsmooth with respect to the change of the control parameters. For example, in Figure 5.11, the orbit 2 is tangent to the boundary. After grazing, three different scenarios can be observed (Maggio, Bernardo, and Kennedy 2000).

1. A continuous transition from the orbit involved in the bifurcation to an orbit of a similar or different periodicity.
2. The merging of two different solutions, followed by their disappearance.
3. A sudden transition from a periodic orbit to a chaotic motion.

Here, Figure 5.11b is of interest, since soft impacts are considered in this section. A soft impact system with the contact stiffness value $k_c = 1.27 \times 10^5$ N/m and the contact damping coefficient values $c_c = 5.99$ N/(m/s) is considered. The amplitude of the impactor motion D is fixed at 0.164 mm, the separation z_c between the impactor and the tip-mass

center is 0.1 mm, and the excitation frequency is decreased in a quasi-static fashion. The Poincaré section is selected as shown in equation (5.18), and the results obtained are shown in Figure 5.12. In Figure 5.12, one can observe a “jump” from a periodic motion to a chaotic motion when the excitation frequency is decreased to 31.4 Hz. This can be explained as a consequence of a grazing impact, as illustrated by the results shown in Figure 5.13. As shown in Figure 5.13b, the inner lobe of the periodic orbit becomes tangent to the hyper surface at the excitation frequency of 31.6 Hz. This is followed by a jump to chaotic motion at 31.4 Hz and this behavior is associated with a grazing bifurcation.

In Figure 5.14, the experimental results obtained for a system with soft impact are shown. In these experiments, a soft material is placed on the contact surface of the tip mass and the contact time is finite. The amplitude of the motion of the impactor D is fixed at 0.164 mm, the separation z_c between the impactor and the tip-mass center is 0.1mm, and the excitation frequency is decreased in a quasi-static fashion. At the excitation frequency of 30.5 Hz, a periodic motion is observed, and as the excitation frequency is decreased, the inner lobe of the periodic orbit becomes tangent to the hyper surface at 30.3 Hz. Then, a jump to a chaotic orbit from a periodic orbit is observed at



Figure 5.11: Possible grazing motions: (a) system with hard impact and (b) piecewise linear system.

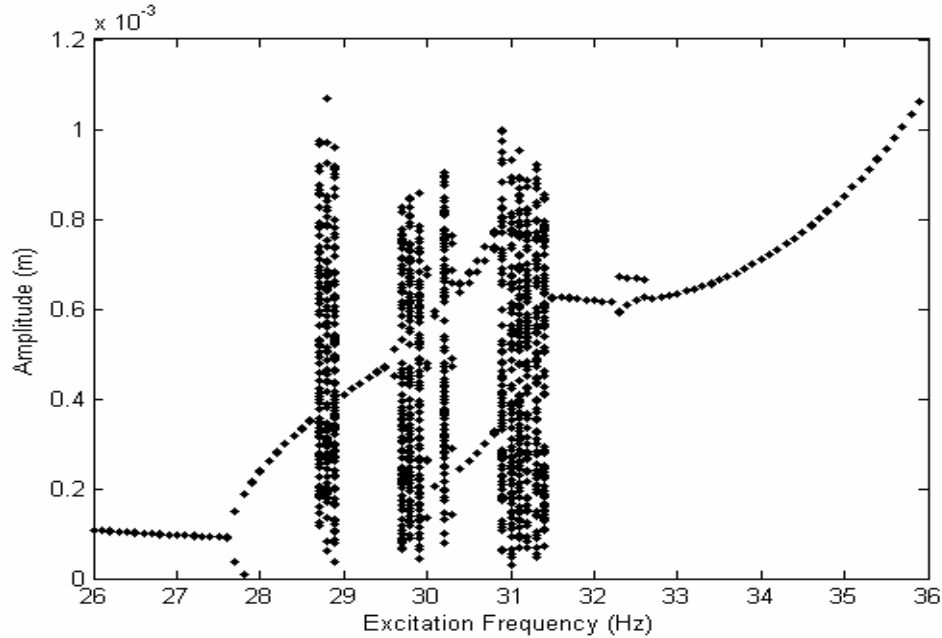


Figure 5.12: Numerically obtained bifurcation diagram on a Poincaré section for $D=0.164$ mm,

$$k_c = 1.27 \times 10^5 \text{ N/m}, c_c = 5.99 \text{ N/(m/s)}, \text{ and } z_c = 0.1 \text{ mm} .$$

30.0 Hz. These results, which show a sudden transition from a periodic orbit to a chaotic motion, agree well with the numerical results. In Figure 5.15, the experimentally measured contact forces for the system with the soft impact are shown. These results confirm the conclusions reached by observing and discussing the results shown in Figure 5.14.

Aside from grazing bifurcations, smooth bifurcations also exist in the soft impact system. Representative results illustrating a period-doubling bifurcation are shown in Figure 5.15. Corresponding experimental results are shown in Figure 5.17 and Figure 5.18. Again, the numerical simulations capture the features of the experimentally observed dynamics.

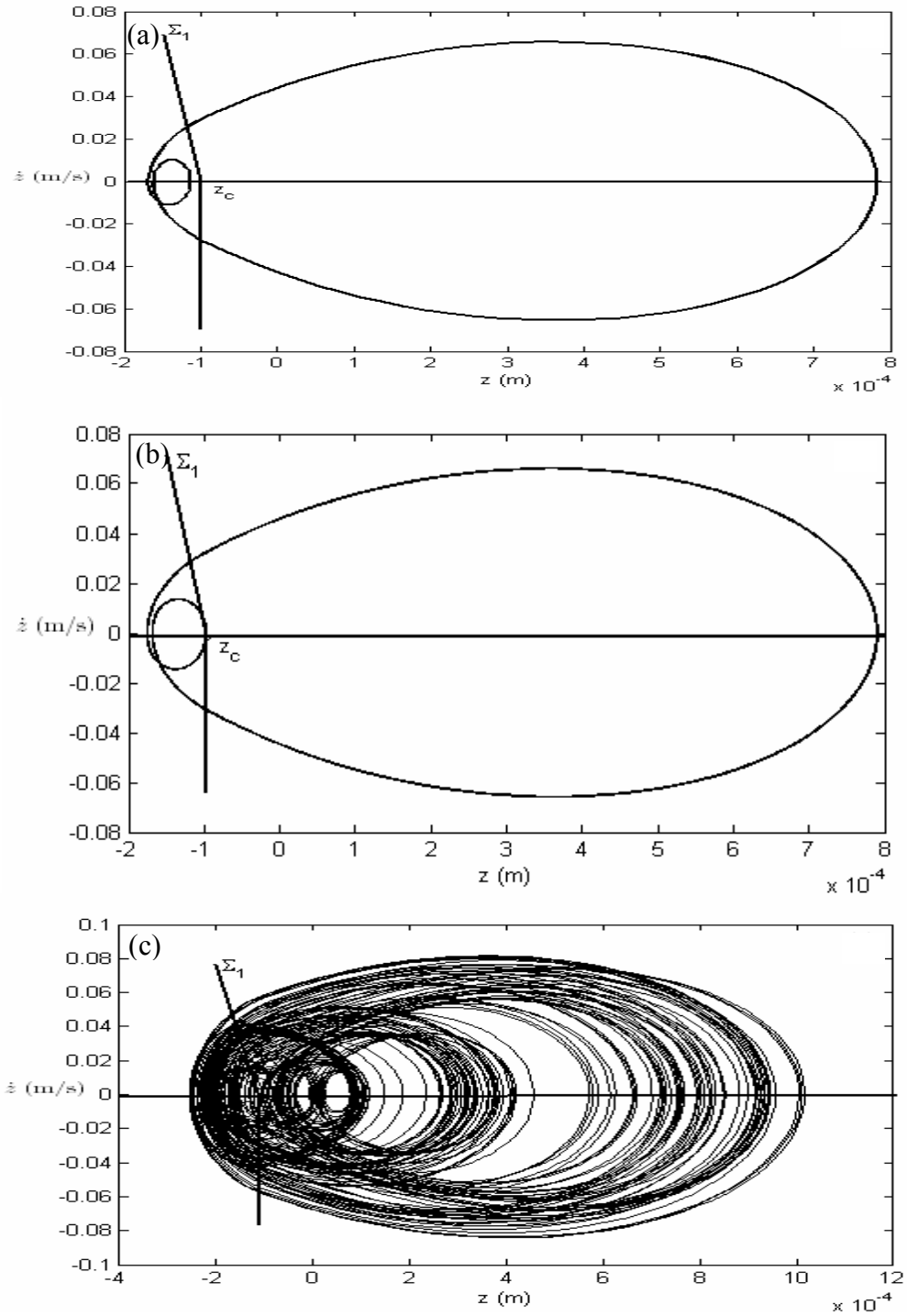


Figure 5.13: Numerical results obtained to illustrate a grazing bifurcation in a system with a soft impact: (a) $\Omega/2\pi = 32.0$ Hz, periodic orbit prior to grazing, (b) $\Omega/2\pi = 31.6$ Hz, periodic orbit grazing the hyper surface, and (c) $\Omega/2\pi = 31.4$ Hz, chaotic orbit, immediately following the grazing impact.

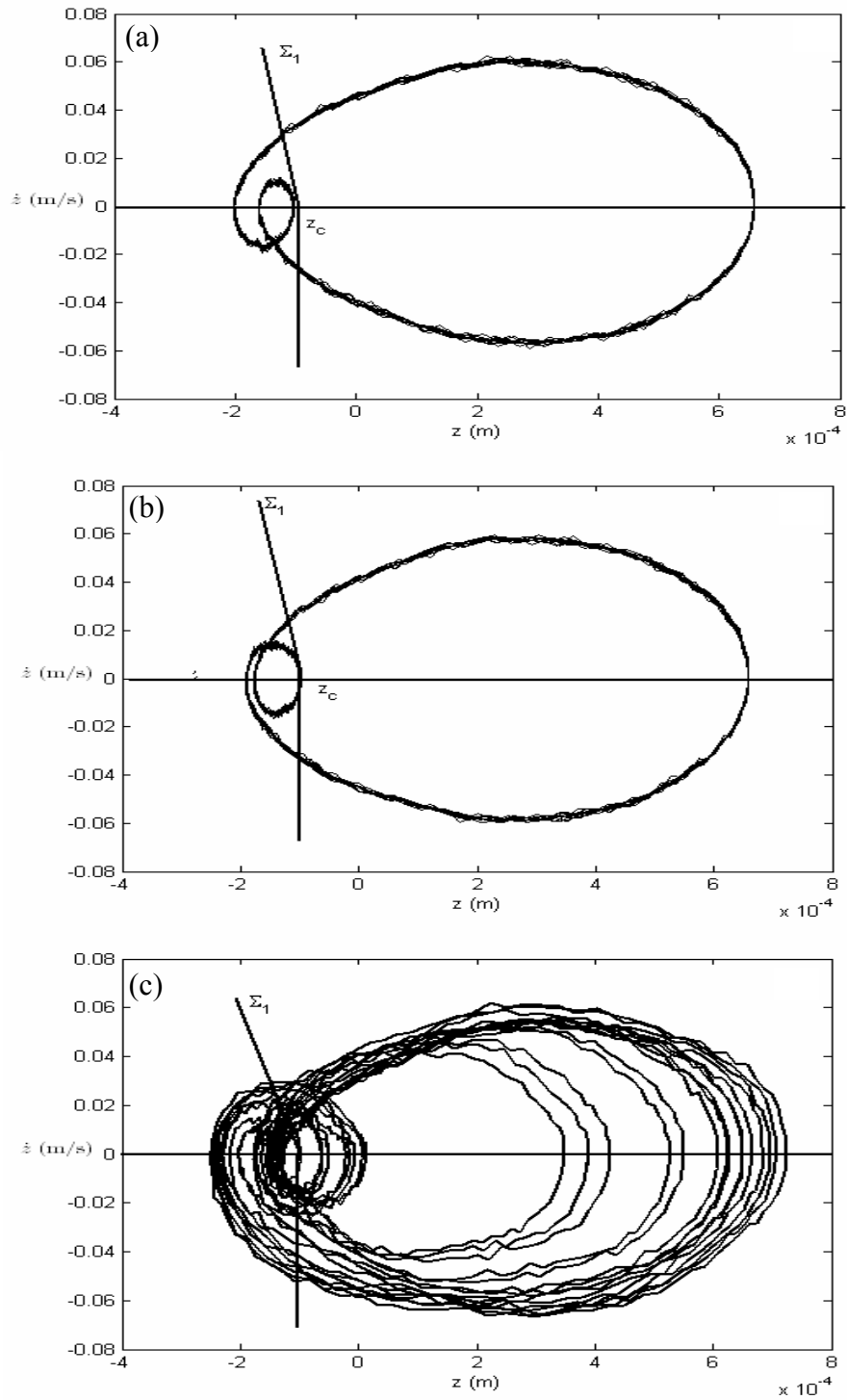


Figure 5.14: Experimental results obtained to illustrate a grazing bifurcation in a system with a soft impact: (a) $\Omega/2\pi = 30.5$ Hz, periodic orbit prior to grazing, (b) $\Omega/2\pi = 30.3$ Hz, periodic orbit grazing the hyper surface, and (c) $\Omega/2\pi = 30.0$ Hz, chaotic orbit, immediately following the grazing impact.

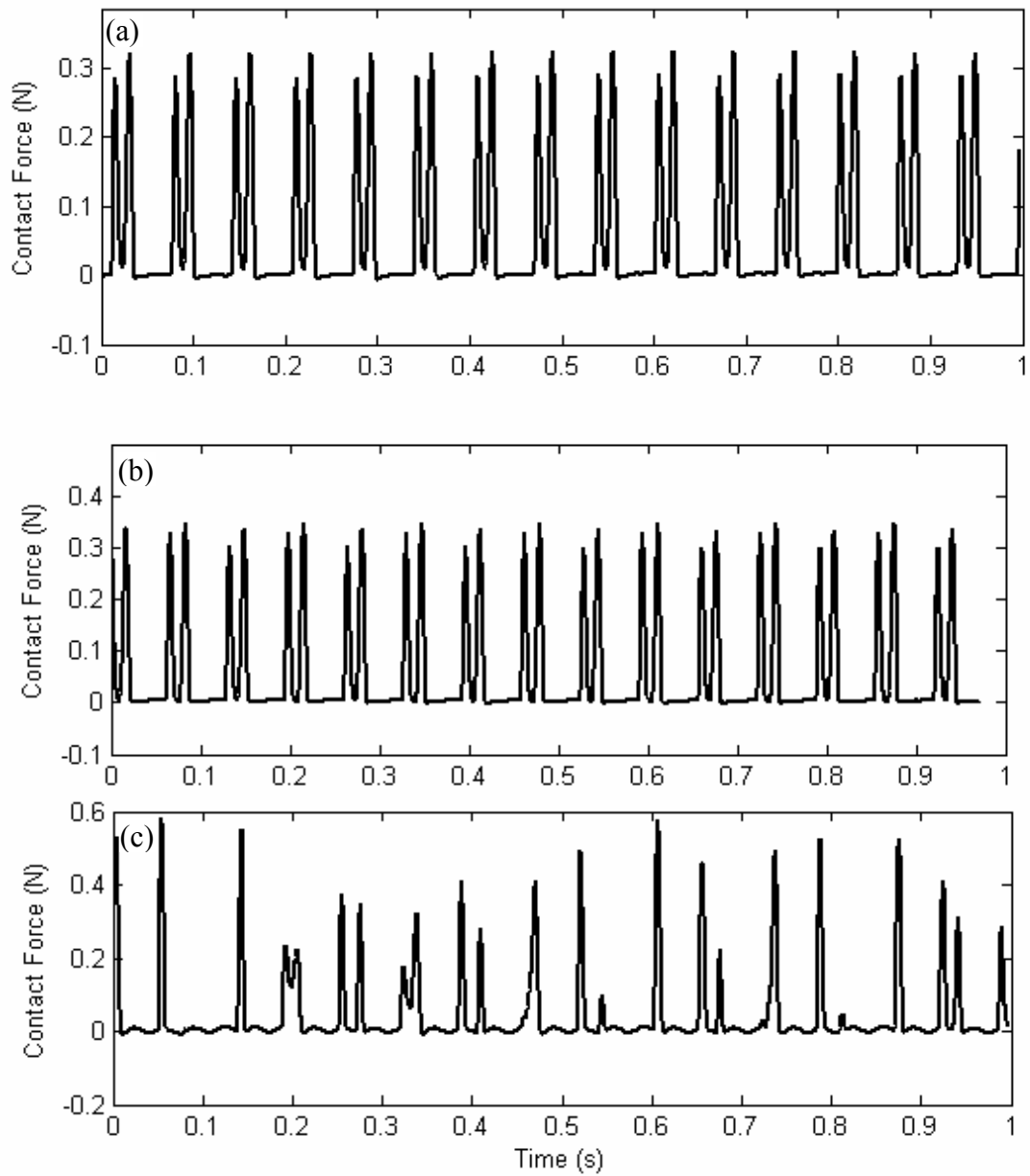


Figure 5.15: Experimental measurements of contact force in a system with a soft impact: (a) $\Omega/2\pi = 30.5$ Hz, periodic orbit prior to grazing, (b) $\Omega/2\pi = 30.3$ Hz, periodic orbit grazing the hyper surface, and (c) $\Omega/2\pi = 30.0$ Hz, chaotic orbit, immediately following the grazing impact.

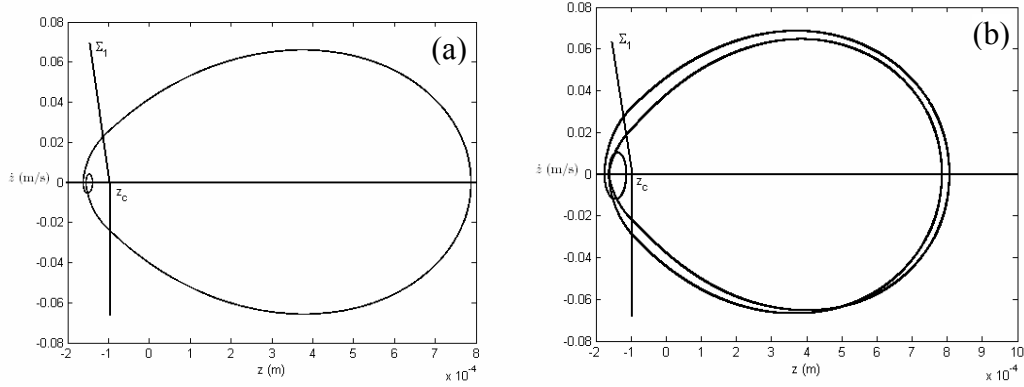


Figure 5.16: Numerical results used to illustrate a smooth bifurcation of a soft impact system: (a) $\Omega / 2\pi = 32.7$ Hz , periodic orbit and (b) $\Omega / 2\pi = 32.63$ Hz , period-doubled orbit.

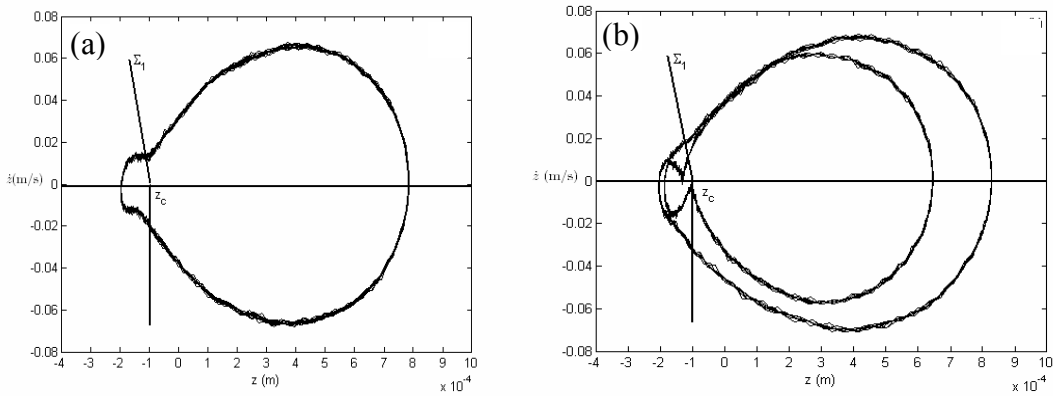


Figure 5.17: Experimental results used to illustrate a smooth bifurcation of a soft impact system: (a) $\Omega / 2\pi = 34.0$ Hz , periodic orbit and (b) $\Omega / 2\pi = 33.0$ Hz , period-doubled orbit.

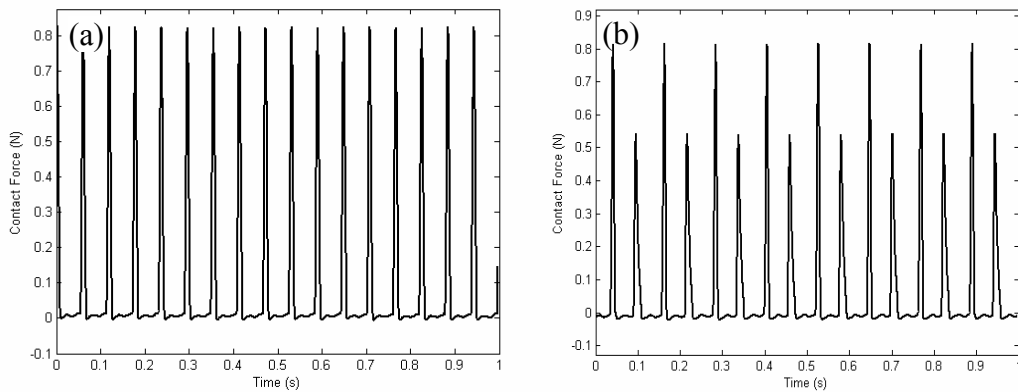


Figure 5.18: Experimental measurements of contact force in a system with a soft impact: (a) $\Omega / 2\pi = 34.0$ Hz , periodic orbit and (b) $\Omega / 2\pi = 33.0$ Hz , period-doubled orbit.

5.4.3. Bifurcation control

The objective of bifurcation control is to design a controller to modify the bifurcation properties of a given nonlinear system so that some desirable dynamical behavior can be achieved [Wang and Abed (1995) and Tesi, Abed, Genesio, and Wang (1996)]. Here, feedback control is used to modify the bifurcation diagram and shift the bifurcation location in a selected range of the excitation frequency. The mechanical system given by (5.7) is modified through feedback control, so that the resulting system has the form

$$m_1\ddot{q}_1 + k_1q_1 + c_1\dot{q}_1 + a_{11}q_1^3 + a_{12}\left[\dot{q}_1^2q_1 + q_1^2\ddot{q}_1\right] + bu(q_1) = 0 \quad (5.19)$$

In Figure 5.19, the numerical results obtained for hard impact with feedback control are shown. Comparing the results of Figure 5.19a (with control $bu(q_1) = 0.2k_1|q_1(t)|$) with those shown in Figure 5.8, one can find the bifurcation locations have been shifted along the axis which is labeled as the excitation frequency. The first bifurcation point shifts from 60 Hz to about 66 Hz, the second bifurcation point shifts from 85 Hz to about 94 Hz, and the third bifurcation point that shifts from 111 Hz to a value larger than 120 Hz, which is not shown in this figure. The feedback effect is equivalent to an increase of the system stiffness. In the uncontrolled case, there is an aperiodic motion, when the excitation frequency is 86 Hz as shown in Figure 5.8. However, with the feedback controller, this is no longer the case. In Figure 5.19b, it is shown that when the control is $bu(q_1) = -0.2k_1|q_1(t)|$, the bifurcation locations shift in the opposite direction compared with those observed in the open-loop system. The feedback is equivalent to a decrease of the system stiffness.

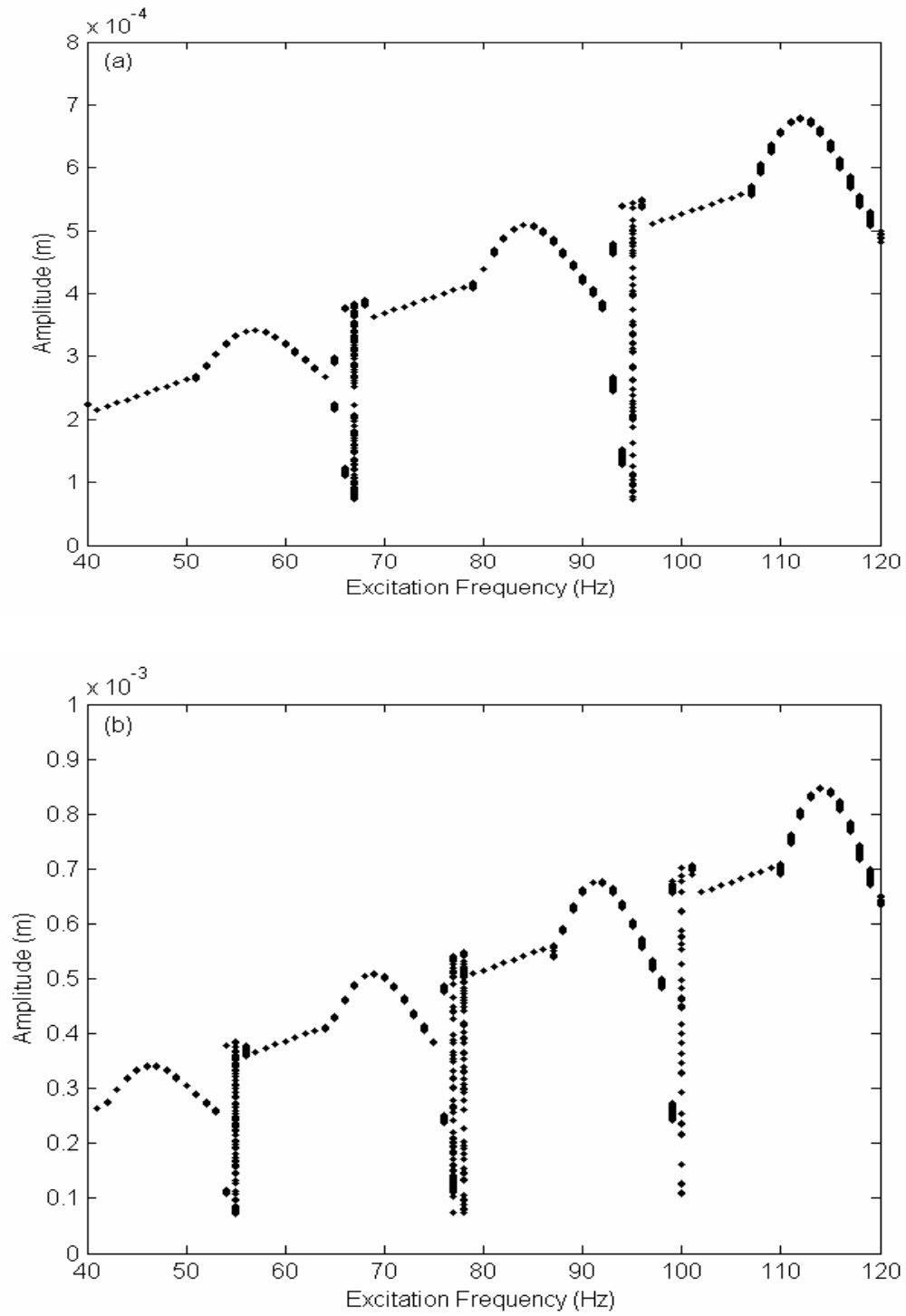


Figure 5.19: Numerically obtained bifurcation diagrams for hard impact and feedback control: (a)

$$bu(q_1) = 0.2k_1 |q_1(t)| \text{ and (b) } bu(q_1) = -0.2k_1 |q_1(t)|.$$

Chapter 6

Summary and Recommendation for Future Work

A new formulation for analyzing the dynamics and stability of end milling operations has been developed in this study. In this formulation, the consideration of the feed-rate effects leads to a non-autonomous delay-differential system with a variable time delay. Besides the feed-rate effects on the time delay, the effects on the entry cutting angle and exit cutting angle have also been presented. Based on the variable time delay formulation, the amplitudes of the feed-mark waves obtained during up-milling and down-milling are also examined and discussed. Apart from the feed motion leading to a variable time delay, the variation of spindle speed during a VSS milling process also results in a system with a variable time delay.

A numerical scheme with an analytical basis, semi-discretization method, has been extended and refined to examine the stability of periodic solutions of system with periodic coefficients and variable delay. This scheme can be used to predict not only the stability but also the chatter frequencies for a wide range of milling operations ranging from full-immersion to partial-immersion operations. Prior to analyzing the stability of the system with variable time delay, a system with two time delays is examined. It is shown through representative examples that this scheme predicts stability charts in fairly good agreement with experimental results and those obtained by using time-domain simulations. In addition, the results obtained by using this scheme indicate that apart from secondary Hopf-bifurcations of periodic orbits, period-doubling bifurcations of periodic orbits can occur in low-immersion

operations. A point to note is that the stability analysis based on the semi-discretization scheme consumes less time compared to the time-domain simulations. The stability limit improvement due to spindle speed variation method has been illustrated by comparing the stability charts of VSS milling operations with those obtained for CSS milling operations. Simulated cutting forces have been presented to illustrate the nonsmooth characteristics of a milling operation. The dynamics of an elastic beam subjected to impacts is also examined to explore possible instabilities in low-immersion operations.

The following points highlight the contributions and inferences of the study:

- Including the feed motion effects, a new model with a variable time delay is presented for the first time. In addition, feed motion effects on the static uncut chip thickness, the entry cutting angle, exit cutting angle are also discussed, and the amplitudes of the feed-mark waves are obtained by up-milling and down-milling operation. The results obtained by using the current model are in good agreement with the experimental data. From the results, it can be concluded that the feed-rate effects on the stability of milling processes are minimal for full and high-immersion operations and become pronounced for low-immersion operations with the increase of the feed rate.
- The semi-discretization method is improved to examine the stability of periodic solution of system with periodic coefficients and two time delays and a variable time delay. Features that make this method a unique one include the following: a) numerical scheme with an analytical basis, b) can be used to

predict the stability charts and multiple chatter frequencies for a milling process, c) can be used to examine the stability of milling processes over a wide range of operations from full-immersion to partial-immersion operations, d) efficiently able to examine the periodic solution of both systems with a constant delay and a periodic time varying delay. Results obtained by using this method agree well with experimental data and the previously published numerical results.

- A new delay approximation is used in the current research on VSS milling processes. The improvement of the stability limit by using VSS machining is discussed and the sensitivity to the system natural frequencies is addressed. The results show VSS machining has a high stability limit and it is robust to the nominal spindle speed when it is operated at relatively low nominal spindle speeds with respect to the system's dominant modal frequency.
- The governing equations of motion can be referred to as nonsmooth system due to the loss of contact between workpiece and tool. The nonsmooth characteristic will raise new bifurcations such as grazing bifurcation, which is different with the traditional bifurcation. Prior works on a simple nonsmooth system are investigated. Numerical and experimental evidence for grazing bifurcation in cantilever beam with repeated impacts is presented.

The following suggestions are made for future work:

1. Milling experiments with different feed rate operations can be carried out to achieve a comprehensive verification of the predictions of the current model.

2. In the ball-end milling process, the radius of tool is very small at the end of tool. This results in a high ratio f/R and the feed-rate effects are pronounced. The current model can be expanded to analyze the dynamics of ball-end milling processes.
3. Bifurcations associated with the non-smooth dynamics of milling processes need to be further explored.
4. Possible control strategies for the bifurcations control of milling processes need to be investigated.
5. Numerical predictions of stability can be used to plan optimal operation for different milling operations.

Appendix A

Coefficients in Impact Model

The coefficients in equation (5.7) are determined from

$$m_1 = \rho A + m \left\{ \phi_1(s = \hat{l}) \right\}^2 \quad (\text{A1})$$

$$k_1 = -EI \int_0^{\hat{l}} \phi_1''' \phi_1' ds - mg \int_0^{\hat{l}} (\phi_1')^2 ds + \rho A \hat{l} \int_0^{\hat{l}} \phi_1'' \phi_1 ds - \rho A g \int_0^{\hat{l}} (\phi_1' \phi_1 + s \phi_1'' \phi_1) ds \quad (\text{A2})$$

$$c_1 = 2m_1 \zeta_1 \omega_1 \quad (\text{A3})$$

$$a_{11} = EI \int_0^{\hat{l}} \left[\phi_1^{iv} (\phi_1')^2 \phi_1 + 4\phi_1''' \phi_1'' \phi_1' \phi_1 + (\phi_1''')^3 \phi_1 \right] ds + \frac{3}{2} mg \int_0^{\hat{l}} (\phi_1')^2 \phi_1'' \phi_1 ds - \frac{1}{2} \rho A g \int_0^{\hat{l}} \left[(\phi_1')^3 \phi_1 + 3(s - \hat{l})(\phi_1')^2 \phi_1'' \phi_1 \right] ds \quad (\text{A4})$$

$$a_{12} = -m \int_0^{\hat{l}} \phi_1'' \phi_1 ds \int_0^{\hat{l}} (\phi_1')^2 ds + \rho A \int_0^{\hat{l}} \phi_1'' \phi_1 \left(1 + \frac{\partial}{\partial s} \right) \left[\int_i^s \int_0^s (\phi_1')^2 d\hat{s} ds_2 \right] ds \quad (\text{A5})$$

Appendix B

Matlab Program for Semi-Discretization Method for System with Two Time Delays

```
% MAIN PROGRAM TO GET THE STABILITY LOBE BY SEMI-
DISCRETIZATION METHOD
%
function main
% num_tooth - Number of teeth on the cutter
% r        - Radius of cutter (m)
% phi_n    - Normal rake angle (degree)
% omega    - Spindle Speed (rev./min.)
% feed     - Feed rate along x direction (m/s)
% feedcut  - Feed per tooth along x direction (m/pertooth)
% rdoc     - Radial depth of cut (m)
% adoc     - Axial depth of cut (m)
% kt       - Tangential cutting coefficient from orthogonal cutting (N/m^2)
% kn       - Cutting coefficient proportional constant
% cp       - Viscous damping in the cutting process (N.s/m^2)
% friction  - Coulomb friction coefficient
% eta      - Helix angle of cylindrical end mill (degree)
% mx       - Modal mass in x direction (Kg)
% kx       - Modal stiffness in x direction (N/m)
% cx       - Viscous damping in x direction (N.s/m)
% theta_enter - Cutter entering angle (degree)
% theta_exit - Cutter exit angle (degree)
% z1       - Dynamic integration lower limit (m)
% z2       - Dynamic integration upper limit (m)
% step     - Integration time step (s)

global mx xix kx my xiy ky mu ku xiu mv kv xiv feed;
global kt kn friction cp r eta phi_n num_tooth feedcut;
global omega1 omega2 delta_omega theta_enter theta_exit;
global adocL adocH delta_adoc int_time;

% CALL THE INPUT FUNCTION TO INPUT THE SYSTEM PARAMETERS
PI=3.14159;
N=40; % THE NUMBER OF STEP FOR EVERY PERIODIC
input2_41;
% CHANGE THE DIMENSIONLESS DAMPING INTO CX,CY ETC.
cx=xix*2.0*sqrt(mx*kx);
cy=xiy*2.0*sqrt(my*ky);
cu=xiu*2.0*sqrt(mu*ku);
cv=xiv*2.0*sqrt(mv*kv);
% FORMING THE MASS, DAMPING AND STIFFNESS MATRICES
mm=[mx,my,mu,mv];
```

```

MC=diag(mm,0);
MC=inv(MC);
cc=[cx,cy,cu,cv];
CC=diag(cc,0);
kk=[kx,ky,ku,kv];
KC=diag(kk,0);
% CREAT TWO MATRICES FOR STATE EQUATIONS
AA=zeros(8,8);
BB=zeros(8,8);
kbar=zeros(4,4);
cbar=zeros(4,4);
zerobar=zeros(4,1);
s=zeros(2,2);
q=zeros(2,2);
% CHANGE THE ANGULE FROM DEGREE TO ARCH
eta=eta*PI/180.0;
omega1=2*PI*omega1/60.0;
omega2=2*PI*omega2/60.0;
delta_omega=2*PI*delta_omega/60.0;
theta_enter=theta_enter*PI/180.0;
theta_exit=theta_exit*PI/180.0;
% GET K1, K2
k1 = kn/cos(eta);
k2 = 1.0 + friction*(cos(phi_n)-kn*sin(phi_n))*tan(eta);
% DEFINE RANK OF MAPPING MATRICES
rankn=(N+1)*8;
% GET THE LOBE DIAGRAM OF STABILITY BY PARAMETERS OF SPINDLE
SPEED
% AND AXIAL CUTTING DEEPTH
BI=zeros(rankn,rankn);
jj=1;
for omega=omega1:delta_omega:omega2
    step=2*PI/omega/(N+0.5)/num_tooth;
    tn=2*PI/omega/num_tooth;
    feed=omega/(2*PI)*num_tooth*feedcut;
    % Cutting entering or exit angle variations due to feed
    delta_theta = asin(2*PI*feed/(2*omega*r*num_tooth));

    xdelay = floor(2*PI/(omega*num_tooth*step));
    ydelay = floor(4*PI*r/(num_tooth*step*(2*r*omega+feed)));
    xresidue = 2*PI/(omega*num_tooth*step) - xdelay+0.5;
    yresidue = 4*PI*r/(num_tooth*step*(2*r*omega+feed)) - ydelay+0.5;
    adoc1=0.0;
    adoc2=adocH;
    adoc=adocL;
    stable1=1;

```

```

delta_adoc1=delta_adoc;
while abs((adoc1-adoc))>2e-6
% PHI=eye(rankn,rankn);
kbar=zeros(4,4);
cbar=zeros(4,4);
adoc1=adoc;
for t=0:step:tn-step
    BI=[zeros(8,rankn);eye(rankn-8),zeros(rankn-8,8)];
    % CALL THE SUBROUTINE TO GET THE S, Q MATRICES

[s,q]=cutzone1(t,theta_enter,theta_exit,delta_theta,adoc,r,omega,eta,num_tooth,...
    step,k1,k2,kt,cp);
kbar=kbar+[s,s;s,s];
cbar=cbar+[q,q;q,q];
end
kbar=kbar/N;
cbar=cbar/N;
kbar=[kbar(1,1),zeros(1,3);zeros(3,1),zeros(3,3)];
kbar1=kbar(:,1);
cbar1=cbar(:,1);
kbar2=kbar(:,2);
cbar2=cbar(:,2);

% X DIRECTION DELAY COEFFICIENT MATRICES
kbar11=[kbar1,zerobar,kbar1,zerobar];
cbar11=[cbar1,zerobar,cbar1,zerobar];

% Y DIRECTION DELAY COEFFICIENT MATRICES
kbar22=[zerobar,kbar2,zerobar,kbar2];
cbar22=[zerobar,cbar2,zerobar,cbar2];

% FORMING THE STATE EQUATION MATRICES
% THE EFFECT COEFFICIENCES OF
AA=[zeros(4,4),eye(4,4);-MC*(KC-kbar),-MC*(CC-cbar)];
INVA=inv(AA);
% if xdelay==ydelay
% THE EFFECT COEFFICIENCES OF DELAY
BB1=[zeros(4,8);-MC*kbar11,-MC*cbar11];
BB2=[zeros(4,8);-MC*kbar22,-MC*cbar22];
mi0=expm(AA*step);
mi1=(1-xresidue)*(mi0-eye(8,8))*INVA*BB1;
mi2=xresidue*(mi0-eye(8,8))*INVA*BB1;
mi3=(1-yresidue)*(mi0-eye(8,8))*INVA*BB2;
mi4=yresidue*(mi0-eye(8,8))*INVA*BB2;
BI(1:8,1:8)=BI(1:8,1:8)+mi0;
BI(1:8,8*xdelay-7:8*xdelay)=BI(1:8,8*xdelay-7:8*xdelay)+mi1;

```

```

    BI(1:8,8*xdelay+1:8*xdelay+8)=BI(1:8,8*xdelay+1:8*xdelay+8)+mi2;
    BI(1:8,8*ydelay-7:8*ydelay)=BI(1:8,8*ydelay-7:8*ydelay)+mi3;
    BI(1:8,8*ydelay+1:8*ydelay+8)=BI(1:8,8*ydelay+1:8*ydelay+8)+mi4;
%   PHI=BI*PHI;
    E=eig(BI^40);
    max_eig=max(abs(E));
    max_eig
    if (max_eig>1) & (abs(stable1-1)>0.1)
        %printf();
        stable=-1;
        adoc=adoc-delta_adoc1;
    elseif (max_eig>1) & (abs(stable1-1)<0.1)
        %printf();
        stable=-1;
        delta_adoc1=delta_adoc1/2.0;
        adoc=adoc-delta_adoc1;
    elseif (max_eig<1) & (abs(stable1+1)<0.1)
        %printf();
        stable=1;
        delta_adoc1=delta_adoc1/2.0;
        adoc=adoc+delta_adoc1;
    elseif (max_eig<1) & (abs(stable1+1)>0.1)
        %printf();
        stable=1;
        adoc=adoc+delta_adoc1;
    end
    stable1=stable;
    adoc
    stable
end
adoc
omega*60/2/PI
omeg(jj)=omega*60/2/PI;
ado(jj)=adoc;
jj=jj+1;
end

save ad4s41.dat omeg ado -ascii -double;

% DEFINE THE CUTTING ZONE
% FORM THE STIFFNESS AND DAMPING MATRICES DUE TO CUTTING
FORCE
function [s,q]=cutzone(tn,theta_enter,theta_exit,delta_theta,r,omega,eta,num_tooth,...
                    step,k1,k2,kt,cp,num_harmonic)

```

```

PI=3.14159;
tn_1=tn-step;
s=zeros(2,2);
q=zeros(2,2);
normal1=zeros(num_tooth,1);
normal2=zeros(num_tooth,1);
adoc=0.0;
for i = 1:num_tooth
    normal1(i) = -2*PI*(i-1)/num_tooth + theta_enter;
    normal2(i) = normal1(i) - 2*PI;
end
theta_en=theta_enter;
theta_ex=theta_exit;
% Non-cutting
% -PI is for straight tooth cutter in non-cutting condition

    % Compensation of delta_theta for up and down milling
if theta_en == 0.0
    theta_en = theta_en - delta_theta;
end
if theta_ex == PI
    theta_ex = theta_ex + delta_theta;
end
if theta_en >= theta_ex
    theta_en = -PI;
    theta_ex = -PI;
end
for i = 1:num_tooth
    % For cylindrical mills with non-zero helix angles
    if(eta ~= 0.0)
        theta_en1 = theta_en;
        theta_ex1 = theta_ex;
        % Normalization of the cutting zone angles
        if (theta_en1-normal1(i))*(theta_en1-normal2(i)) > 0.0
            while (theta_en1-normal2(i)) > 2*PI
                theta_en1 = theta_en1 - 2*PI;
            end
        end
        if (theta_en1-normal1(i))*(theta_en1-normal2(i)) > 0.0
            while (theta_en1-normal1(i)) < (-2*PI)
                theta_en1 = theta_en1 + 2*PI;
            end
        end
        if (theta_en1-normal1(i))*(theta_en1-normal2(i)) == 0.0
            theta_en1 = normal1(i);
        end
    end
end

```

```

if (theta_ex1-normal1(i))*(theta_ex1-normal2(i)) > 0.0
    while (theta_ex1-normal2(i)) > 2*PI
        theta_ex1 = theta_ex1 - 2*PI;
    end
end
if (theta_ex1-normal1(i))*(theta_ex1-normal2(i)) > 0.0
    while (theta_ex1-normal1(i)) < (-2*PI)
        theta_ex1 = theta_ex1 + 2*PI;
    end
end
if (theta_ex1-normal1(i))*(theta_ex1-normal2(i)) == 0.0
    theta_ex1 = normal1(i);
end
% Rotate the cutting zone in the opposite direction
theta_en1 = theta_en1 - omega*tn;
theta_ex1 = theta_ex1 - omega*tn;
if theta_en1 <= normal2(i)
    theta_en1 = theta_en1 + 2*PI;
end
if (theta_ex1 <= normal2(i))
    theta_ex1 = theta_ex1 + 2*PI;
end
% z_en and z_ex values always nonnegative
z_en = (-(i-1)*2*PI/num_tooth+theta_enter-theta_en1)*r/tan(eta);
z_ex = (-(i-1)*2*PI/num_tooth+theta_enter-theta_ex1)*r/tan(eta);

% Non-cutting positions
if ((z_ex>=adoc)&(z_en>z_ex))|((z_en<=0.0)&(z_ex>adoc))|(z_en==z_ex)
    %ai=0.0;
    %bi=0.0;
    z1 = 0.0;
    z2 = 0.0;
    % Cutting positions
else
    if (z_en<adoc)&(z_en>0.0)&((z_ex<=0.0)|(z_ex>adoc))
        z1 = 0.0;
        z2 = z_en;
%
        ai=1/2*(omega/2*(tn*tn-tn_1*tn_1)/step-(i-
1)*2*PI/num_tooth+theta_enter-theta_en1);
%
        bi=(1/step)*r/4/tan(eta)/(2*omega)*(cos(2*omega*tn_1-(i-
1)*4*PI/num_tooth...
%
+2*theta_enter)-cos(2*omega*tn-(i-1)*4*PI/num_tooth+2*theta_enter))...
%
-r/4/tan(eta)*sin(2*theta_en1);
    elseif (z_en>=adoc)&((z_ex<=0.0)|(z_ex>adoc))
        z1 = 0.0;
        z2 = adoc;
    end
end

```

```

%      ai=1/2*adoc;
%      bi=1/step*r/2/tan(eta)/(2*omega)*sin(tan(eta)/r*adoc)...
%      *(sin(2*omega*tn-(i-1)*4*PI/num_tooth+2*theta_enter-tan(eta)/r*adoc)...
%      -sin(2*omega*tn_1-(i-1)*4*PI/num_tooth+2*theta_enter-tan(eta)/r*adoc));
      elseif (z_en<adoc)&(z_ex<adoc)&(z_ex<z_en)&(z_ex>0.0)
          z1 = z_ex;
          z2 = z_en;
%      ai=r/tan(eta)*(theta_ex1-theta_en1);
%      bi=r/(4*tan(eta))*(sin(2*theta_ex1)-sin(2*theta_en1));
      elseif (z_en>=adoc)&(z_ex<adoc)&(z_ex>0.0)
          z1 = z_ex;
          z2 = adoc;
%      ai=1/2*(adoc-omega/2*(tn*tn-tn_1*tn_1)/step+(i-1)*2*PI/num_tooth-
theta_enter+theta_ex1);
%      bi=1/step*r/4/tan(eta)/(2*omega)*(cos(2*omega*tn-(i-
1)*4*PI/num_tooth...
%      +2*theta_enter-2*tan(eta)/r*adoc)-cos(2*omega*tn_1-(i-
1)*4*PI/num_tooth...
%      +2*theta_enter-2*tan(eta)/r*adoc))+r/4/tan(eta)*sin(2*theta_ex1);
      else
          % You should not enter this block if all situations have been included
          % puts("There is a bug for helical tooth cutter!\n");
          z1 = 0.0;
          z2 = 0.0;
      end
  end
  end
%      ss = ai-bi;
%      cc = ai+bi;
%      sc = bi;
          ss = (z2-z1)/2.0+r*sin(tan(eta)*(z1-z2)/r)*...
          cos(2*omega*tn-(i-1)*4*PI/num_tooth-
tan(eta)*(z1+z2)/r+2*theta_enter)/(2*tan(eta));

          cc = (z2-z1)/2.0-r*sin(tan(eta)*(z1-z2)/r)*...
          cos(2*omega*tn-(i-1)*4*PI/num_tooth-
tan(eta)*(z1+z2)/r+2*theta_enter)/(2*tan(eta));

          sc = r*sin(tan(eta)*(z2-z1)/r)*...
          sin(2*omega*tn-(i-1)*4*PI/num_tooth-
tan(eta)*(z1+z2)/r+2*theta_enter)/(2*tan(eta));
% For flat end milling with zero helix angle
elseif(eta==0)
    theta_t = 2*PI*omega*tn - (i-1)*2*PI/num_tooth + theta_enter;
    % Rotational angle
    theta_angle= theta_t;
    %/*Normalize tooth angle in <theta_enter, theta_enter+2*PI> mode*/

```

```

if ((theta_t-theta_enter)*(theta_t-theta_enter-2*PI) > 0.0)
    while ((theta_t-theta_enter) > 2*PI)
        theta_t = theta_t - 2*PI;
    end
end
if ((theta_t-theta_enter)*(theta_t-theta_enter-2*PI) > 0.0)
    while ((theta_t-theta_enter-2*PI) < (-2*PI))
        theta_t = theta_t + 2*PI;
    end
end
if ((theta_t-theta_enter)*(theta_t-theta_enter-2*PI) == 0.0)
    theta_t = theta_enter;
    /*Non-cutting positions*/
end
if (((theta_t-theta_en)*(theta_t-theta_ex)>0.0)|((theta_en==-PI)&(theta_ex==
PI)))
    ss=0.0;
    cc=0.0;
    sc=0.0;
    /*Cutting positions*/
    elseif (((theta_t-theta_en)*(theta_t-theta_ex)<=0.0)&(theta_en~=
PI)&(theta_ex~=-PI))
        ss = sin(theta_t)*sin(theta_t);
        cc = cos(theta_t)*cos(theta_t);
        sc = 0.5*sin(2*theta_t);
    end
end
end
for ii=0,num_harmonic
    bs1 = (-k1*kt*ss-k2*kt*sc-
omega*cp*(k2*cc+k1*sc))*exp(i*ii*num_tooth*omega);
    bq1 = (-k1*cp*ss-k2*cp*sc)*exp(i*ii*num_tooth*omega);
    bs2 = (-k2*kt*cc-
k1*kt*sc+omega*cp*(k1*ss+k2*sc))*exp(i*ii*num_tooth*omega);
    bq2 = (-k2*cp*cc-k1*cp*sc)*exp(i*ii*num_tooth*omega);
    bs3 = (k2*kt*ss-k1*kt*sc+omega*cp*(k2*sc-
k1*cc))*exp(i*ii*num_tooth*omega);
    bq3 = (k2*cp*ss-k1*cp*sc)*exp(i*ii*num_tooth*omega);
    bs4 = (k2*kt*sc-k1*kt*cc+omega*cp*(k1*sc-
k2*ss))*exp(i*ii*num_tooth*omega);
    bq4 = (k2*cp*sc-k1*cp*cc)*exp(i*ii*num_tooth*omega);
    s(1:1,1:1) = s(1:1,1:1) + bs1;
    s(1:1,2:2) = s(1:1,2:2) + bs2;
    s(2:2,1:1) = s(2:2,1:1) + bs3;
    s(2:2,2:2) = s(2:2,2:2) + bs4;

```

```

    q(1:1,1:1) = q(1:1,1:1) + bq1;
    q(1:1,2:2) = q(1:1,2:2) + bq2;
    q(2:2,1:1) = q(2:2,1:1) + bq3;
    q(2:2,2:2) = q(2:2,2:2) + bq4;
end
end

```

Input the parameters of system (For Figure 3.7)

```

function input2_4
global mx xix kx my xiy ky mu ku xiu mv kv xiv feed;
global kt kn friction cp r eta phi_n num_tooth feedcut;
global omega1 omega2 delta_omega theta_enter theta_exit;
global adocL adocH delta_adoc int_time;
% MASS DAMPING STIFFNESS (X)
mx=2.0e-2;
xix=0.01;
kx=8.0e+5;
% MASS DAMPING STIFFNESS (Y)
my=2.4e-2;
xiy=0.015;
ky=1.0e+6;
% MASS DAMPING STIFFNESS (U)
mu=1.0e-1;
xiu=0.01;
ku=1.0e+6;
% MASS DAMPING STIFFNESS (V)
mv=1.5e-1;
xiv=0.01;
kv=3.0e+6;
%WORKPIECE MATERIAL
%WORKPIECE MATERIAL
material='aluminum';
% CUTTING STIFFNESS (KT KN)
kt=6.0e+8;
kn=0.3;
% CUTTING FRICTION AND DAMPING (FRICTION CP)
friction=0.20;
cp=0.0;
% CUTTING RADIUS (R)
r=6.35e-3;
% HELIC ANGLE (ETA)
eta=30.0;
% NORMAL RAKE ANGLE (PHI_N)
phi_n=15.0;
% NUMBER OF TEETH (NUM_TOOTH)

```

```
num_tooth=2;
% FEED PER TOOTH (FEEDCUT)
feedcut=5.1e-4;
% MINIMAL SPINDLE SPEED, MAXIMUM SPINDLE SPEED,
% CHANGE SPINDLE SPEED(OMEGA1 OMEGA2 DELTA_OMEGA)
omega1=5000.0;
omega2=20000.0;
delta_omega=250.0;
% ENTRY AND EXIT ANGLES (THETA_ENTER THETA_EXIT)
theta_enter=0.0;
theta_exit=36.13;
% MINIMAL, MAXIMUM AND CHANGE AXIAL DEPTH OF CUT
% (ADOC1,ADOC2,DELTA_ADOC)
adocL=50.0e-6;
adocH=8.0e-3;
delta_adoc=0.0;
```

Appendix C

Matlab Program for Semi-Discretization Method for System with Variable Time Delay

```
% MAIN PROGRAM TO GET THE STABILITY LOBE BY SEMI-
DISCRETIZATION METHOD
% In this case, we will consider the effect of feed rate on time delay
% Taylor approximation is not used. This is differently with the old one ()
function main
% num_tooth - Number of teeth on the cutter
% r - Radius of cutter (m)
% phi_n - Normal rake angle (degree)
% omega - Spindle Speed (rev./min.)
% feed - Feed rate along x direction (m/s)
% feedcut - Feed per tooth along x direction (m/pertooth)
% rdoc - Radial depth of cut (m)
% adoc - Axial depth of cut (m)
% kt - Tangential cutting coefficient from orthogonal cutting (N/m^2)
% kn - Cutting coefficient proportional constant
% cp - Viscous damping in the cutting process (N.s/m^2)
% friction - Coulomb friction coefficient
% eta - Helix angle of cylindrical end mill (degree)
% mx - Modal mass in x direction (Kg)
% kx - Modal stiffness in x direction (N/m)
% cx - Viscous damping in x direction (N.s/m)
% theta_enter - Cutter entering angle (degree)
% theta_exit - Cutter exit angle (degree)
% z1 - Dynamic integration lower limit (m)
% z2 - Dynamic integration upper limit (m)
% step - Integration time step (s)
clear all

global mx xix kx my xiy ky mu ku xiu mv kv xiv feed;
global kt kn friction cp r eta phi_n num_tooth feedcut;
global omega1 omega2 delta_omega theta_enter theta_exit;
global adocL adocH delta_adoc int_time;

% CALL THE INPUT FUNCTION TO INPUT THE SYSTEM PARAMETERS
PI=3.14159;
N=60; % THE NUMBER OF STEP FOR EVERY PERIODIC
input_brian_05;
```

```

% CHANGE THE DIMENSIONLESS DAMPING INTO CX,CY ETC.
cx=xix*2.0*sqrt(mx*kx);
cy=xiy*2.0*sqrt(my*ky);
cu=xiu*2.0*sqrt(mu*ku);
cv=xiv*2.0*sqrt(mv*kv);
% FORMING THE MASS, DAMPING AND STIFFNESS MATRICES
mm=[mx,my,mu,mv];
MC=diag(mm,0);
MC=inv(MC);
cc=[cx,cy,cu,cv];
CC=diag(cc,0);
kk=[kx,ky,ku,kv];
KC=diag(kk,0);
% CREAT TWO MATRICES FOR STATE EQUATIONS
AA=zeros(8,8);
BB=zeros(8,8);
kbar=zeros(4,4);
cbar=zeros(4,4);
zeroibar=zeros(4,1);

s=zeros(2,2);
q=zeros(2,2);
bs=zeros(2,2,num_tooth);
bq=zeros(2,2,num_tooth);

% CHANGE THE ANGULE FROM DEGREE TO ARCH
eta=eta*PI/180.0;
omega1=2*PI*omega1/60.0;
omega2=2*PI*omega2/60.0;
delta_omega=2*PI*delta_omega/60.0;
theta_enter=theta_enter*PI/180.0;
theta_exit=theta_exit*PI/180.0;
% GET K1, K2
k1 = kn/cos(eta);
k2 = 1.0 + friction*(cos(phi_n)-kn*sin(phi_n))*tan(eta);

% DEFINE RANK OF MAPPING MATRICES
rankn=(N+3)*8;

% GET THE LOBE DIAGRAM OF STABILITY BY PARAMETERS OF SPINDLE
SPEED
% AND AXIAL CUTTING DEEPTH
BI=zeros(rankn,rankn);
jj=1;
ii=0;

```

```

for omega=omega1:delta_omega:omega2
    step=2*PI/omega/N/num_tooth;
    tn=2*PI/omega/num_tooth;

    excite_harmonics=(-omega:omega:6*omega)/2/PI*num_tooth;

    feed=omega/(2*PI)*num_tooth*feedcut;
    % Cutting entering or exit angle variations due to feed
    delta_theta = asin(2*PI*feed/(2*omega*r*num_tooth));

    adoc1=adocL;
    adoc2=adocH;
    adoc=adocH/2.0;
    while (adoc-adoc1)>1e-6 & (adoc2-adoc)>1e-6
        PHI=eye(rankn,rankn);
        for t=0:step:tn-step
            BI=[zeros(8,rankn);eye(rankn-8),zeros(rankn-8,8)];
            % CALL THE SUBROUTINE TO GET THE S, Q MATRICES

[bs,bq,s,q,t_delay]=cutzone_continue2(t,theta_enter,theta_exit,delta_theta,adoc,r,ome
ga,eta,num_tooth,...
            step,k1,k2,kt,cp,feed);
            kbar=[s,s;s,s];
            cbar=[q,q;q,q];

            % FORMING THE STATE EQUATION MATRICES
            % THE EFFECT COEFFICIENCES OF
            AA=[zeros(4,4),eye(4,4);-MC*(KC-kbar),-MC*(CC-cbar)];
            INVA=inv(AA);
            mi0=expm(AA*step);
            BI(1:8,1:8)=BI(1:8,1:8)+mi0;
            % THE EFFECT COEFFICIENCES OF DELAY
            for i2=1:num_tooth

                BB=[zeros(4,8);-
MC*[bs(1:2,1:2,i2),bs(1:2,1:2,i2);bs(1:2,1:2,i2),bs(1:2,1:2,i2)],...
                -MC*[bq(1:2,1:2,i2),bq(1:2,1:2,i2);bq(1:2,1:2,i2),bq(1:2,1:2,i2)]];
                xdelay=floor(t_delay(i2)/step-0.5);
                xresidue=t_delay(i2)/step-xdelay-0.5;

                mi1=(1-xresidue)*(mi0-eye(8,8))*INVA*BB;
                mi2=xresidue*(mi0-eye(8,8))*INVA*BB;
                BI(1:8,8*xdelay+1:8*xdelay+8)=BI(1:8,8*xdelay+1:8*xdelay+8)+mi1;
                BI(1:8,8*xdelay+9:8*xdelay+16)=BI(1:8,8*xdelay+9:8*xdelay+16)+mi2;
            end
end

```

```

    PHI=BI*PHI;
end
E=eig(PHI);
max_eig=max(abs(E));
if max_eig>1
    %printf();
    adoc2=adoc;
    adoc=(adoc1+adoc)/2;
else
    %printf()
    adoc1=adoc;
    adoc=(adoc2+adoc)/2;
end
end
[y,i]=sort(abs(E));
if abs(E(i(rankn))+1)<1e-2
    ii=1+ii;
    E(i(rankn))
    period2(ii)=adoc
    omega2(ii)=omega*60/2/pi
end
Floquetmult=E(i(rankn))

chatter_freq1=-imag(log(Floquetmult))/tn/2/PI+excite_harmonics;
chatter_freq2=imag(log(Floquetmult))/tn/2/PI+excite_harmonics;
l_c_f=length(chatter_freq1);
chatter_freq(1+2*(jj-1)*l_c_f:2*(jj-1)*l_c_f+l_c_f)=chatter_freq1;
chatter_freq(2*(jj-1)*l_c_f+l_c_f+1:2*jj*l_c_f)=chatter_freq2;
s_spindle(1+2*(jj-1)*l_c_f:2*jj*l_c_f)=omega*60/2/PI*ones(1,2*l_c_f);
adoc
omega*60/2/PI
omeg(jj)=omega*60/2/PI;
ado(jj)=adoc;
jj=jj+1;
end
save fl_b_d2r05.dat omeg ado -ascii -double;
save fl_b_d2r05_cf.dat s_spindle chatter_freq -ascii -double;
save fl_b_d2r05p2.dat omega2 period2 -ascii -double;
load fl_b_d2r05.dat;
figure(1)
plot(fl_s_d2r05(2,:)/1000,1000*fl_s_d2r05(1,:));
xlabel('Spindle Speed (krpm)');
ylabel('ADOC (mm)');

load fl_b_d2r05_cf.dat;
figure(2)

```

```

plot(f1_b_d2r05_cf(2,:)/1000,f1_b_d2r05_cf(1,:)*1000,'!');
xlabel('Spindle Speed (krpm)');
ylabel('Chatter Frequency (Hz)');

% DEFINE THE CUTTING ZONE
% FORM THE STIFFNESS AND DAMPING MATRICES DUE TO CUTTING
FORCE
% Time delay is time varying due to the feed rate
% Helix cutter
function
[bs,bq,s,q,t_delay]=cutzone(tn,theta_enter,theta_exit,delta_theta,adoc,r,omega,eta,num
m_tooth,...
                             step,k1,k2,kt,cp,feed,t_delay)

PI=3.14159;
tn_1=tn-step;
bs=zeros(2,2,num_tooth);
s=zeros(2,2);
q=zeros(2,2);
qs=zeros(2,2);
normal1=zeros(num_tooth,1);
normal2=zeros(num_tooth,1);
t_delay=zeros(num_tooth,1);
%*** Define the initial angle range for each tooth at t=0 and z=0***
% the initial angle of the first tooth is the enter angle
for i = 1:num_tooth
    normal1(i) = -2*PI*(i-1)/num_tooth + theta_enter;
    normal2(i) = normal1(i) - 2*PI;
end
theta_en=theta_enter;
theta_ex=theta_exit;
% Non-cutting
% -PI is for straight tooth cutter in non-cutting condition

    % Compensation of delta_theta for up and down-milling

if theta_en == 0.0
    theta_en = theta_en - delta_theta;
end
if theta_ex == PI
    theta_ex = theta_ex + delta_theta;
end
if theta_en >= theta_ex
    theta_en = -PI;
    theta_ex = -PI;
end

```

```

for i = 1:num_tooth
    % For cylindrical mills with non-zero helix angles
    theta=omega*tn-(i-1)*2*PI/num_tooth+theta_enter;

    if eta ~= 0.0
        theta_en1 = theta_en;
        theta_ex1 = theta_ex;

        % Normalization of the cutting zone angles
        if (theta_en1-normal1(i))*(theta_en1-normal2(i)) > 0.0
            while (theta_en1-normal2(i)) > 2*PI
                theta_en1 = theta_en1 - 2*PI;
            end
        end
        if (theta_en1-normal1(i))*(theta_en1-normal2(i)) > 0.0
            while (theta_en1-normal1(i)) < (-2*PI)
                theta_en1 = theta_en1 + 2*PI;
            end
        end
        if (theta_en1-normal1(i))*(theta_en1-normal2(i)) == 0.0
            theta_en1 = normal1(i);
        end
        if (theta_ex1-normal1(i))*(theta_ex1-normal2(i)) > 0.0
            while (theta_ex1-normal2(i)) > 2*PI
                theta_ex1 = theta_ex1 - 2*PI;
            end
        end
        if (theta_ex1-normal1(i))*(theta_ex1-normal2(i)) > 0.0
            while (theta_ex1-normal1(i)) < (-2*PI)
                theta_ex1 = theta_ex1 + 2*PI;
            end
        end
        if (theta_ex1-normal1(i))*(theta_ex1-normal2(i)) == 0.0
            theta_ex1 = normal1(i);
        end

        % Rotate the cutting zone in the opposite direction
        theta_en1 = theta_en1 - omega*tn;
        theta_ex1 = theta_ex1 - omega*tn;
        if theta_en1 <= normal2(i)
            theta_en1 = theta_en1 + 2*PI;
        end

        if theta_ex1 <= normal2(i)
            theta_ex1 = theta_ex1 + 2*PI;
        end
    end
end

```

```

end

% z_en and z_ex values always nonnegative

z_en = -(i-1)*2*PI/num_tooth+theta_enter-theta_en1)*r/tan(eta);
z_ex = -(i-1)*2*PI/num_tooth+theta_enter-theta_ex1)*r/tan(eta);

% Non-cutting positions
if ((z_ex>=adoc)&(z_en>z_ex))|((z_en<=0.0)&(z_ex>adoc))|(z_en==z_ex)
    z1 = 0.0;
    z2 = 0.0;
    % Cutting positions
elseif (z_en<adoc)&(z_en>0.0)&((z_ex<=0.0)|(z_ex>adoc))
    z1 = 0.0;
    z2 = z_en;
elseif (z_en>=adoc)&((z_ex<=0.0)|(z_ex>adoc))
    z1 = 0.0;
    z2 = adoc;
elseif (z_en<adoc)&(z_ex<adoc)&(z_ex<z_en)&(z_ex>0.0)
    z1 = z_ex;
    z2 = z_en;
elseif (z_en>=adoc)&(z_ex<adoc)&(z_ex>0.0)
    z1 = z_ex;
    z2 = adoc;
else
    % You should not enter this block if all situations have been included
    % puts("There is a bug for helical tooth cutter!\n");
    z1 = 0.0;
    z2 = 0.0;
end
ss = (z2-z1)/2.0+r*sin(tan(eta)*(z1-z2)/r)*...
cos(2*omega*tn-(i-1)*4*PI/num_tooth-
tan(eta)*(z1+z2)/r+2*theta_enter)/(2*tan(eta));

cc = (z2-z1)/2.0-r*sin(tan(eta)*(z1-z2)/r)*...
cos(2*omega*tn-(i-1)*4*PI/num_tooth-
tan(eta)*(z1+z2)/r+2*theta_enter)/(2*tan(eta));

sc = r*sin(tan(eta)*(z2-z1)/r)*...
sin(2*omega*tn-(i-1)*4*PI/num_tooth-
tan(eta)*(z1+z2)/r+2*theta_enter)/(2*tan(eta));
else
theta=omega*tn-(i-1)*2*PI/num_tooth+theta_enter;
theta=theta-floor(theta/2/PI)*2*PI;
if(theta<=theta_ex&theta>=theta_en)
    ss=adoc*sin(theta)*sin(theta);

```

```

        cc=adoc*cos(theta)*cos(theta);
        sc=adoc*sin(theta)*cos(theta);
    else
        ss=0;
        cc=0;
        sc=0;
    end
end
end

bs(1,1,i)= -k1*kt*ss-k2*kt*sc-omega*cp*(k2*cc+k1*sc);
bq(1,1,i)= -k1*cp*ss-k2*cp*sc;
bs(1,2,i)= -k2*kt*cc-k1*kt*sc+omega*cp*(k1*ss+k2*sc);
bq(1,2,i)= -k2*cp*cc-k1*cp*sc;
bs(2,1,i)= k2*kt*ss-k1*kt*sc+omega*cp*(k2*sc-k1*cc);
bq(2,1,i)= k2*cp*ss-k1*cp*sc;
bs(2,2,i)= k2*kt*sc-k1*kt*cc+omega*cp*(k1*sc-k2*ss);
bq(2,2,i)= k2*cp*sc-k1*cp*cc;

s(1:1,1:1) = s(1:1,1:1) + bs(1,1,i);
s(1:1,2:2) = s(1:1,2:2) + bs(1,2,i);
s(2:2,1:1) = s(2:2,1:1) + bs(2,1,i);
s(2:2,2:2) = s(2:2,2:2) + bs(2,2,i);

q(1:1,1:1) = q(1:1,1:1) + bq(1,1,i);
q(1:1,2:2) = q(1:1,2:2) + bq(1,2,i);
q(2:2,1:1) = q(2:2,1:1) + bq(2,1,i);
q(2:2,2:2) = q(2:2,2:2) + bq(2,2,i);

t_delay(i)=2*PI*r/(num_tooth*(omega*r+feed*cos(theta)));

end

```

Input the parameters of system (For Figure 3.13, 1.14)

```

function input2_4
global mx xix kx my xiy ky mu ku xiu mv kv xiv feed;
global kt kn friction cp r eta phi_n num_tooth feedcut;
global omega1 omega2 delta_omega theta_enter theta_exit;
global adocL adocH delta_adoc int_time;
% MASS DAMPING STIFFNESS (X)
mx = 0.0436;
xix = 0.0107;
kx = 9.1397e+05;
% MASS DAMPING STIFFNESS (Y)%
my = 0.0478;
xiy = 0.009949;

```

```

ky = 1.0020e+06;
% MASS DAMPING STIFFNESS (U)
mu=1.0e+5;
xiu=100.0;
ku=1.0e+15;
% MASS DAMPING STIFFNESS (V)
mv=1.0e+5;
xiv=100.0;
kv=1.0e+15;
%WORKPIECE MATERIAL
%WORKPIECE MATERIAL
material='aluminum';
% CUTTING STIFFNESS (KT KN)
kt=6.0e+8;
kn=2.5/6;
% CUTTING FRICTION AND DAMPING (FRICTION CP)
friction=0.20;
cp=0.0;
% CUTTING RADIUS (R)
r=6.35e-3;
% HELIC ANGLE (ETA)
eta=40.0;
% NORMAL RAKE ANGLE (PHI_N)
phi_n=6.0;
% NUMBER OF TEETH (NUM_TOOTH)
num_tooth=2;
% FEED PER TOOTH (FEEDCUT)
feedcut=1*0.000127;
% MINIMAL SPINDLE SPEED, MAXIMUM SPINDLE SPEED,
% CHANGE SPINDLE SPEED(OMEGA1 OMEGA2 DELTA_OMEGA)
omega1=5000.0;
omega2=20000.0;
delta_omega=100.0;
% ENTRY AND EXIT ANGLES (THETA_ENTER THETA_EXIT)
theta_enter=154.16;
theta_exit=180.0;
% MINIMAL, MAXIMUM AND CHANGE AXIAL DEPTH OF CUT
% (ADOC1,ADOC2,DELTA_ADOC)
adocL=50.0e-6;
adocH=48.0e-3;
delta_adoc=0.0;

```

Appendix D

Matlab Program for Semi-Discretization Method for Stability Analysis of VSS Milling Processes

```
% MAIN PROGRAM TO GET THE STABILITY LOBE BY SEMI-
DISCRETIZATION METHOD
% In this case, we will consider the effect of feed rate on time delay
% Taylor approximation is not used. This is differently with the old one ()
function main
% num_tooth - Number of teeth on the cutter
% r - Radius of cutter (m)
% phi_n - Normal rake angle (degree)
% omega - Spindle Speed (rev./min.)
% feed - Feed rate along x direction (m/s)
% feedcut - Feed per tooth along x direction (m/pertooth)
% rdoc - Radial depth of cut (m)
% adoc - Axial depth of cut (m)
% kt - Tangential cutting coefficient from orthogonal cutting (N/m^2)
% kn - Cutting coefficient proportional constant
% cp - Viscous damping in the cutting process (N.s/m^2)
% friction - Coulomb friction coefficient
% eta - Helix angle of cylindrical end mill (degree)
% mx - Modal mass in x direction (Kg)
% kx - Modal stiffness in x direction (N/m)
% cx - Viscous damping in x direction (N.s/m)
% theta_enter - Cutter entering angle (degree)
% theta_exit - Cutter exit angle (degree)
% z1 - Dynamic integration lower limit (m)
% z2 - Dynamic integration upper limit (m)
% step - Integration time step (s)

global mx xix kx my xiy ky mu ku xiu mv kv xiv feed;
global kt kn friction cp r eta phi_n num_tooth feedcut;
global omega1 omega2 delta_omega theta_enter theta_exit;
global adocL adocH delta_adoc int_time RVA RVF;

% CALL THE INPUT FUNCTION TO INPUT THE SYSTEM PARAMETERS
N=40; % THE NUMBER OF STEP FOR EVERY PERIODIC
INPUT_brian_05_VSM;
% CHANGE THE DIMENSIONLESS DAMPING INTO CX,CY ETC.
cx=xix*2.0*sqrt(mx*kx);
cy=xiy*2.0*sqrt(my*ky);
cu=xiu*2.0*sqrt(mu*ku);
cv=xiv*2.0*sqrt(mv*kv);
% FORMING THE MASS, DAMPING AND STIFFNESS MATRICES
mm=[mx,my,mu,mv];
```

```

MC=diag(mm,0);
MC=inv(MC);
cc=[cx,cy,cu,cv];
CC=diag(cc,0);
kk=[kx,ky,ku,kv];
KC=diag(kk,0);
% CREAT TWO MATRICES FOR STATE EQUATIONS
AA=zeros(8,8);
BB=zeros(8,8);
kbar=zeros(4,4);
cbar=zeros(4,4);
zeroibar=zeros(4,1);

s=zeros(3,1);

% CHANGE THE ANGLE FROM DEGREE TO ARCH
eta=eta*pi/180.0;
omega1=2*pi*omega1/60.0;
omega2=2*pi*omega2/60.0;
delta_omega=2*pi*delta_omega/60.0;
theta_enter=theta_enter*pi/180.0;
theta_exit=theta_exit*pi/180.0;
% GET K1, K2
k1 = kn/cos(eta);
k2 = 1.0 + friction*(cos(phi_n)-kn*sin(phi_n))*tan(eta);

% DEFINE RANK OF MAPPING MATRICES
% rankn=(N+1)*8;

% GET THE LOBE DIAGRAM OF STABILITY BY PARAMETERS OF SPINDLE
SPEED
% AND AXIAL CUTTING DEEPHTH
jj=1;
ii=0;
for omega=omega1:delta_omega:omega2
    step=2*pi/omega/N/num_tooth;
    tn=2*pi/omega/RVF;

    tau_0=2*pi/omega/num_tooth;

    omega_m=RVF*omega;
    omega_A=RVA*omega;

    t_delay_max=tau_0*(1+(1+RVA)*RVA);
    t_delay_min=tau_0*(1-(1+RVA)*RVA);

```

```

rankn=(floor(t_delay_max/step-0.5)+2)*8;
BI=zeros(rankn,rankn);

excite_harmonics=-1/tn:1/tn:6*1/tn;

feed=omega/(2*pi)*num_tooth*feedcut;
% Cutting entering or exit angle variations due to feed
delta_theta = asin(2*pi*feed/(2*omega*r*num_tooth));

adoc1=adocL;
adoc2=adocH;
adoc=adocH/2.0;
% Define the constant matrix for the cutting coefficient under different
% cutting conditions.
Rambda=[-k1*kt -k2*kt-omega*cp*k1 -omega*cp*k2; +omega*cp*k1 -
k1*kt+omega*cp*k2 -k2*kt
+k2*kt -k1*kt+omega*cp*k2 -omega*cp*k1; -omega*cp*k2
k2*kt+omega*cp*k1 -k1*kt];
Gamma=[-k1*cp -k2*cp 0; 0 -k1*cp -k2*cp; k2*cp -k1*cp 0; 0 k2*cp -k1*cp];
while (adoc-adoc1)>1e-6 & (adoc2-adoc)>1e-6
    PHI=eye(rankn,rankn);
    for t=0:step:tn-step
        BI=[zeros(8,rankn);eye(rankn-8),zeros(rankn-8,8)];
        % CALL THE SUBROUTINE TO GET THE S, Q MATRICES

[s]=VSM_CUTZONE(t,theta_enter,theta_exit,delta_theta,adoc,r,omega,eta,num_tooth,
h,...
    step,k1,k2,kt,cp,RVA,RVF,omega_m);
dk=[Rambda(1,:)*s Rambda(2,:)*s; Rambda(3,:)*s Rambda(4,:)*s];
dc=[Gamma(1,:)*s Gamma(2,:)*s; Gamma(3,:)*s Gamma(4,:)*s];
kbar=[dk, dk; dk dk];
cbar=[dc,dc;dc,dc];

% FORMING THE STATE EQUATION MATRICES
% THE EFFECT COEFFICIENCES OF
AA=[zeros(4,4),eye(4,4);-MC*(KC-kbar),-MC*(CC-cbar)];
INVA=inv(AA);
mi0=expm(AA*step);
BI(1:8,1:8)=BI(1:8,1:8)+mi0;

t_delay=tau_0*(1-RVA*(1-RVA*sin(omega_m*t-
3.14159*RVF/num_tooth)).*sin(omega_m*t-3.14159*RVF/num_tooth));

% THE EFFECT COEFFICIENCES OF DELAY

BB=[zeros(4,8);-MC*kbar,-MC*cbar];

```

```

xdelay=floor(t_delay/step-0.5);
xresidue=t_delay/step-xdelay-0.5;

mi1=(1-xresidue)*(mi0-eye(8,8))*INVA*BB;
mi2=xresidue*(mi0-eye(8,8))*INVA*BB;
BI(1:8,8*xdelay+1:8*xdelay+8)=BI(1:8,8*xdelay+1:8*xdelay+8)+mi1;
BI(1:8,8*xdelay+9:8*xdelay+16)=BI(1:8,8*xdelay+9:8*xdelay+16)+mi2;

PHI=BI*PHI;
end
E=eig(PHI);
max_eig=max(abs(E));
if max_eig>1
    %printf();
    adoc2=adoc;
    adoc=(adoc1+adoc)/2;
else
    %printf()
    adoc1=adoc;
    adoc=(adoc2+adoc)/2;
end
end
[y,i]=sort(abs(E));
if abs(E(i(rankn))+1)<1e-2
    ii=1+ii;
    E(i(rankn))
    period2(ii)=adoc;
    omega2(ii)=omega*60/2/pi;
end
Floquetmult=E(i(rankn))

chatter_freq1=-imag(log(Floquetmult))/tn/2/pi+excite_harmonics;
chatter_freq2=imag(log(Floquetmult))/tn/2/pi+excite_harmonics;
l_c_f=length(chatter_freq1);
chatter_freq(1+2*(jj-1)*l_c_f:2*(jj-1)*l_c_f+l_c_f)=chatter_freq1;
chatter_freq(2*(jj-1)*l_c_f+l_c_f+1:2*jj*l_c_f)=chatter_freq2;
s_spindle(1+2*(jj-1)*l_c_f:2*jj*l_c_f)=omega*60/2/pi*ones(1,2*l_c_f);
adoc
omega*60/2/pi
omeg(jj)=omega*60/2/pi;
ado(jj)=adoc;
jj=jj+1;
end
save A01F02_b05_r05L.dat omeg ado -ascii -double;
save A01F02_b05_r05L_cf.dat s_spindle chatter_freq -ascii -double;

```

```

save A01F02_b05_r05Lp2.dat omega2 period2 -ascii -double;
load A01F02_b05_r05L.dat;
figure(1)
plot(A01F02_b05_r05L(2,:)/1000,1000*A01F02_b05_r05L(1,:));
xlabel('Spindle Speed (krpm)');
ylabel('ADOC (mm)');

load A01F02_b05_r05L_cf.dat;
figure(2)
plot(A01F02_b05_r05L_cf(2,:)/1000,A01F02_b05_r05L_cf(1,:)*1000,'.');
xlabel('Spindle Speed (krpm)');
ylabel('Chatter Frequency (Hz)');

% DEFINE THE CUTTING ZONE
% FORM THE STIFFNESS AND DAMPING MATRICES DUE TO CUTTING
FORCE
% Time delay is time varying due to the feed rate
% Helix cutter
function
[s]=VSM_cutzone(tn,theta_enter,theta_exit,delta_theta,adoc,r,omega,eta,num_tooth,..
.
    step,k1,k2,kt,cp,RVA,RVF,omega_m);

s=zeros(3,1);
%*** Define the initial angle range for each tooth at t=0 and z=0***
% the initial angle of the first tooth is the enter angle
normal1(1:num_tooth) = -2*pi*((1:num_tooth)-1)/num_tooth + theta_enter;
normal2 = normal1 - 2*pi;

theta_en=theta_enter;
theta_ex=theta_exit;
% Non-cutting
% -pi is for straight tooth cutter in non-cutting condition

    % Compensation of delta_theta for up and down milling
if theta_en == 0.0
    theta_en = theta_en - delta_theta;
end
if theta_ex == pi
    theta_ex = theta_ex + delta_theta;
end
if theta_en >= theta_ex
    theta_en = -pi;
    theta_ex = -pi;
end
end

```

```

for i = 1:num_tooth
    % For cylindrical mills with non-zero helix angles
    theta=omega*tn+RVA/RVF-RVA/RVF*cos(omega_m*tn)-(i-
1)*2*pi/num_tooth+theta_enter;

    if eta ~= 0.0
        theta_en1 = theta_en;
        theta_ex1 = theta_ex;

        % Normalization of the cutting zone angles
        if (theta_en1-normal1(i))*(theta_en1-normal2(i)) > 0.0
            while (theta_en1-normal2(i)) > 2*pi
                theta_en1 = theta_en1 - 2*pi;
            end
        end
        if (theta_en1-normal1(i))*(theta_en1-normal2(i)) > 0.0
            while (theta_en1-normal1(i)) < (-2*pi)
                theta_en1 = theta_en1 + 2*pi;
            end
        end
        if (theta_en1-normal1(i))*(theta_en1-normal2(i)) == 0.0
            theta_en1 = normal1(i);
        end
        if (theta_ex1-normal1(i))*(theta_ex1-normal2(i)) > 0.0
            while (theta_ex1-normal2(i)) > 2*pi
                theta_ex1 = theta_ex1 - 2*pi;
            end
        end
        if (theta_ex1-normal1(i))*(theta_ex1-normal2(i)) > 0.0
            while (theta_ex1-normal1(i)) < (-2*pi)
                theta_ex1 = theta_ex1 + 2*pi;
            end
        end
        if (theta_ex1-normal1(i))*(theta_ex1-normal2(i)) == 0.0
            theta_ex1 = normal1(i);
        end

        % Rotate the cutting zone in the opposite direction
        theta_en1 = theta_en1 - (omega*tn+RVA/RVF-
RVA/RVF*cos(omega_m*tn));
        theta_ex1 = theta_ex1 - (omega*tn+RVA/RVF-
RVA/RVF*cos(omega_m*tn));
        while theta_en1 <= normal2(i)
            theta_en1 = theta_en1 + 2*pi;
        end
    end
end

```

```

while theta_ex1 <= normal2(i)
    theta_ex1 = theta_ex1 + 2*pi;
end

% z_en and z_ex values always nonnegative
z_en = -(i-1)*2*pi/num_tooth+theta_enter-theta_en1)*r/tan(eta);
z_ex = -(i-1)*2*pi/num_tooth+theta_enter-theta_ex1)*r/tan(eta);

% Non-cutting positions
if ((z_ex>=adoc)&(z_en>z_ex))|((z_en<=0.0)&(z_ex>adoc))|(z_en==z_ex)
    z1 = 0.0;
    z2 = 0.0;
    % Cutting positions
elseif (z_en<adoc)&(z_en>0.0)&((z_ex<=0.0)|(z_ex>adoc))
    z1 = 0.0;
    z2 = z_en;
elseif (z_en>=adoc)&((z_ex<=0.0)|(z_ex>adoc))
    z1 = 0.0;
    z2 = adoc;
elseif (z_en<adoc)&(z_ex<adoc)&(z_ex<z_en)&(z_ex>0.0)
    z1 = z_ex;
    z2 = z_en;
elseif (z_en>=adoc)&(z_ex<adoc)&(z_ex>0.0)
    z1 = z_ex;
    z2 = adoc;
else
    % You should not enter this block if all situations have been included
    % puts("There is a bug for helical tooth cutter!\n");
    z1 = 0.0;
    z2 = 0.0;
end
ss = (z2-z1)/2.0+r*sin(tan(eta)*(z1-z2)/r)*...
cos(2*(omega*tn+RVA/RVF-RVA/RVF*cos(omega_m*tn))-...
(i-1)*4*pi/num_tooth-tan(eta)*(z1+z2)/r+2*theta_enter)/(2*tan(eta));

cc = (z2-z1)/2.0-r*sin(tan(eta)*(z1-z2)/r)*...
cos(2*(omega*tn+RVA/RVF-RVA/RVF*cos(omega_m*tn))-...
(i-1)*4*pi/num_tooth-tan(eta)*(z1+z2)/r+2*theta_enter)/(2*tan(eta));

    sc = r*sin(tan(eta)*(z2-z1)/r)*...
    sin(2*(omega*tn+RVA/RVF-RVA/RVF*cos(omega_m*tn))-...
(i-1)*4*pi/num_tooth-tan(eta)*(z1+z2)/r+2*theta_enter)/(2*tan(eta));
else
theta=theta-floor(theta/2/pi)*2*pi;
if(theta<=theta_ex&theta>=theta_en)

```

```

        ss=adoc*sin(theta)*sin(theta);
        cc=adoc*cos(theta)*cos(theta);
        sc=adoc*sin(theta)*cos(theta);
    else
        ss=0;
        cc=0;
        sc=0;
    end
end
end
s=s+[ss; sc; cc];
end

```

Input the parameters of system (for Figure 4.3b)

```

function INPUT_brian_05_VSM
global mx xix kx my xiy ky mu ku xiu mv kv xiv feed;
global kt kn friction cp r eta phi_n num_tooth feedcut;
global omega1 omega2 delta_omega theta_enter theta_exit;
global adocL adocH delta_adoc int_time RVA RVF;
% MASS DAMPING STIFFNESS (X)
mx = 0.0436;
xix = 0.0107;
kx = 9.1397e+05;
% MASS DAMPING STIFFNESS (Y)%
my = 0.0478;
xiy = 0.009949;
ky = 1.0020e+06;
% MASS DAMPING STIFFNESS (U)
mu=1.0e+5;
xiu=100.0;
ku=1.0e+15;
% MASS DAMPING STIFFNESS (V)
mv=1.0e+5;
xiv=100.0;
kv=1.0e+15;
%WORKPIECE MATERIAL
%WORKPIECE MATERIAL
material='aluminum';
%CUTTING STIFFNESS (KT KN)
kt=6.0e+8;
kn=2.5/6;
% CUTTING FRICTION AND DAMPING (FRICTION CP)
friction=0.20;
cp=0.0;
% CUTTING RADIUS (R)
r=6.35e-3;

```

```

% HELIC ANGLE (ETA)
eta=40.0;
% NORMAL RAKE ANGLE (PHI_N)
phi_n=6.0;
% NUMBER OF TEETH (NUM_TOOTH)
num_tooth=2;
% FEED PER TOOTH (FEEDCUT)
feedcut=0.000127;
% MINIMAL SPINDLE SPEED, MAXIMUM SPINDLE SPEED,
% CHANGE SPINDLE SPEED(OMEGA1 OMEGA2 DELTA_OMEGA)
omega1=1000.0;
omega2=5000.0;
delta_omega=50.0;
% RATIO OF NOMINAL SPINDLE SPEED AND AMPLITUDE OF SPEED
VARIATION
RVA=0.1;
% FREQUENCY OF SPEED VARIATION
RVF=0.1;
% ENTRY AND EXIT ANGLES (THETA_ENTER THETA_EXIT)
theta_enter=154.16;
theta_exit=180.0;
% MINIMAL, MAXIMUM AND CHANGE AXIAL DEPTH OF CUT
% (ADOC1,ADOC2,DELTA_ADOC)
adocL=50.0e-6;
adocH=48.0e-3;
delta_adoc=0.0;

```

Appendix E

FORTRAN Program for Studying Impact System

```
C *****
C ***** THIS PROGRAM IS USED TO SIMULATE DYNAMICS *****
C ***** OF SOFT IMPACT SYSTEM *****
C ***** (BILINEAR STIFFNESS AND DAMPING)*****
C ***** POINCARÉ SECTION IS USED TO CONSTRUCT *****
C ***** THE BIFURCATION DIAGRAM *****
C ***** NUMERICAL INTEGRATION (RKT) *****
C *****THE AMPLITUDE OF SHAKER OSCILLATE IS A CONSTANT***
C *****
PROGRAM MAIN
IMPLICIT REAL*8(A-H,O-Z), INTEGER(I-N)
DIMENSION Y(3),D(3),Z(3,1000000),B(3),FIN157220(1000000,2)
DIMENSION FORCE(1000000)
REAL*8 M_M,M_C,M_K,N_D,N_E,K_C,C_C
C DOUBLE PRECISION Y,D,Z,T,H,B
C T IS THE TIME; N IS NUMBER OF INTEGRATION; H IS THE TIME STEP
T=0.0
N=1000000
H=0.0001
PHI_LY=4.5003
PI=3.14159
C MODAL MASS M_A, MODAL DAMPLING M_C, MODAL STIFFNESS
M_K
C NONLINEAR COEFFICIENTS N_D, N_E
C CONTACT STIFFNESS K_C, CONTACT DAMPING C_C
CALL SYSPARAM(M_M,M_C,M_K,N_D,N_E,K_C,C_C,PHI_LY)
C DEFINE THE INITIAL CONDITION Y(1) AND Y(2) INITIAL
DISPLACEMENT AND VELOCITY
C Y(3) EXCITATION FREQUENCY
Y(1)=0.0
Y(2)=0.0
M=3
C DEFINE THE CLEARANCE BETWEEN THE SHAKER AND THE END OF
BEAM
X_C=0.0001
C OPEN THE OUT FILES
CALL FILES
NCOUNT=0
C SDMAX, THE MAXIMUM DISPLACEMENT OF SHAKER (CONSTANT)

SDMAX=2.6/(2*PI*2*PI*20*20)
DO 100 I=1,100
```

```

WRITE(*,*) I
Y(3)=36-I/10.0
C SDMAX=FORCE/(2*PI*2*PI*Y(3)*Y(3)*0.05985)
C AA=PHI_LY/SDMAX
T=0.0
CALL GRKT1(T,Y,M,H,N,Z,D,B,X_C,SDMAX,
1 M_M,M_C,M_K,N_D,N_E,K_C,C_C,FORCE,PHI_LY)
N1=19*N/20+1
DO 10 K=N1,N-1
IF (Z(2,K).LT.0.0 .AND. Z(2,K+1).EQ.0.0) THEN
NCOUNT=NCOUNT+1
FIN157220(NCOUNT,2)=Z(1,K)
FIN157220(NCOUNT,1)=Y(3)
ELSE IF ((Z(2,K+1).LT.0.0) .AND. (Z(2,K).GT.0.0)) THEN
NCOUNT=NCOUNT+1
FIN157220(NCOUNT,2)=(Z(1,K)+Z(1,K+1))/2
FIN157220(NCOUNT,1)=Y(3)
END IF
10 CONTINUE
IF (abs(Y(3)-32.61).LT.1E-4) THEN
DO 20 K=N1,N,5
WRITE(12,160) K*H,FORCE(K)
20 WRITE(2,150) K*H,PHI_LY*Z(1,K),PHI_LY*Z(2,K)
END IF
IF (abs(Y(3)-32.63).LT.1E-4) THEN
DO 30 K=N1,N
WRITE(13,160) K*H,FORCE(K)
30 WRITE(3,150) K*H,PHI_LY*Z(1,K),PHI_LY*Z(2,K)
END IF
IF (abs(Y(3)-32.65).LT.1E-4) THEN
DO 40 K=N1,N,5
WRITE(14,160) K*H,FORCE(K)
40 WRITE(4,150) K*H,PHI_LY*Z(1,K),PHI_LY*Z(2,K)
END IF
IF (abs(Y(3)-32.67).LT.1E-4) THEN
DO 50 K=N1,N,5
WRITE(15,160) K*H,FORCE(K)
50 WRITE(5,150) K*H,PHI_LY*Z(1,K),PHI_LY*Z(2,K)
END IF
IF (abs(Y(3)-32.69).LT.1E-4) THEN
DO 60 K=N1,N,5
WRITE(16,160) K*H,FORCE(K)
60 WRITE(6,150) K*H,PHI_LY*Z(1,K),PHI_LY*Z(2,K)
END IF
IF (abs(Y(3)-32.21).LT.1E-4) THEN
DO 70 K=N1,N,5

```

```

WRITE(17,160) K*H,FORCE(K)
70  WRITE(7,150) K*H,PHI_LY*Z(1,K),PHI_LY*Z(2,K)
END IF
IF (abs(Y(3)-32.23).LT.1E-4) THEN
DO 80 K=N1,N,5
WRITE(18,160) K*H,FORCE(K)
80  WRITE(8,150) K*H,PHI_LY*Z(1,K),PHI_LY*Z(2,K)
END IF
IF (abs(Y(3)-32.25).LT.1E-4) THEN
DO 90 K=N1,N,5
WRITE(19,160) K*H,FORCE(K)
90  WRITE(9,150) K*H,PHI_LY*Z(1,K),PHI_LY*Z(2,K)
END IF
IF (abs(Y(3)-32.27).LT.1E-4) THEN
DO 105 K=N1,N,5
WRITE(20,160) K*H,FORCE(K)
105  WRITE(10,150) K*H,PHI_LY*Z(1,K),PHI_LY*Z(2,K)
END IF
100 CONTINUE
DO 120 I=1,NCOUNT
120  WRITE(11,160) FIN157220(I,1),PHI_LY*FIN157220(I,2)
150  FORMAT(3F15.9)
160  FORMAT(2F15.9)
CLOSE UNIT=2
CLOSE UNIT=3
CLOSE UNIT=4
CLOSE UNIT=5
CLOSE UNIT=6
CLOSE UNIT=7
CLOSE UNIT=8
CLOSE UNIT=9
CLOSE UNIT=10
CLOSE UNIT=11
CLOSE UNIT=12
CLOSE UNIT=13
CLOSE UNIT=14
CLOSE UNIT=15
CLOSE UNIT=16
CLOSE UNIT=17
CLOSE UNIT=18
CLOSE UNIT=19
CLOSE UNIT=20
END

```

```

SUBROUTINE GRKT1(T,Y,M,H,N,Z,D,B,X_C,SDMAX,
1          M_M,M_C,M_K,N_D,N_E,K_C,C_C,FORCE,PHI_LY)

```

```

      IMPLICIT REAL*8(A-H,O-Z), INTEGER(I-N)
      DIMENSION Y(M),D(M),Z(M,N),A(4),B(M),FORCE(N)
      REAL*8 M_M,M_C,M_K,N_D,N_E,K_C,C_C,PHI_LY

C      DOUBLE PRECISION Y,D,Z,A,B,T,H,X,TT
      PI=3.14159
      A(1)=H/2.0
      A(2)=A(1)
      A(3)=H
      A(4)=H
      DO 5 I=1,M
5     Z(I,1)=Y(I)
      X=T
C      DEFINE THE CONTACT TIME
      NCONTACTT=0
      TI=0.0
      DO 100 J=2,N
C      DETERMINE THE DISPLACEMENT OF SHAKER
      SD=SDMAX*SIN(2*PI*Y(3)*(J-1)*H)
      SV=SDMAX*2*PI*Y(3)*COS(2*PI*Y(3)*(J-1)*H)
      SA=-SDMAX*2*PI*Y(3)*2*PI*Y(3)*SIN(2*PI*Y(3)*(J-1)*H)
C      DETERMINE THE TIME WHEN THE SHAKER CONTACT WITH THE
      BEAM
C      CONTACT CONDITION, CONTACT FORCE>=0
C      CON_FORCE REPRESENT THE CONTACT FORCE
      IF ((SD-PHI_LY*Z(1,J-1)-X_C) .GT. 0.0) THEN
          CON_FORCE=K_C*(SD-PHI_LY*Z(1,J-1)-X_C)+
1          C_C*(SV-PHI_LY*Z(2,J-1))
      ELSE
          CON_FORCE=0.0
      END IF
      IF (CON_FORCE .LT. 0.0) THEN
          CON_FORCE=0.0
      END IF

      CALL FF(M_M,M_C,M_K,N_D,N_E,Y,M,D,CON_FORCE,PHI_LY)
      FORCE(J)=CON_FORCE
      DO 10 I=1,M
10     B(I)=Y(I)
      DO 30 K=1,3
          DO 20 I=1,M
              Y(I)=Z(I,J-1)+A(K)*D(I)
              B(I)=B(I)+A(K+1)*D(I)/3.0
20     CONTINUE
      TT=T+A(K)
      CALL FF(M_M,M_C,M_K,N_D,N_E,Y,M,D,CON_FORCE,PHI_LY)

```

```

30  CONTINUE
    DO 40 I=1,M
40  Y(I)=B(I)+H*D(I)/6.0
    DO 50 I=1,M
50  Z(I,J)=Y(I)
    T=T+H
100 CONTINUE
    T=X
    RETURN
    END

    SUBROUTINE SYSPARAM(M_M,M_C,M_K,N_D,N_E,K_C,C_C,phi_ly)
    IMPLICIT REAL*8(A-H,O-Z),INTEGER(I-N)
    DIMENSION S(15)
    REAL*8 M_M,M_C,M_K,N_D,N_E,K_C,C_C,phi_ly
    rho1 = 0.3332
    xm = 0.0704
    g = 9.810
    E = 1.93e11
    XI = 8.6699e-012
    yl = 207.3e-3
c   %excitation force in Newton
C   force = 0.314
    pi=3.14159
C   normalized mode shape at the top
C   phi_ly = 4.501

C   from parametric integration

S(1) = -6.8109e+003
S(2) = 116.5171
S(3) = 27.9306
S(4) = 10.1265
S(5) = 3.3173
S(6) = 1.1892e+006
S(7) = -1.0833e+006
S(8) = 5.8726e+005
S(9) = 3.2544e+003
S(10) = 7.1495e+002
S(11) = 1.8820e+004
S(12) = -1.6464e+002
S(13) = 8.9084e+003
S(14) = 2.5383e+003
S(15) = 1.8820e+004

```

```

c  generalized mass
M_M = rho1 + xm*phi_ly*phi_ly
C  generalized stiffness
M_K = -E*XI*S(1) - xm*g*S(2) + rho1*g*y1*S(3) - rho1*g*(S(4)+S(5))
C  viscous damping factor from experiment
et = 0.0028
C  c is viscous damping.
M_C = et*2*M_M*2*pi*12.817

C  The first undamped natural frequency 12.89Hz
C  DETERMINE THE CONTACT STIFFNESS (N/M) AND DAMPING (N.S/M)
K_C=2.5*M_K*phi_ly
  C_C=6.0*et*sqrt(K_C)

N_D=E*XI*(S(6)+4*S(7)+S(8))+3*xm*g*S(11)/2-rho1*g
  1 *(S(13)+3*S(14)-3*y1*S(15))/2

N_E = -xm*S(9) + rho1*S(10) + rho1*S(12)
  RETURN
  END

  SUBROUTINE
FF(M_M,M_C,M_K,N_D,N_E,Y,M,yp,CON_FORCE,phi_ly)
  IMPLICIT REAL*8(A-H,O-Z),INTEGER(I-N)
  DIMENSION Y(M),yp(M)
  REAL*8 M_M,M_C,M_K,N_D,N_E,phi_ly
  pi=3.14159
C  y(3) is the excitation frequency from main program
C  normalized mode shape at the top
  CON_FORCE1=CON_FORCE/phi_ly
C  y(2) IS velocity  y(1) is displacement
yp(1) = y(2)
yp(2) = -(-CON_FORCE1+M_K*y(1)+M_C*y(2)+N_D*y(1)**3+
1  N_E*y(1)*y(2)**2)/(M_M+N_E*y(1)*y(1))
yp(3)=0.0
  return
  end

SUBROUTINE FILES
  OPEN(UNIT=2,FILE='N_FREQF3261.DAT',TYPE='UNKNOWN')
  OPEN(UNIT=3,FILE='N_FREQF3263.DAT',TYPE='UNKNOWN')
  OPEN(UNIT=4,FILE='N_FREQF3265.DAT',TYPE='UNKNOWN')
  OPEN(UNIT=5,FILE='N_FREQF3267.DAT',TYPE='UNKNOWN')
  OPEN(UNIT=6,FILE='N_FREQF3269.DAT',TYPE='UNKNOWN')
  OPEN(UNIT=7,FILE='N_FREQF3221.DAT',TYPE='UNKNOWN')

```

```
OPEN(UNIT=8,FILE='N_FREQF3223.DAT',TYPE='UNKNOWN')
OPEN(UNIT=9,FILE='N_FREQF3225.DAT',TYPE='UNKNOWN')
OPEN(UNIT=10,FILE='N_FREQF3227.DAT',TYPE='UNKNOWN')
OPEN(UNIT=11,FILE='BIF157F032.DAT',TYPE='UNKNOWN')
OPEN(UNIT=12,FILE='F_FREQF3261.DAT',TYPE='UNKNOWN')
OPEN(UNIT=13,FILE='F_FREQF3263.DAT',TYPE='UNKNOWN')
OPEN(UNIT=14,FILE='F_FREQF3265.DAT',TYPE='UNKNOWN')
OPEN(UNIT=15,FILE='F_FREQF3267.DAT',TYPE='UNKNOWN')
OPEN(UNIT=16,FILE='F_FREQF3269.DAT',TYPE='UNKNOWN')
OPEN(UNIT=17,FILE='F_FREQF3221.DAT',TYPE='UNKNOWN')
OPEN(UNIT=18,FILE='F_FREQF3223.DAT',TYPE='UNKNOWN')
OPEN(UNIT=19,FILE='F_FREQF3225.DAT',TYPE='UNKNOWN')
OPEN(UNIT=20,FILE='F_FREQF3227.DAT',TYPE='UNKNOWN')
RETURN
END
```

Bibliography

- Altintas, Y. (2000). *Manufacturing Automation, Cambridge University Press.*
- Altintas, Y. and Budak, E. (1995). "Analytical Prediction of Stability Lobes in Milling," *Annals of CIRP*, Vol. 44, pp. 357–362.
- Altintas, Y. and Chan, P. K. (1992). "In-process Detection and Suppression of Chatter in Milling," *International Journal of Machine Tools & Manufacture*, Vol. 32, pp. 329–347.
- Balachandran, B. (2001). "Nonlinear Dynamics of Milling Processes," *Phil Trans. R. Soc. Lond. A*, Vol. 359, pp. 793–819.
- Balachandran, B. (2003). "Dynamics of an Elastic Structure Excited by Harmonic and Aharmonic Impactor Motions," *Journal of Vibration and Control*, Vol. 9, pp. 265–279.
- Balachandran, B. and Gilsinn, D. (2005). "Nonlinear Oscillations of Milling," *Mathematical and Computer Modelling of Dynamical Systems*, Vol. 11, pp. 273–290.
- Balachandran, B. and Zhao, M. X. (2000). "A Mechanics Based Model for Study of Dynamics of Milling Operations," *Meccanica*, Vol. 35, pp. 89–109.
- Banerjee, S. and Grebogi, C. (1999). "Border Collision Bifurcations in Two-Dimensional Piecewise Smooth Maps," *Physical Reviews E*, Vol. 59, pp.4052–4061.
- Canniere, J. D., Brussel, V. H., and Bogaert, J. V. (1981). "A Contribution to Mathematical Analysis of Variable Spindle Speed Machining," *Appl. Math. Model.*, Vol. 5, pp. 158–164.
- Casas, F and Grebogi, C. (1997). "Control of Chaotic Impacts," *International Journal of Bifurcation and Chaos*, Vol. 7, pp. 951–955.
- Davis, M. and Balachandran, B. (2000). "Impact Dyanmics in the Milling in the Thin-Walled Structures," *Nonlinear Dynamics*, Vol. 22, pp. 375–392.

di Bernardo, M., Budd, C.J. and Champneys, A.R. (2001a). "Normal Form Maps for Grazing Bifurcations in n -dimensional Piecewise-Smooth Dynamical Systems," *Physica D*, Vol. 160, pp. 222–254.

di Bernardo, M., Budd, C.J., and Champneys, A.R. (2001b). "Grazing and Border-Collision in Piecewise-Smooth Systems: A Unified Analytical Framework," *Physical Review Letters*, Vol. 86, pp. 2553–2556.

Endres, W. J., Devor, R. E., and Kapoor, S. G. (1995). "A Dual-Mechanism Approach to the Prediction of Machining Forces. Part 1. Model Development," *ASME Journal of Engineering for Industry*, Vol. 117, pp. 526–533.

Faassen, R.P.H, van de Wouw, N., Oosterling, J.A.J., and Nijmeijer, H. (2003). "Prediction of Regenerative Chatter by Modelling and Analysis of High-Speed Milling," *International Journal of Machine Tools & Manufacture*, Vol. 43, pp. 1437–1446.

Fang, F. and Wickert, J. A. (1994). "Response of a Periodically Driven Impact Oscillator," *Journal of Sound and Vibration*. Vol. 170. pp. 397–409.

Farkas, M. (1994). *Periodic Motions*, Springer-Verlag, New York.

Feigin, M.I. (1970). "Doubling of the Oscillation Period with C-bifurcation in Piece-Wise Continuous Systems," *Journal of Applied Mathematics and Mechanics*, Vol. 34, pp. 861–869.

Feigin, M.I. (1974). "On the Generation of Sets of Subharmonic Modes in a Piecewise Continuous System," *Journal of Applied Mathematics and Mechanics*, Vol. 38, pp. 810–818.

Feigin, M.I. (1995). "The Increasingly Complex Structure of the Bifurcation Tree of a Piecewise-Smooth System," *Journal of Applied Mathematics and Mechanics*, Vol. 59, pp. 853–863.

Galvanetto, U. (2001). "Some Discontinuous Bifurcations in a Two-Block Stick-Slip System," *Journal of Sound and Vibration*, Vol. 248, pp. 653–669.

- Galvanetto, U. (2004). "Sliding Bifurcations in the Dynamics of Mechanical Systems with Dry Friction Remarks for Engineers and Applied Scientists," *Journal of Sound and Vibration*, Vol. 276, pp. 121–139.
- Gasparetto, A. (2001). "Eigenvalue Analysis of Mode Coupling Chatter for Machine-Tool Stabilization," *Journal of Vibration and Control*, Vol. 7, pp. 181–198.
- Hale, J. K. and Lunel, S M. V. (1993). Introduction to Functional Differential Equations, *Springer-Verlag*, New York.
- Hahn, W. (1961). "On Difference-Differential Equations with Periodic Coefficients," *Journal of Mathematical Analysis and Applications*, Vol. 3, pp. 70–101.
- Hanna, N. H. and Tobias, S. A. (1974). "A Theory of Nonlinear Regenerative Chatter," *ASME Journal of Engineering for Industry*, Vol. 96, pp. 247–255.
- Inamura, T. and Sata, T. (1974). "Stability Analysis of Cutting Under Varying Spindle Speed," *Annals of the CIRP*, Vol. 23, pp. 119–120.
- Inspurger, T., Mann, B.P., Stépán, G., and Bayly, P.V. (2003). "Stability of Up-Milling and Down-Milling, Part 1: Alternative Analytical Methods," *International Journal of Machine Tools & Manufacture*, Vol. 43, pp. 25–34.
- Inspurger, T. and Stépán, G. (2001). "Semi-discretization of Delayed Dynamical Systems," *Proceedings of DETC'01 ASME 2001 Design Engineering Technical Conference and Computers and Information in Engineering Conference Pittsburgh, PA*, September 9-12, CD-ROM, DETC2001/VIB-21446.
- Inspurger, T., and Stépán, G. (2002). "Semi-discretization Method for Delayed Systems," *International Journal of Numerical Methods in Engineering*, Vol. 55, pp. 503–518.
- Inspurger, T., and Stépán, G., (2004). "Stability Analysis of Turning with Periodic Spindle Speed Modulation Via Semidiscretization," *Journal of Vibration and Control*, Vol. 10, pp. 1835–1855.
- Inspurger, T., and Stépán, G. (2005). "State Dependent Regenerative Delay in Milling Processes," *ASME 2005 International Design Engineering Technical Conferences &*

Computers and Information in Engineering Conference, Long Beach, California USA, September 24-28, DETC/CIE2005-85282,

Insperger, T., Stépán, G., Mann, B.P., and Bayly, P.V. (2003). "Multiple Chatter Frequencies in Milling Processes," *Journal of Sound and Vibration*, Vol. 262, pp. 333–345

Insperger, T., Stépán, G., and Namachchivaya, N. S. (2001). "Comparison of the Dynamics of Low Immersion Milling and Cutting with Varying Spindle Speed," *Proceedings of DETC'01 ASME 2001 Design Engineering Technical Conference and Computers and Information in Engineering Conference Pittsburgh, PA*, September 9-12, CD-ROM, DETC2001/VIB-21616.

Kalpakjian, S. and Schmid, S. R. (2003) *Manufacturing Processes for Engineering materials*, Prentice Hall.

Kolmanovskii, V. and Myshkis, A. (1999). *Introduction to the Theory and Applications of Functional Differential Equation*, Kluwer Academic Publishers.

Kuster, F. and Gygax, P. E. (1990). "Cutting Dynamics and Stability of Boring Bars," *Annals of CIRP*, Vol. 39, pp. 361–366.

Lamba, H. and Budd, C. J. (1994). "Scalling of Lyapunov Exponents of Nonsmooth Bifurcations," *Physical Review E*, Vol. 50, pp. 84–90.

Leine, R. I. (2000). *Bifurcations in Discontinuous Mechanical Systems of Fillippov-Type*, Ph.D. Dissertation, Eindhoven University of Technology, The Netherlands.

Leine, R. I. and van Campen, D. H. (2002). "Discontinuous Bifurcations of Periodic Solutions," *Mathematical and Computer Modelling*, Vol. 36, pp. 259–273.

Lin, S. C., DeVor, R. E., and Kapoor, S. G. (1990). "The Effects of Variable Speed Cutting on Vibration Control in Face Milling," *ASME Journal of Engineering for Industry*, Vol. 112, pp.1–11

Long, X.H., and Balachandran, B. (2004). "Milling Model with Variable Time Delay," *Proceedings of IMECE 2004 ASME International Mechanical Engineering Congress and RD&D Expo, Anaheim, CA*, November 13-19, CD-ROM, IMECE2004-59207.

Long, X.H., and Balachandran, B. (2005a). "Elastic Structure Excited By harmonic Impactor Motion: Experimental and Numerical Investigations," *ENOC-2005*, Eindhoven, Netherlands, Aug. 7-12, 2005.

Long, X.H., and Balachandran, B. (2005b). "Stability Analysis of A Variable Spindle Speed Milling Process," *ASME 2005 International Design Engineering Technical Conferences & Computers and Information in Engineering Conference*, Long Beach, California USA, September 24-28, DETC/CIE2005-85065.

Long, X.H., and Balachandran, B. (2006). "Stability of Milling Process," *Nonlinear Dynamics*, in press.

Long, X.H., Balachandran, B., and Mann, B. P. (2006). "Dynamics of Milling Processes with Variable Time Delay," *Nonlinear Dynamics*, accept for publication

Maggio G. M., di Bernardo, M., and Kennedy, M. P. (2000). "Nonsmooth Bifurcations in a Piecewise-Linear Model of the Colpitts Oscillator," *IEEE Transactions on Circuits and Systems-E Fundamental theory and Applications*. Vol. 47, pp. 1160-1177.

Mann, B.P., Insperger, T., Bayly, P.V., and Stépán, G. (2003). "Stability of Up-Milling and Down-Milling, Part 2: Experimental Verification," *International Journal of Machine Tools & Manufacture*, Vol. 43, pp. 35-40.

Martellotti, M.E. (1941). "An Analysis of the Milling Process," *Transactions of the ASME*, Vol. 63, pp. 677-700.

Martellotti, M.E. (1945). "An Analysis of the Milling Process. Part II: Down Milling," *Transactions of the ASME*, Vol. 67, pp. 233-251.

Minis, I., Yanushevsky, R. (1993). "A New Theoretical Approach for the Prediction of Machine Tool Chatter in Milling," *ASME Journal of Engineering for Industry*, Vol. 115, pp. 1-8.

- Moon, F. C. and Holmes, P. J. (1979). "A Magnetoelastic Strange Attractor," *Journal of Sound and Vibration*. Vol. 65. pp. 275–296.
- Namachchivaya, N. S. and Beddini, R. (2003). "Spindle Speed Variation for the Suppression of Regenerative Chatter," *Journal of Nonlinear Science*, Vol. 13, pp. 265–288.
- Nayfeh, A. H. and Balachandran, B. (1995). *Applied Nonlinear Dynamics: Analytical, Computational, and Experimental Methods*, Wiley, New York.
- Nayfeh, A. H. and Mook, D. T. (1979). *Nonlinear Oscillations*, Wiley, New York.
- Normark, A. B. (1991). "Non-periodic Motion Caused by Grazing Incidence in an Impact Oscillator," *Journal of Sound and Vibration*. Vol. 145. pp. 279–297.
- Nusse, H. E., Ott, E., and Yorke, J. A. (1994). "Border-Collision Bifurcations: An Explanation for Observed Bifurcation Phenomena," *Physical Review E*, Vol. 49, pp. 1073–1076.
- Opitz, H., Dregger, E.U., and Roese, H. (1966). "Improvement of the Dynamic Stability of the Milling Process by Irregular Tooth Pitch," *Proceedings of the 7th International MTDR Conference*, Pergamon Press, New York.
- Ott, E., Grebogi, E., and Yorke, J.A. (1990). "Controlling Chaos," *Physical Review Letters*, Vol. 64, pp. 1196–1199.
- Peterka, F., Kotera, T, and Čipera, S. (2001). "Explanation of Appearance and Characteristics of Intermittency Chaos of the Impact Oscillator," *Proceedings of DETC'01 ASME 2001 Design Engineering Technical Conference and Computers and Information in Engineering Conference* Pittsburgh, PA, September 9-12, CD-ROM, DETC2001/VIB-21440.
- Pfeiffer, F., and Glocker, C. (1996). *Multibody Dynamics with Unilateral Contacts*. Wiley, New York.
- Popp, K., Oestreich, M., and Hinrichs, N. (1997). "Numerical and Experimental Investigation of Nonsmooth Mechanical Systems," *Proceedings of the IUTAM-*

Symposium on New Applications of Nonlinear and Chaotic Dynamics in Mechanics , Moon, F. C. (Ed.), Ithaca, NY, pp. 293–302 .

Radulescu, R., Kapoor, S. G., and Devor, R. E. (1997a). “An Investigation of Variable Spindle Speed Face Milling for Tool-Work Structures With Complex Dynamics, Part 1: Simulation Results,” *Transactions of the ASME, Journal of Manufacturing Science and Engineering*, Vol. 119, pp. 266–272.

Radulescu, R., Kapoor, S.G., and DeVor, R. E. (1997b). “An Investigation of Variable Spindle Speed Face Milling for Tool-work Structure with Complex Dynamics, Part 2: Physical Explanation,” *ASME Journal of Manufacturing Science and Engineering*, Vol. 119, pp.273–280.

Sastry, S., Kapoor, S. G., and Devor, R. E. (2002). “Floquet Theory Based Approach for Stability Analysis of the Variable Speed Face-Milling Process,” *Transactions of the ASME, Journal of Manufacturing Science and Engineering*, Vol. 124, pp. 10–17.

Sastry, S., Kapoor, S.G., DeVor, R. E., and Dullerud, G. E. (2001). “Chatter Stability Analysis of the Variable Speed Face-Milling Process,” *ASME Journal of Manufacturing Science and Engineering*, Vol. 123, pp.753–756.

Shaw, S. W. (1985). “Forced Vibrations of a Beam with One-sided Amplitude Constraint: Theory and Experiment,” *Journal of Sound and Vibration*. Vol. 99. pp. 199–212.

Sexton, J. S., Milne, R. D., and Stone, B. J. (1977). “A Stability Analysis of Single Point Machining with Varying Spindle Speed,” *Appl. Math. Model*, Vol. 19, pp. 310–318.

Smith, S. and Tlusty, J. (1997). “Current Trends in High-Speed Maching,” *Journal of Manufacturing Science and Engineering*, Vol. 119, pp. 664–666.

Sridhar, R., Hohn, R. E., and Long, G. W. (1968). “A Stability Algorithm for the General Milling Process,” *ASME Journal of Engineering for Industry*, Vol. 90, pp. 330–334.

Stensson, A. and Nordmark, A. B. (1994). “Experimental Investigation of Some Consequences of Low Velocity Impacts in the Chaotic Dynamics of a Mechanical System,” *Phil. Trans. R. Soc. Lond. A*. Vol. 347, pp. 439–448.

- Stépán, G. (1998). "Delay-Differential Equation Models for Machine Tool Chatter," in: F. C. Moon (Ed.), *Dynamics and Chaos in Manufacturing Processes*, Wiley, pp. 162–192.
- Stépán, G. (2001). "Modeling Nonlinear Regenerative Effects in Metal Cutting," *Philosophical Transactions of the Royal Society London A*, Vol. 359, pp. 739–757.
- Stépán, G., Szalai, R., Mann, B. P., Bayly, P. V., Insperger, T., Gradišek, J., Govekar E. (2005). "Nonlinear Dynamics of High-Speed Milling – Analyses, Numerics and Experiments," *Journal of Vibration and Acoustics*, Vol. 127, pp. 197–203.
- Takemura, T., Hoshi, T., and Okushima, K. (1974). "Active Suppression of Chatter by Programmed Variation of Spindle Speed," *Annals of the CIRP*, Vol. 23, pp. 121–122.
- Taylor, F. W. (1907). "On the Art of Cutting Materials," *Trans. ASME* Vol. 28, pp. 31–35.
- Tlusty, J. and Polacek, M. (1963). "The Stability of the Machine Tool Against Self-Excited Vibration in Machining," *Proceedings of the Conference on International Research in Production Engineering*, Pittsburgh, PA, pp. 465–474.
- Tobias, S. A. (1965). *Machine-Tool Vibration*, John Wiley & Sons.
- Tobias, S. A. and Fishwick, W. (1958a). "The Chatter of Lathe Tools Under Other Cutting Conditions," *Transactions of the ASME*, Vol. 80, pp. 1079–1088.
- Tobias, S. A. and Fishwick, W. (1958b). "Theory of Regenerative Machine Tool Chatter," *The Engineer*, Vol. 205, London.
- Tsao, T. C., McCarthy, M. W., and Kapoor, S. G. (1993). "A New Approach to Stability Analysis of Variable Speed Machining Systems," *International Journal of Machine Tools & Manufacture*, Vol. 33, pp. 79–808.
- Tesi, A., Abed, E. H., Genesio, R. and Wang, H. O. (1996). "Harmonic Balance Analysis of Period-Doubling Bifurcations with Implications for Control of Nonlinear Dynamics," *Automatica*, Vol. 32, pp. 1255–1271.

Wagg, D. J. and Bishop, S. R. (2002). “Application of Non-smooth Modeling Techniques to the Dynamics of a Flexible Impacting Beam,” *Journal of Sound and Vibration*. Vol. 256. pp. 803–820.

Wang, H. O. and Abed, E. H. (1995). “Bifurcation Control of a Chaotic System,” *Automatica*, Vol. 31. pp. 1213–1226.

Yilmaz, A., Al-Regib, E., and Ni, J. (2002). “Machine Tool Chatter Suppression by Multi-Level Random Spindle Speed Variation,” *Transactions of the ASME, Journal of Manufacturing Science and Engineering*, Vol. 124, pp.208–216.

Zhao, M. X. and Balachandran, B. (2001). “Dynamics and Stability of Milling Process,” *International Journal of Solids and Structures*, Vol. 38, pp. 2233–2248.

Zhusubaliyev, ZH. T. and Mosekilde, E. (2004). *Bifurcations and Chaos in Piecewise-Smooth Dynamical System, World Scientific Series on Nonlinear Science*.